



Publicly Accessible Penn Dissertations

---


1-1-2016

# 3d Biomimetic Model for Cellular Invasion in Angiogenesis and Cancer

Duc-Huy Nguyen

*University of Pennsylvania*, [ducng@seas.upenn.edu](mailto:ducng@seas.upenn.edu)

Follow this and additional works at: <http://repository.upenn.edu/edissertations>

 Part of the [Biomedical Commons](#), and the [Chemical Engineering Commons](#)

---

## Recommended Citation

Nguyen, Duc-Huy, "3d Biomimetic Model for Cellular Invasion in Angiogenesis and Cancer" (2016). *Publicly Accessible Penn Dissertations*. 1915.

<http://repository.upenn.edu/edissertations/1915>

This paper is posted at ScholarlyCommons. <http://repository.upenn.edu/edissertations/1915>

For more information, please contact [libraryrepository@pobox.upenn.edu](mailto:libraryrepository@pobox.upenn.edu).

---

# 3d Biomimetic Model for Cellular Invasion in Angiogenesis and Cancer

## **Abstract**

Cell migration is an essential and highly regulated process. Cells migrate to vascularize tissues, to form tissue, and to respond to inflammation. Unfortunately, cell migration is also involved in numerous pathological conditions such as in invasive tumors. Cells can migrate as individual cells or as collective groups of cells. Particularly important in cell migration is the collective migration of cells as it is a hallmark of tissue remodeling events during embryonic morphogenesis, wound repair, and cancer invasion. Perhaps, angiogenesis is one of the most crucial collective migration processes as it is involved in multiple physiological and pathological conditions such as formation of vasculature, wound healing, cancer progression and metastasis. During angiogenesis, endothelial cells migrate collectively from existing vasculature in response to a complex biochemical and mechanical cues to form multicellular structures that eventually develop into new functional blood vessels. Angiogenesis is also a highly dynamic process where multiple cells rearrange and coordinate within a sprout. Such dynamic rearrangement requires different cytoskeletal regulators such as Rho GTPases proteins (RhoA, Rac, and Cdc42). Although the roles of Rho GTPase proteins have been well characterized in 2D cell migration, little is known about their contributions in angiogenic morphogenesis. Here, we engineered a 3D biomimetic microfluidic-based device, called AngioChip, where endothelial cells are induced to migrate collectively from a pre-formed biomimetic cylindrical blood vessel into a 3D interstitial collagen matrix. The sprouts in our AngioChip demonstrate in vivo-like morphogenetic features such as formation of tip-stalk cells, lumen formation, filopodial-like protrusions in leading tip cells, and formation of perfusable neovessels. Using this system, we examine the roles of Cdc42 to regulate many aspects of angiogenic morphogenesis. We find that disturbing Cdc42 activity reduces formation of branches, migration speed, and collective migration. Additionally, Cdc42 also negatively regulate filopodia formation. We also develop the AngioChip into a pancreatic ductal adenocarcinoma (PDAC) on a chip to investigate the interactions between pancreatic cancer cells and blood vessels. Vascular invasion, where PDAC cells invaded towards the vasculature during tumor progression, is a hallmark of metastatic PDAC. Nevertheless, how pancreatic tumor cells interact with the blood vessels remains largely unknown. Using our PDAC-on-a-chip, we reveal a striking observation where PDAC cells invade and de-endothelialize the blood vessels. This de-endothelialization process leads to vascular replacement in the blood vessels and is mediated by proliferation of PDAC through Nodal/Activin-ALK7 signaling.

## **Degree Type**

Dissertation

## **Degree Name**

Doctor of Philosophy (PhD)

## **Graduate Group**

Chemical and Biomolecular Engineering

## **First Advisor**

Christopher S. Chen

---

**Keywords**

angiogenesis, biomimetic, cancer, Cdc42, microfluidic, pancreatic

**Subject Categories**

Biomedical | Chemical Engineering

**3D BIOMIMETIC MODEL FOR CELLULAR INVASION IN ANGIOGENESIS AND CANCER**

Duc-Huy Tran Nguyen

A DISSERTATION

In

Chemical and Biomolecular Engineering

Presented to the Faculties of the University of Pennsylvania

In

Partial Fulfillment of the Requirements for the

Degree of Doctor of Philosophy

2016

Supervisor of Dissertation

Signature: \_\_\_\_\_

Christopher S. Chen, M.D., Ph.D., Adjunct Professor of Bioengineering and Chemical and Biomolecular Engineering; Professor of Biomedical Engineering, Boston University; Wyss Institute for Biologically Inspired Engineering at Harvard University

Graduate Group Chairperson

Signature: \_\_\_\_\_

John C. Crocker, Ph.D., Professor of Chemical and Biomolecular Engineering.

Dissertation Committee:

Christopher S. Chen, M.D., Ph.D., Adjunct Professor of Bioengineering and Chemical and Biomolecular Engineering; Professor of Biomedical Engineering, Boston University; Wyss Institute for Biologically Inspired Engineering at Harvard University  
Kathleen J. Stebe, Ph.D., Richer and Elizabeth Goodwin Professor, Department of Chemical and Biomolecular Engineering, University of Pennsylvania  
Scott L. Diamond, Ph.D., Arthur E. Humphrey Professor, Department of Chemical and Biomolecular Engineering, University of Pennsylvania  
Sandra W. Ryeom, Ph.D., Assistant Professor, Department of Cancer Biology, University of Pennsylvania

3D BIOMIMETIC MODEL FOR CELLULAR INVASION IN ANGIOGENESIS AND CANCER

COPYRIGHT

2016

Duc-Huy Tran Nguyen

This work is licensed under the  
Creative Commons Attribution-  
NonCommercial-ShareAlike 3.0  
License

To view a copy of this license, visit

<http://creativecommons.org/licenses/by-nc-sa/2.0/>

## ACKNOWLEDGMENTS

Thank you to the following people:

### **Family**

To my parents, Minh-Lien Tran and Duc Van Nguyen: As I am writing my dissertation, I remember you said this to me many times when I was young: “We don’t have money for you to inherit, so we hope to leave you with a great education, and we hope you continue to learn and thrive to succeed in life”. This was the reason you both had given up a comfortable life in Vietnam to allow me a chance to arrive in the US, the land of opportunities to acquire a better education and a better life.

I also remember vividly that you both full-heartedly supported me when I was a young kid learning about science. Dad, whenever I asked, without any hesitation, you drove me to bookstores, and despite me spending hours reading chemistry, physics, and math books, you patiently waited outside. This was how I discovered my passion for science. Mom, you have always supported me fully as I explored my different interests from learning how to play an electronic keyboard to practicing Aikido. I know how hard it is that you let your only child live across the country, whom you only get to see once or twice a year. I am deeply grateful for all your moral supports and the sacrifices to let me follow my dreams and passions.

To my aunt, Loc Tran: I admire you for being such a generous, caring and loving individual. It is very inspiring to be around you. Thank you very much for being our rock of supports as we first stepped our first few footsteps into the land of opportunities. And thank you very much for always being there for my parents and me all these years.

To all my extended family members in Vietnam and in the US: thank you for your support and always believing in me.

To Andrew Menning: Sometimes, my labmates ask why I am often optimistic and positive about science despite how much frustrating sometimes science can be. I have no one else but you to be thankful for. You have always listened and cheered me up when my experiments failed. Thanks for

your patience, kindness, and words of wisdom and through those, I have discovered many things about myself. It has been an amazing 3+ years of adventure with you and many more years to come. Thank you very much for always being there and believing in me.

### **Scientific Mentors**

Dr. Christopher Chen: Thank you very much for creating a very open and collaborative scientific environment. I cannot thank you enough for being an extremely supportive and encouraging advisor. Your words of wisdom, your mentorship and career advice are invaluable. Looking back on all of these years, I will always be proud to say that I made the right decision to join and do great science in your lab. Thanks for setting up a great model of what it is to be a great leader in a scientific community.

Dr. Sandra Ryeom: I am very thankful for your mentorship and guidance. Thank you for your invaluable inputs as we were writing our AngioChip paper, and especially your valuable career advice as I started to apply for postdoctoral positions.

Dr. Kathleen Stebe and Dr. Scott Diamond: thank you very much for your guidance and support of my work, and your valuable scientific inputs whether it is during my thesis committee meetings or at the CBE department's social happy hours.

### **Members of Chenlab**

I have had a privileged opportunity to be surrounded by many wonderful minds and smart people in Chenlab. Not only you inspired me to think outside of the box, but you also set up an example of hard work and dedication. You are not only my colleagues but also my true friends over the years: Styliani Alimperti, Brendon Baker, Jan Baranski, Evangelia Bellas, Brandon Blakely, Thomas Boudou, Mark Breckenridge, Ritika Chaturvedi, Daniel Cheng, Colin Choi, Anant Chopra, Daniel Cohen, Ravi Desai, Jeroen Eyckmans, Peter Galie, Lin Gao, Elaine Jenson, Laurie Kelleher, Matt Kutys, Esak Lee, Wesley Legant, Jennifer Leight, Grace Lin, Zhijun Liu, Michelle Lynch, Jordan Miller, Teodelinda Mirabella, Jaisree Moorthy, William Polacheck, Natalia Rodriguez, Colette Shen,

Hyun-Ho Greco Song, Sarah Stapleton, Esteban Toro, Britta Trappmann, Michele Wozniak, Kexiang Xu, Michael Yang, Christine Yoon, Chris Yu, Xiang Yu.

I specially extend my immense gratitude to the following Chenlab members who have trained, collaborated, and contributed to the success of my PhD dissertation: Michael Yang, Daniel Cohen, Sarah Stapleton, Stella Alimperti, Esak Lee, Colin Choi, Peter Galie, Lin Gao, Susie Cha, and Alec Wong.



## ABSTRACT

### 3D BIOMIMETIC MODEL FOR CELLULAR INVASION IN ANGIOGENESIS AND CANCER

Duc-Huy T. Nguyen

Christopher S. Chen

Cell migration is an essential and highly regulated process. Cells migrate to vascularize tissues, to form tissue, and to respond to inflammation. Unfortunately, cell migration is also involved in numerous pathological conditions such as in invasive tumors. Cells can migrate as individual cells or as collective groups of cells. Particularly important in cell migration is the collective migration of cells as it is a hallmark of tissue remodeling events during embryonic morphogenesis, wound repair, and cancer invasion. Perhaps, angiogenesis is one of the most crucial collective migration processes as it is involved in multiple physiological and pathological conditions such as formation of vasculature, wound healing, cancer progression and metastasis. During angiogenesis, endothelial cells migrate collectively from existing vasculature in response to a complex biochemical and mechanical cues to form multicellular structures that eventually develop into new functional blood vessels. Angiogenesis is also a highly dynamic process where multiple cells rearrange and coordinate within a sprout. Such dynamic rearrangement requires different cytoskeletal regulators such as Rho GTPases proteins (RhoA, Rac, and Cdc42). Although the roles of Rho GTPase proteins have been well characterized in 2D cell migration, little is known about their contributions in angiogenic morphogenesis. Here, we engineered a 3D biomimetic microfluidic-based device, called *AngioChip*, where endothelial cells are induced to migrate collectively from a pre-formed biomimetic cylindrical blood vessel into a 3D interstitial collagen matrix. The sprouts in our *AngioChip* demonstrate *in vivo*-like morphogenetic features such as formation of tip-stalk cells, lumen formation, filopodial-like protrusions in leading tip cells, and formation of perfusable neovessels. Using this system, we examine the roles of Cdc42 to regulate many aspects of angiogenic morphogenesis. We find that disturbing Cdc42 activity reduces formation of branches, migration speed, and collective migration. Additionally, Cdc42 also

negatively regulate filopodia formation. We also develop the AngioChip into a pancreatic ductal adenocarcinoma (PDAC) on a chip to investigate the interactions between pancreatic cancer cells and blood vessels. Vascular invasion, where PDAC cells invaded towards the vasculature during tumor progression, is a hallmark of metastatic PDAC. Nevertheless, how pancreatic tumor cells interact with the blood vessels remains largely unknown. Using our PDAC-on-a-chip, we reveal a striking observation where PDAC cells invade and de-endothelialize the blood vessels. This de-endothelialization process leads to vascular replacement in the blood vessels and is mediated by proliferation of PDAC through Nodal/Activin-ALK7 signaling.

## TABLE OF CONTENTS

<b>ACKNOWLEDGEMENTS</b> .....	iii
<b>ABSTRACT</b> .....	vi
<b>LIST OF TABLES</b> .....	x
<b>LIST OF ILLUSTRATIONS</b> .....	xi
<b>CHAPTER 1: INTRODUCTION</b> .....	1
<b>1.1 Cellular invasion in physiological and pathological contexts</b> .....	1
1.1.1 Cellular invasion in morphogenesis and cancer.....	1
1.1.2 Molecular mechanism to regulate collective cell migration.....	4
1.1.3 The morphogenetic process of angiogenesis.....	7
1.1.4 Molecular mechanism of angiogenesis.....	9
1.1.5 Models to study angiogenesis.....	15
1.1.6 Rho GTPases as regulators for cell migration, cell-cell adhesion, and angiogenesis.....	22
<b>1.2 Pathology of pancreatic cancer and vascular invasion in pancreatic cancer</b> .....	26
1.2.1 Pancreatic adenocarcinoma.....	26
1.2.2 TGF- $\beta$ signaling in cancer and in pancreatic cancer.....	29
1.2.3 Roles of other TGF- $\beta$ superfamily members in cancer.....	32
1.2.4 Tumor-blood vessel interactions during tumor metastasis-cascade.....	34
1.2.5 Vascular invasion in pancreatic cancer and carcino-endothelialization.....	36
<b>CHAPTER 2: ANGIOCHIP, A BIOMIMETIC MODEL TO RECONSTITUTE ANGIOGENIC SPROUTING MORPHOGENESIS IN VITRO</b> .....	38
2.1 Abstract.....	38
2.2 Introduction.....	39
2.3 Materials and Methods.....	40
2.4 Results.....	44
2.5 Discussion.....	58
<b>CHAPTER 3: THE ROLE OF CDC42 IN BRANCHING MORPHOGENESIS IN</b>	

<b>ANGIOGENESIS</b> .....	61
3.1 Abstract.....	61
3.2 Introduction.....	61
3.3 Materials and Methods.....	63
3.4 Results.....	65
3.5 Discussion.....	73
<b>CHAPTER 4: A PRECLINIAL ORGANOTYPIC MODEL TO EXAMINE VASCULAR INVASION AND VASCULAR REPLACEMENT IN PANCREATIC DUCTAL ADENOCARCINOMA</b> .....	76
4.1 Abstract.....	76
4.2 Introduction.....	76
4.3 Materials and Methods.....	78
4.4 Results.....	81
4.5 Discussion.....	90
<b>CHAPTER 5: CONCLUSIONS AND FUTURE DIRECTIONS</b> .....	97
<b>REFERENCES</b> .....	103

## LIST OF TABLES

Table 4.1. Primers for qPCR.....	95
Table 4.2 Oligo sequences for CRISPR.....	96

## LIST OF ILLUSTRATIONS

<b>Figure 1.1.</b> The morphogenetic processes of angiogenesis.....	8
<b>Figure 1.2.</b> Carcino-endothelialization in human pancreatic cancer.....	37
<b>Figure 2.1.</b> 3D formation of endothelial sprouts and neovessels in a microfluidic device, AngioChip.....	46
<b>Figure 2.2.</b> Characterization of early and late sprouts and neovessels.....	48
<b>Figure 2.3.</b> Effects of VEGFR2 inhibition on angiogenic sprouting.....	50
<b>Figure 2.4.</b> Effects of S1P receptor inhibition on angiogenic sprouting.....	52
<b>Figure 2.S1.</b> Characterization of gradient between parent vessel and source channel.....	53
<b>Figure 2.S2.</b> Quantitative metrics for scoring number and length of sprouts and single cell.....	54
<b>Figure 2.S3.</b> Characterization of cell-deposited extracellular matrices by the endothelium.....	55
<b>Figure 2.S4.</b> Quantification of sprout length for the MVPS and MPS cocktail at day 4.....	56
<b>Figure 2.S5.</b> Quantification of sprout length for different S1P gradients.....	56
<b>Figure 2.S6.</b> Effects of MMP inhibition on angiogenic sprouting. ....	57
<b>Figure 2.S7.</b> Schematic of device manufacturing process.....	57
<b>Figure 3.1.</b> Inhibition of Cdc42 in the AngioChip.....	66
<b>Figure 3.2.</b> The effects of Cdc42 on sprout length and density during angiogenic sprouting.....	67
<b>Figure 3.3.</b> The effects of Cdc42 on collective migration of endothelial sprouting.....	68
<b>Figure 3.4.</b> The effects of inhibiting Cdc42 on branching morphogenesis in angiogenic sprouting.....	70
<b>Figure 3.5.</b> Filopodia formation of angiogenic sprouting upon Cdc42 inhibition.....	72
<b>Figure 4.1.</b> Preclinical organotypic model, PDAC-on-a-chip to capture vascular invasion and vascular replacement.....	83
<b>Figure 4.2.</b> Inhibition of TGF- $\beta$ signaling prohibited vascular apoptosis and vascular replacement.....	86
<b>Figure 4.3.</b> Vascular replacement is inhibited by blocking TGF $\beta$ signaling.....	88
<b>Figure 4.4.</b> Vascular replacement is driven through invasive forces by pancreatic cancer cells.....	89
<b>Figure 4.S1.</b> Vascular invasion and replacement were also observed in other murine primary PDAC cell lines and human pancreatic cancer cell line in our 3D biomimetic PDAC-on-a-chip model.....	93
<b>Figure 4.S2.</b> Vascular invasion and replacement of human pancreatic cancer cell lines in 2D heterotypic patterning coculture.....	94

## CHAPTER 1: INTRODUCTION

### 1.1 Cellular invasion in physiological and pathological contexts

#### 1.1.1 Cellular invasion in morphogenesis and cancer

The ability for cells to migrate is essential for physiological functions such as immune-surveillance, wound healing, and tissue morphogenesis during embryo development. Pathological processes such as in cancer invasion and metastasis also depend on the ability of malignant cells to transform, acquire motility and invasiveness to break away from their tissue of origin and seed distant organs to form secondary tumors (1). There are different modes of cell invasions: single cell migration, multicellular streaming, and collective migration (2). Although different modes of cellular invasion are important for many physiological and pathological processes, the purpose of this thesis will mostly focus on collective migration.

Distinguished from collective migration is single-cell migration. Single-cell migration is characterized by invasion of individual cells without cell-cell interactions during migration and a low correlation in the migration pattern between a cell and its neighbors. Single-cell migration is further classified into two subtypes comprised of amoeboid and mesenchymal migration. In amoeboid migration, cells obtain a round cell-body and there are several variants depending on the protrusive activity of migrating cells. Examples for different variants of amoeboid migrations are 1) cells that change morphology rapidly with short thin protrusions, without blebs and move with high velocities (0.4–5  $\mu\text{m}/\text{min}$ ); 2) cells with blebbing morphology and move slower in chaotic movements; and 3) cells with short protrusions associated with proteolytic activity with speed  $\sim 0.1 \mu\text{m}/\text{min}$  (2). In mesenchymal phenotype, cells have an elongated or spindle-shaped body and long protrusions. The front protrusions are dynamic and rapidly extend and retract while the rear of the cells can stay immobile, resulting in a relatively slow net migration at  $\sim 0.2 \mu\text{m}/\text{min}$  (2).

In contrast to single cell migration, both multicellular streaming and collective cell migration have common features such as movement of a group of cells and the migrating path is straighter

as compared to single cell migration. However, these two invasive modes share distinct characteristics. In multicellular streaming, cells that migrate along the same path are loosely or non-adherent. The streaming cells typically have speeds of 1-2  $\mu\text{m}/\text{min}$  (3). On the other hand, in collective migration, cells within the group are held together by cell-cell junctions. There is also a high correlation of directionality between neighboring cells. These cells move as a single strand of cells led by a single leader cell or as broad sheet of cells led by several leader cells (3-5). Collective migration is typically the slowest mode of cell migration (0.01–0.05  $\mu\text{m}/\text{min}$ ) in multiple cell types including cancer, but faster collective migration (0.2–1  $\mu\text{m}/\text{min}$ ) is also observed in development (6-8).

In single cell migration, a classified cyclic 5-step process has been described (9). The first step of single cell migration requires initial polarization of the cell cytoskeleton to distinguish between the front and rear of the migrating cells. During this step, extensive protrusions, either ruffles or pseudopods, are formed. The subsequent step requires the engagement of adhesion receptors of the integrin families (alpha and beta integrins). Adhesion receptors are clustered and recruit additional scaffolding proteins to form nascent adhesion complexes and mature focal adhesions. These focal adhesions bind cells to the substrata or extracellular matrix proteins (ECMs). In step 3, surface proteins, such as proteases (MT1-MMP, uPA/uPAR), are recruited to proteolytically cleave the ECMs providing space for the cells to expand forward. In step 4, shortly after integrin-ligand binding, actin filaments engage with adaptor as well as cross-linking and contractile proteins, such as myosin II, which stabilize and contract the actin polymers. In step 5, under tension and contraction created by myosin II, actin filaments are shortened to provide contraction, which allows the front end of the cell body to glide forward and rear end to retract. These five steps provide an adaptive and dynamic framework in most of the cell types. However, they might undergo adaptive modifications depending on the inherent molecular repertoire or specific functions of various cell types (9).



In collective cell migration, steps 1-4 of the migration cycle of each individual cell are retained. However, the mode of rear retraction and forward gliding of the cell body is now placed under an important modification. If the moving cells in the group are to remain connected to the rest of the moving cells within the group, trailing edge retracting drags the following cells along the emerging migration track. Therefore, the trailing edge exerts forces to the ECMs and cell-cell junctions. It is very likely that rear retraction and release of adhesive bonds towards the substrata are involved, yet the maintenance of cell-cell junctions allows transferring of the net migration vector on the following cells. Tracking of single cells within a cohesive migration group of cells in different locations reveals intact inner architecture of cells within a group (10). One additional important feature of collective migration is that leading edge extension, and force generation as well as trailing edge retraction is a shared process by several cells. In other words, there are three distinct set of cells within a cohesive migration group of cells: a group of leading edge cells that generates force, a group of passively dragged cells, and a trailing group of cells that execute retraction. All these three groups provide an asymmetry to the moving group.

During development, many morphogenetic processes involved collective migration such as morphogenetic movement of inner blastocysts (11), epithelial budding and developing ducts during branching morphogenesis (12), and migration of epithelial cells at the rim of the optic and the invaginating thyroid gland (13). More complex collective migration examples include collective movement during the converging extension of the vertebrate embryo in the *Xenopus* (14, 15) or the closure of dorsal surface in *Drosophila* embryo (16). Outside the context of development, collective migration is also seen in adults, such as in physiological wound healing. During wound healing, the horizontal migration of epithelial cell sheets across the wound tissue helps contract and close the wound (17). At the same time, endothelial cells sprout from existing blood vessels to form new blood vessels to support the repaired tissues (18).

While collective migration plays many important roles during embryo development, it is also a putative mechanism for invasion and metastasis of cancer. Evidence of collective migration

in cancer is present in not fully dedifferentiated tumors, high and intermediate differentiated tumors of epithelial origins such as lobular breast cancer, epithelial prostate cancer, large-cell lung cancer (19, 20), melanoma (21), and rhabdomyosarcoma (22). Two morphological and functional variants of collective migration in tumors have been observed in vivo through histology. The first mode is a result of protruding sheets and strands of cells that maintain contact with the primary site. This mode is typically observed in oral squamous-cell carcinoma, mammary carcinoma (19), colon carcinoma (23), melanoma, and basal cell carcinoma. A second mode is characterized as groups of cells, seen in histology and referred to as 'nests', which detach from the primary site and extend along interstitial tissue gaps. This second mode is observed in epithelial cancer and melanoma (21). Interestingly, collective migration is observed in multiple stages of the metastasis cascade including clusters of cells circulating in the peripheral blood or lymphatic vessels (24-26). The dissemination of collectives of cells has a greater implication for cancer metastasis rather than single cells.

### **1.1.2 Molecular mechanism to regulate collective cell migration**

One of the most distinctive features of collective migration is the formation of leader and follower cells. Leader cells localize at the front of the group, where they receive instructive signals to guide follower cells at the rear to migrate in the same direction. This process may be regulated through chemical or mechanical signaling (27, 28). The existence of the leader and follower cells secure front-rear polarity for the entire moving process. Delta-Notch signaling is implicated in determining the leader and follower cells as demonstrated in angiogenic (29). An additional example of negative feedback loops to inhibit formation of leader cells in neighboring cells is within 2D sheet migration (28). Interestingly, the fate of leader cells may be transiently determined as leader cells and follower cells might dynamically exchange position such as in angiogenic sprouting and in the developing mammary gland. The extracellular cues and downstream signaling to specify leader and follower cells are probably cell type-specific. Previously described signaling pathways

include mitogen-activated protein kinase, focal adhesion kinase, phosphoinositide-3-kinase, Src kinases, Notch, and Rho GTPases.

Once leader and follower cells are specified, individual cells in the group have to respond to a plethora of instructive cues from the microenvironment to move as a collective group. These signals can be topographic, chemical, or electrical. Topographic cues are consisted of extracellular matrix proteins, molecules bound by the ECM or the resident cells within the group. Haptokinesis is a topographic guidance in which cells orient their axis and movement along the topography provided by the anisotropy of the environment (30). Topography of guiding structures enables alignment of adhesion sites in parallel to the substrate, followed by a longitudinal actin cytoskeleton. For example, in 1D migration, fibroblasts patterned on a narrow line of adhesive substrate migrate in a string-like fashion, discouraging cells to migrate next to each other. Other examples in 3D topography guidance include collective groups of cells moving as a continuous sheet at the interfaces between muscle fibers or larger nerves and network formed by ECM fibers (31). If haptokinesis describes adhesion receptor-dependent migration along an isotropic substrate, haptotaxis indicates migration along a gradient of immobilized ligands in the substrate. Cells usually orient their migration toward the increasing availability of ligands. However, cell movement may also oppose the increasing gradient of ligands depending on the cell type and context (32, 33). Leader cells can guide collective migration of the group through sensing the guiding cues, depositing or removing the ECMs to alter adhesion sites or releasing or depositing immobilized cytokines/chemokines on the ECMs (31, 34). Lastly in topographic guidance, groups of cells also respond to the stiffness gradient of the microenvironment, a phenomenon called durotaxis. Positive durotaxis or migration towards a stiffer region is previously described in fibroblasts. Similarly, sarcoma cell sheets exhibit greater degree of collective migration on a stiffer substrate (35). During durotaxis, cells integrate different mechanosensory machineries such as focal adhesion, integrins and myosin II-mediated contractility in response to tissue stiffness.

In addition to the topographical cues, cell instructive signals also include biochemical and electrical signals. In chemical guidance, collective cell migration is influenced by gradient of soluble chemical factors, a phenomenon also called chemotaxis. Chemotactic guidance is essential during developmental processes but also a powerful tool to direct collective migration in experimental systems (36). Gradient of soluble biochemical factors can be generated through intrinsic diffusion ability of molecules within tissues or through convection due to interstitial fluid flow or a combination of both. Receptor binding and activation by biochemical factors induce and stabilize polarizing cell groups to move towards the increasing availability of biochemical cues (37). Chemotaxis is generally a paracrine mechanism but also induced by the cells themselves. Cells in a group may self-generate a gradient by different mechanisms: releasing chemokine-degrading enzymes that diffuse along the cell group and clear chemokines in the rear cells (38), or expressing migration-enhance factors/receptors in the front and decoy receptors in the rear that bind and internalize the chemokines to limit the biological function of the chemokines in rear cells (39, 40). In addition to chemoattractant in chemotaxis migration, chemorepulsive cues impose a constraint to direct migration away from the cues (41, 42). Such factors include FGF8 and Wnt3a, which induce mesendodermal cell sheet to migrate away from the primitive streak during gastrulation (43). Lastly, electrical guidance also known as galvanotaxis or electrotaxis is probably the least studied in collective cell migration. Electrotaxis describes directional migration of cells relative to direct-current electric field, which can be generated by cathode and anode (44). It has been shown to influence migration of many cell types including fibroblasts, epithelial and endothelial cells, neurons, immune cells, and cancer cells (45). Electric field can open voltage-gated ion channels to enable influx of ions and downstream signaling through activation of ion transport proteins, and cytoskeletal polarization (46, 47). For example, migration-inducing cell surface receptors including EGFR, acetylcholine receptor, and integrins were reported to respond to electric fields to locally activate PI3K/Akt and MAP/ERK signaling.

In tissues, there is a plethora of instructive guidance signals including both physical and biochemical cues. These cues act parallel to a group of cells. Therefore, migrating collective cells

need to integrate concurrent, potentially cooperative or opposing inputs to make their decision and adjust their migrating direction. The integrative inputs may lead to strengthen the cellular cohesion of cells within group to encourage collective migration or permit dispersal and transition from migration group to single cell migration (48). Therefore, cells within a group need to process and prioritize the instructive signals. Particularly interesting is the process of collective migration in angiogenesis where endothelial cells not only sprout out from a vessel in a collective manner, they also process microenvironment cues to undergo morphogenesis to develop multiple branches and well-structured hierarchical networks to support the tissue homeostasis, growth and regeneration.

### **1.1.3 The morphogenetic process of angiogenesis**

The vasculature develops shortly after gastrulation. Starting as blood islands from progenitor cells (hemangioblasts) in the visceral yolk sac, hemangioblasts differentiate into either hematopoietic or endothelial cells. The endothelial cells undergo the first phase of blood vessel formation in a process called vasculogenesis where they coalesce to form the primitive network of the vasculature. A second phase of blood vessel formation, called angiogenesis, begins, as endothelial cells from the existing primitive vascular plexus sprout out to form new blood vessels. These new blood vessels also undergo extensive remodeling via fusion and regression to finally form a fetal vasculature (49).

During angiogenesis, in response to various stimuli including biochemical and mechanical, some endothelial cells within the capillary walls are selected to become tip cells. These tip cells first digest the basement membrane proteins in the blood vessel and extend their cellular protrusions, filopodia, into the interstitial tissues to lead the sprouts. Tip cells do not proliferate in response to angiogenic cues (50). Though tip cells in zebrafish undergo a single proliferation during intersegmental vessel development (51). Other cells follow the tip cells to become stalk cells. Tip cells express higher level of VEGFR2 and DLL4 than following stalk cells. However, at any given time, stalk cells which express higher level of VEGFR2 and DLL4 can overtake tip cell to resume

tip cell position (52). Tip-stalk shuffling is a highly dynamic process. As multicellular sprout structures penetrate into the interstitial tissues, stalk cells from the trunk of the sprouts may undergo phenotypic transition into tip cells to initiate formation of branches.

Many steps further are essential to convert a sprout into fully functional blood-carrying vessels. For example, sprout extension requires migration of stalk cells. At the same time, stalk cells also proliferate to contribute to the extension of sprouts. To form new vascular connections, tip cells need to suppress their motile, exploratory behavior as they encounter their targets, which are either tips of other sprouts or existing vessels. Strong adhesive interactions between the tip/tip, tip/stalk enable connections of 2 sprouts or a sprout to an existing blood vessel. Once connection is established, cytoskeletal rearrangement allows opening of the sprouts to form lumen throughout the sprouts. Interestingly, existing evidence in zebrafish during intersegmental vessel formation suggests the role of fluid shear stress to initiate the formation of lumen within the intersegmental vessels (53). Failure of fusion might also help preventing formation of arteriovenous shunts or serve as a positive regulation of regression of unnecessary vessels.

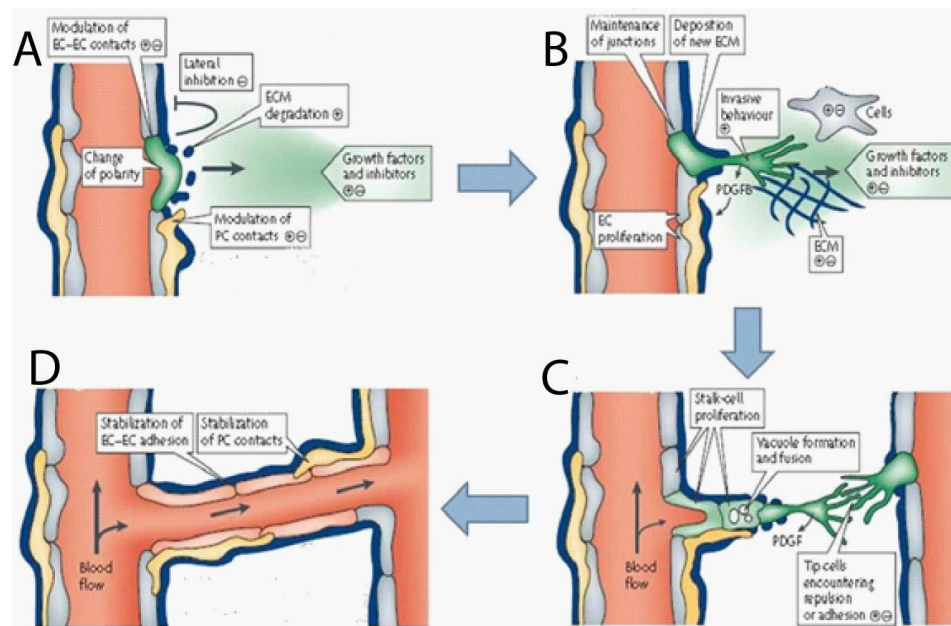


**Figure 1.1.** The morphogenetic processes of angiogenesis (modified and adapted from Alitalo. *Nature* (2006): **8**, 464-478). (A) Endothelial cells in the vessels are exposed to pro-angiogenic factors and begin to digest the basement membrane protein. (B) The tip cells extend filopodia into

the matrix in the direction of pro-angiogenic cues. (C) Tip cells lead the way while stalk cells are following. Lumen begins to develop. Tip cell of one sprout can encounter tip cell of another sprout during their migration. (D) Fusion of sprouts results in a blood vessel, which is lumenized throughout and perfused with blood vessels. Newly formed vessels are eventually mature to with deposition of basement membrane proteins.

Angiogenesis undoubtedly plays a critical role during embryo development. Nevertheless, dysregulations of angiogenesis in adults can contribute to many diseases. Historically, pathological angiogenesis is only implicated in cancer through ground-breaking work by Judah Folkman and many other labs to demonstrate that angiogenesis is a hallmark of cancer (54). To support the over-demanding growth of tumor, cancer cells secrete angiogenic factors to recruit blood vessels to supply nutrients and oxygen. These blood vessels then become escaping routes for the cancer cells to metastasize and seed distant organs to form secondary tumors. In recent years it has become increasingly evident that insufficient or abnormal angiogenesis also contributes to the pathogenesis of many more disorders. Another example of pathological disease due to excessive angiogenesis is retinopathy in diabetes patients which ultimately leads to blindness. Insufficient angiogenesis or damaged endothelium is also implicated in multiple diseases such as Alzheimer disease, diabetic neuropathy, atherosclerosis, hypertension, restenosis, Crohn disease, hair loss, nephropathy, osteoporosis, and so on (54).

#### **1.1.4 Molecular mechanism of angiogenesis**

Because angiogenesis is a critical process, it is tightly regulated by several mechanisms including expression of different family members, expression of alternatively spliced variants and ligand binding to different receptors. One of the most important molecule that controls blood-vessel sprouting is vascular endothelial growth factor A (VEGFA). VEGFA is required for chemotaxis and differentiation of endothelial cell precursor cells, endothelial cell proliferation, vasculogenesis, and blood vessel remodeling. Alternative splicing of VEGFA generate several variants. Binding of VEGFA to the receptor tyrosine kinase VEGFR2 (or KDR or FLK1) promotes downstream signaling

to enable angiogenic responses. VEGFR1 (or FLT1), secreted as a soluble receptor, is known to act as an antagonist or ligand trap for VEGFA signaling pathway (55, 56). Hypoxia is an important stimulus for expansion of the vasculature (57), and VEGF expression is upregulated during hypoxic conditions. Specifically, during organ development, cells are first oxygenated by simple diffusion until the tissue grows larger than the diffusion limit can permit to support tissue growth. Locally hypoxic environment triggers vessel growth through hypoxia-inducible transcription factors (HIFs) (57). Loss of a single allele of VEGF can cause vascular defects during embryogenesis (58, 59). A 25% reduction of VEGF levels impairs spinal cord perfusion and results in motor neuron degeneration (60). The role of VEGFB remains to be determined in angiogenesis while VEGFC is implicated in controlling lymphangiogenesis.

Platelet-derived growth factors share a significant degree of sequence to VEGF but their functions are distinct. For instance, PDGF-B is implicated in the maturation of vascular development. PDGF-B is expressed on the endothelium while PDGFR is present on vascular smooth muscle cells and pericytes. PDGF-B null mice had reduced pericyte coverage on capillaries. Similarly, PDGFR-B-null mice had decreased numbers and proliferation of smooth muscle cells and pericyte progenitors and most predominantly in the brain, heart, and brown adipose tissue (61, 62). Another protein also regulating smooth muscle cell attachment to blood vessel is angiopoietin. There are four members of angiopoietins (Ang 1-4) (63). Among these Angiopoietin 1 and 2 are the most understood due to their roles in developmental and pathological angiogenesis. Angiopoietin signals through Tie2 receptor kinase. Ang2 can induce phosphorylation of Tie2 in endothelial cells in autocrine or paracrine manners (64, 65). During angiogenic and vascular remodeling, Ang2 is expressed in endothelial cells and contributes to the detachment of smooth muscle cells. Genetic knock out of Ang-1 leads to embryonic lethality due to cardiovascular abnormalities (66).

The superfamily of FGFs and their receptors control a wide range of biological functions (67). Among the FGF ligands, bFGF is one of the first discovered angiogenic factors. FGF1 has



angiogenic and arteriogenic properties while FGF9 stimulate angiogenesis in bone repair. FGF can act on endothelial cells directly or indirectly via activating the secretion of angiogenic factors of other cell types (67). For instance, FGF activates secretion of hedgehog, ANG-2, and VEGF-B. Aberrant FGF signaling also promotes tumor angiogenesis and mediates the escape of tumor vascularization from VEGF-inhibition treatment (68). Interestingly, FGF1 and FGF2 deficiency in mice didn't result in vascular defects and there exists substantial redundancy in the FGF superfamily (67).

The large TGF- $\beta$  superfamily also contributes to angiogenesis and vascular malformations. Particularly important is the role of ALK1 or endoglin, one of the receptors for TGF- $\beta$  family. Loss of ALK1, ALK5, or TGF- $\beta$ R-2 leads to arteriovenous malfunctions. Human hereditary hemorrhagic telangiectasia or the formation of dilated capillaries is a result of mutation of ALK1 gene (69). TGF- $\beta$  signaling plays an important role for differentiation of endothelial cells. TGF- $\beta$  also promotes vascular smooth muscle cell differentiation. As a result, deficiency of ALK1 impairs mural cell development (69). However, the effects of TGF- $\beta$  in angiogenesis remains to be further explored due to the inconsistent results whether they promote or inhibit angiogenesis (70).

Notch and Wnt signaling pathways also contribute to the formation of blood vessels. Studies of tip-stalk cell formation in vessel, particularly, in the retina model indicate the roles of NOTCH to mediate the tip-stalk phenotype through DLL4-Notch signaling axis (71). More specifically, JAGGED1, a NOTCH ligand is expressed in stalk cells during tip-cell selection by disturbing the reciprocal DLL4 and NOTCH signaling from the stalk cell to the tip cell (72).

Tip-stalk cell selection is a competitive and dynamic process. Besides NOTCH and DLL4, endothelial cells also express various types of various WNT ligands and their frizzled receptors that can stimulate endothelial cell proliferation. NOTCH activates WNT signaling in proliferating stalk cells during vessel branching. WNT also activates NOTCH in a reciprocal-feedback loop (73, 74). Gene-inactivation of some of the WNT and Frizzle members in mice such as Wnt2, Wnt5a, Fzd4,

and Fzd5 causes vascular defects and combined loss of Wnt7a and Wnt7b impairs angiogenesis in the brain and disturb blood brain barrier formation(75).

Though less studied in the context of angiogenesis, hepatocyte growth factor (HGF), and monocyte chemotactic protein-1 (MCP-1) have also been shown to be involved in angiogenesis. HGF, also known as a scatter factor, is a large multidomain protein structurally similar to plasminogen with c-met as a receptor with tyrosine kinase activity. HGF is a potent mitogen, and morphogen for endothelial cells(76, 77). Administration of HGF as a protein or through adenoviral vector promotes angiogenesis without increasing vascular permeability or inflammation (78, 79). Combining HGF and VEGF enables more robust proliferative and chemotactic response of endothelial cells than either factor alone. Similarly, in 3D collagen gels, neither HGF or VEGF alone is sufficient to promote survival or tubulogenesis in endothelial cells, but a combination of the two growth factors will promote these responses (80, 81).

MCP-1 is a key chemokine responsible for trafficking and activation of monocytes/macrophages through its receptor CCR2. However, it has also been implicated in inflammation and angiogenesis. In fact, administration of exogenous MCP-1 increases monocyte/macrophage recruitment, and indirectly results in collateral vessel formation, and ultimately blood flow to the ischemic tissue in ischemic hindlimb models (82, 83) and in ischemic myocardium (84). Additionally, MCP-1 can also exert direct effects on endothelial cells to trigger angiogenesis (85).

Besides the growing list of angiogenic proteins (e.g.: VEGF, PDGF, FGF, HGF, MCP-1, TGF- $\beta$ , etc.), recent discoveries also indicate the crucial role of lipids as mediators for angiogenesis. Among them, sphingosine-1-phosphate emerges as an important regulator of angiogenesis and vessel maturation (86). Sphingosine-1-phosphate (S1P) is a blood-borne lipid mediator with pleiotropic biological activities including growth, survival, migration of mammalian cells (87). S1P is generated by converting ceramide to sphingosine by the enzyme ceramidase. Sphingosine is further converted into S1P by sphingosine kinases (SK1 and SK2). Knockout of

either SK1 or SK2 doesn't affect development of mice as it is fully compensated by the other functional enzyme. However, double knockout mice of SK1 and SK2 is embryonic lethal without detectable S1P level in the blood stream, suggesting that S1P is mainly generated through SK1 and SK2 (88).

The red blood cells are a major source of S1P, but other cell types such as vascular endothelial cells, and activated platelets also produce S1P (89-92). S1P binds to a family of five G protein-coupled receptors (GPCRs), called S1P<sub>1</sub>-S1P<sub>5</sub> (87). S1P<sub>1</sub>, S1P<sub>2</sub>, and S1P<sub>3</sub> are widely expressed in various tissues and the major receptor subtypes in blood vessels. S1P<sub>1</sub> is coupled exclusively via G<sub>i</sub> to Ras-mitogen activated protein kinase, phosphoinositide 3-kinase/ Akt pathway, and phospholipase C pathway, whereas S1P<sub>2</sub> and S1P<sub>3</sub> are coupled to multiple G proteins to activate phospholipase C, Rho pathways and as well as G<sub>i</sub>-dependent pathway (86). Endothelial cells and vascular smooth muscle cells show distinct patterns of expression of S1P<sub>1</sub>, S1P<sub>2</sub>, and S1P<sub>3</sub>. Endothelial cells largely express S1P<sub>1</sub> and S1P<sub>3</sub>, whereas S1P<sub>2</sub> is expressed only in certain vascular beds (93, 94). S1P<sub>3</sub> is abundantly expressed in both in endothelial cells and medial smooth muscle cells. S1P<sub>3</sub> stimulates nitric oxide synthase and nitric oxide production in endothelial cells while it mediates vaso-constriction in smooth muscle cells (95). S1P regulates endothelial cell growth, survival, migration, and barrier function (82, 90, 91, 96-98).

S1P stimulates angiogenesis mainly through S1P<sub>1</sub> and to a lesser extent through S1P<sub>3</sub> (86). Angiogenesis mediated by S1P<sub>1</sub> and S1P<sub>3</sub> is through activation of Rho GTPase Rac (93, 99-102) . S1P<sub>1</sub> ablation in mice impairs accumulation of pericytes and smooth muscle cells to the blood vessels (103). In contrast to S1P<sub>1</sub>, S1P<sub>2</sub> inhibits Rac activation, endothelial cell migration, and tube formation (94). Consistent with in vitro models, S1P<sub>2</sub> on retinal endothelial cells exerts an inhibitory effect on angiogenesis in avascular areas of the retina (104). Mice null for S1P<sub>2</sub> or S1P<sub>3</sub> develop normally without vascular defects, but combinatory deletion of S1P<sub>2</sub> and S1P<sub>3</sub> results in 50% lethality but without a defect in smooth muscle cell coverage on vessels. This suggests the importance of S1P<sub>1</sub> in vascular formation (86).

During the processes of angiogenic sprouting, the endothelial cells directly interact with the extracellular matrix. Linking the endothelial cells to ECMs are surface receptors such as integrins, which are heterodimeric receptors that mediate adhesion to ECM and immunoglobulin superfamily molecules (105, 106). Sprouting endothelial cells highly express  $\alpha v\beta 3$  and  $\alpha v\beta 5$  in tumor, which enables engaging of adhesion sites to multiple ECM proteins such as vitronectin, fibrinogen, and fibronectin to provide survival and traction for invading endothelial cells. Additionally, other integrins have also been reported to play a role in angiogenesis such as  $\alpha 1\beta 1$ ,  $\alpha 2\beta 1$ ,  $\alpha 4\beta 1$ ,  $\alpha 5\beta 1$ ,  $\alpha 9\beta 1$ , and  $\alpha 6\beta 4$  (105, 106). Apart from promoting adhesions to ECMs, integrins also regulate angiogenesis through other mechanisms. They bind to growth factors (VEGF, FGFs, ANG-1) or their receptors (VEGFR2, FGFRs) to activate the signaling and stimulate vessel growth (105, 106).

A significant part of angiogenic sprouting involves matrix degradation and remodeling mediated by enzymatic cleavage of ECMs through proteases. In fact, endothelial tip cells actively digest the basement membrane proteins to initiate the invasion into the interstitial tissue. Additionally, during branching, proteolytic remodeling of the ECM liberates cell unrestricted movement and convert anti-angiogenic peptides of the basement membrane into pro-angiogenic peptides. Among the enzymatic proteases, MMPs, a family of over 20 zinc- containing endopeptidases, have been shown to play multiple roles in angiogenesis (107). They degrade various components of ECMs (108). In addition to degrading ECM components, they also act to activate other MMPs and more importantly make available active growth factors and cytokines. For instances, MMP degrades insulin-like growth factor (IGF) binding proteins to release active IGFs, degrades proteoglycan perlecan in basement membranes to liberate FGFs, and degrade latent TGF- $\beta$  binding proteins to activate active form of TGF- $\beta$  ligands (109, 110). MMP-9 cleaves the pro-inflammatory cytokine IL-8 to increase its activity tenfold, and inactivate the angiogenic inhibitor platelet factor-4 (111). MMP activity is regulated by endogenous inhibitors, primarily by the tissue inhibitors of metalloproteinases (TIMPs). There are 4 TIMPs (TIMP-1 to -4), which bind tightly to all MMPs to regulate their activation. For example, TIMP-2 and TIMP-3 are efficient inhibitors of MT-MMP2 (112). TIMPs also have additional biological activities independent of their MMP inhibitory

activity. For example, in angiogenesis, TIMP-2 can inhibit bFGF-induced endothelial cell proliferation (113).

Last but not least is the role of junctional proteins as regulators of angiogenesis. Cell-cell communication is an inherent part of angiogenic sprouting. It is fundamentally important to synchronize cell-cell cohesive units in angiogenic sprouting but also regulates angiogenic sprouting initiation. Quiescent endothelial cells are growth-arrested through their interconnected junctional proteins but angiogenic endothelial cells dissociate their junctions to migrate and invade into the tissue. Tight junctional proteins such as claudins, occludins maintain blood brain barriers whereas adherent junctions such as VE-cadherins establish cell-cell adhesion during collective migration of sprouts (114). Among the adherent junctions, VE-cadherin is probably the most studied. Loss of VE-cadherin does not prevent development of vessels but causes defects in vascular remodeling and integrity (54). VE-cadherin is also required to localize CD34 to cell-cell contact for lumen formation (115). Localization of VE-cadherin at filopodia allows tip cells to establish new contacts with cells on outreaching sprouts to enable anastomosis between vessels (70).

### **1.1.5 Models to study angiogenesis**

Vascular dysfunctions causally contribute to many diseases, including but not limited to cardiovascular diseases. The endothelium also plays a critical role in the pathobiology of illnesses. Angiogenesis is necessary to form new blood vessels in ischemic tissues or wounded tissues. However, excessive angiogenesis may be harmful in disease development such as in cancer, diabetic retinopathy, atheroma growth or the expansion of vasa vasorum (116). Recent studies also suggest that the endothelium secret angiocrine factors to balance between tissue regeneration and fibrosis after injury. Increasing evidence suggests even though endothelial cells are essential players of neovascularization, their cross-talks to other stromal cells such as pericytes, vascular smooth muscle cells, and immune cells are also very important to regulate the processes of neovascularization. Simple in vitro models possess some advantages to examine the many

processes of angiogenesis such as lumen formation, biochemical and mechanical interactions in high resolution imaging. However, in vivo models are also necessary to study the more complex interactions that enable functional and hierarchical blood vessel networks. Therefore, it is essential to utilize both in vitro and in vivo angiogenesis models to recapitulate angiogenesis in different stages of development and in different contexts (116).

#### **a) In vivo models of developmental angiogenesis**

In all vertebrates, blood vessels form through successive steps of vasculogenesis and angiogenesis. Upon differentiation of angioblasts, the endothelial cell precursors coalesce to form a primitive plexus of the vasculature. Expansion of the initial network of vessels through angiogenesis develops into fully functional and blood perfused networks of vessels. Immediately or during the vascular network expansions, remodeling of the vessels also occurs to prevent excessive formation of vessels and enable formation of mature vessels with mural cell coverage. A larger number of signaling pathways have been described to regulate vascular network formation during development (117) using various in vivo models of developmental angiogenesis including mouse embryonic hindbrain, postnatal retina, avian embryos of chick and quail, and avian models of zebrafish and *Xenopus*.

Mouse hindbrain is vascularized before birth (118). The vasculature commences as vessels sprout into the hindbrain from a perineural vascular plexus at E9.5. First, these vessels grow perpendicular to the hindbrain surface toward the ventricular zone and then change direction to be parallel with the ventricular hindbrain surface and later anastomose with each other. This model is particularly important for the spatiotemporal analysis of organ vasculature due to their utilities for whole-mount staining and high-resolution imaging. Genetic manipulations are also available and more powerful when used with Cre-recombinase technology to study the roles of genes that might be lethal before birth of the embryos.

In contrast to the mouse hindbrain vasculature, the retinal vasculature is only formed after birth (119, 120). Right on the day of birth, the vessels from the optic nerve head sprout

perpendicularly over the surface of the retina on a network of astrocytes. As the vascular network continues to advance at the front, the rear vasculature begins to remodel to form arteries and veins. Further recruitment of pericytes and smooth muscle cells encompasses the blood vessel to form mature vasculature. The primary vascular plexus is completed by day 9 postnatal. However, an additional 10 days is required for the remodeling and maturation of the vessels. One of the major advantages of the retinal model is its 2D structure, enabling high resolution imaging and reliable quantification of vascular migration and angiogenic sprouting. Additional advantage is that vascular formation is postnatal, which can be more easily influenced by environmental factors than hindbrain angiogenesis, which occurs in the utero. However, it is less suitable to quantify network density and vessel calibers as sprouting and remodeling are temporally overlapping, especially at the vessels in the rear of the network (116).

Avian models of angiogenesis include chick and quail. The hallmark advantage of this model is that the animal development is within an eggshell, which may be used as a culture dish by creating a window for visual inspections and mounted on a microscope stage to monitor for extended periods of time. The larger size of the embryos also allows easy grafting of the tissues between different embryos. Previous work on grafting brain endothelial cells into liver shows the plasticity of brain endothelial cells to adapt to the liver environment by losing their blood brain barrier properties to adopt fenestrations (116). The most popular choice of experimental setup within the avian model is the chorioallantois membrane (CAM). The CAM is a highly vascularized extraembryonic appendage that provides nutrients and oxygen to the chick embryo. CAM is situated right beneath the eggshell, making it accessible to monitor the growth of vessels. Although CAM has been widely used to identify pro- and anti-angiogenic factors, validating the relevance of this model to intraembryonic angiogenesis remain a technical challenge (116).

Complimentary to the mentioned above in vivo models of developmental angiogenesis is the aquatic model, which includes zebrafish and *Xenopus*. The hallmark advantage of both of these animal models is their semi-transparency, which makes it attractive for high resolution imaging.

Additionally, when coupled with in vivo labeling of endothelial cells, these models enable noninvasive studies of endothelial cell dynamics during angiogenesis. In the zebrafish model, specified angioblasts originated in the posterior lateral plate mesoderm migrate toward the midline to form a primordial vascular cord or precursor of the dorsal aorta (DA) and posterior cardinal vein (PCV) (121). Once the major axial vessels are established in the trunk, sprouting angiogenesis occurs. Bilateral sprouts branch off from the DA, led by migrating tip cells and follower proliferative stalk cells. These sprouts later anastomose and form arterial intersomitic vessels (ISVs). A secondary sprouting occurs from the PCV between 30 and 50hrs after fertilization. Half of these sprouts form the lymphatic vessels while the other half connect to the arterial ISVs, which lose their original connection with the DA to become venous ISVs and complete the circulation in the trunk of the zebrafish. Unlike the zebrafish, *Xenopus* form 1 DA and 2 paired PCVs, which resemble more closely to higher vertebrates, where DA and PCV each develop from a pair of vessels that later fuse to form a single DA and single PCV (122). Unlike zebrafish, ISVs emerge from both the DA and PCV such that there is a pair of arterial ISV and venous ISV at each intersomitic junction, which is more similar to mammals. ISVs reach the dorsal side of the trunk and anastomose to form the dorsal longitudinal anastomosing vessel (DLAV), which connects to the PCV near the head. Additional sprouting of capillaries is required to cover all the tail area by stage 46 (123).

#### **b) Models of adult angiogenesis**

Postnatal angiogenesis is mostly associated with tissue or organ growth. In some cases, postnatal angiogenesis is caused by reproductive demands or pathologies such as in cancer. Additionally, adult angiogenesis also occurs as the tissue or organ undergoes repairing processes from injury or vascular occlusion.

One of the most visual and physiological assays for adult angiogenesis is the cutaneous wound assay. Tissue repair requires extensive cell proliferation, matrix deposition, and clearance of cell debris, which also demands heavily nutrients from the blood vessels. Thus, new blood



vessels are formed through angiogenesis to increase vascular density. Once the tissue is complete, vascular density returns to its normal level. Vessel density from time of injury to time of complete healing follows a bell-shape curve, with highest vessel density during the wound healing process. Although cutaneous wound healing is a robust model of adult angiogenesis that can be used in mice, rats, pigs, dogs, and primates, there are caveats that need to be considered. The extent of vascularization is highly dependent on the animal age. The angiogenesis process also relies on the blood coagulation system and inflammatory cells, which may complicate the mechanical understanding of the process (116).

In addition to wound healing assay, there are Matrigel plug assay and angioreactors. Matrigel plug is an easy angiogenic setup, in which an injection of Matrigel with or without growth factor supplement is administered subcutaneously into mice. Analysis is followed between 7-14 days post injection. Some analyses include vessel density and hemoglobin contents in the excised plugs. Additional information from the cellular content can also be quantified after fixation of the excised plugs. Some disadvantages of this model include inconsistency between different Matrigel plugs even within one animal. The ingrowth vessels in Matrigel plugs are often leaky and less mature without pericyte coverage, limiting the model to study the remodeling process of the vasculature (124). Similarly, to the Matrigel plug assay, angioreactors are implanted silicon cylinders that contain premixed volume of matrix with or without supplementary growth factors. Angioreactors are often implanted subcutaneously in the dorsal flank of mice (125). Similar analyses to Matrigel plug assay are also performed in the angioreactors.

### **c) In vitro models of angiogenesis**

In vivo models of angiogenesis may better reflect the complex processes of neovascularization and often provide important assessments of therapeutic angiogenic agents in living animals. However, in vivo models require technical expertise, highly complex, time consuming and relatively expensive (126). Additionally, neovascularization in living organisms is not an isolated process but involves multiple cell types, as well as biochemical and mechanical

cues within the environment. Ultimately, these factors may complicate understanding of biological mechanisms of angiogenesis. As a result, in vitro models of angiogenesis become a valuable tool to quickly assess the effects of therapeutic agents, but also allow high resolution imaging and detailed mechanistic studies. There exist various in vitro models of angiogenesis which assess different aspect of angiogenesis including: migration, proliferation, 2D network formation, and 3D sprouting.

Migration is one important aspect of angiogenesis sprouting. To assess migration, scratch wound assay has been employed due to their simple, quick, and inexpensive properties. Simply, endothelial cells are grown into a confluent monolayer and wounded by using a tip, needle or cell scraper (127). The rate and extent of endothelial cell migration towards the 'wounded' area can be microscopically monitored over several hours until the assay complete around 8-18hours. Though wound healing assay is easy and quickly adapted by many labs, there are disadvantages to the models: difficulty in reproducing the scratched area of equal size, variability among wells due to initial cell confluence, mechanical damage to the endothelial cells when creating the wounds with sharp objects, and incapability to separate cell migration from cell spreading and proliferation (127). Several modifications have been made such as introduction of a fence or barrier instead of using the sharp objects to improve the reproducibility. However, cell spreading and proliferation are still inseparable from migration. Additional cell migration model also includes Boyden chamber to study cell migration towards a stimulus, but this set up inherently lacks the capability to be used for high resolution imaging.

The effects of angiogenic factors on endothelial cell proliferation can be assessed by different methods more suitable than wound healing assay. Endothelial cells are often starved in serum-free or low serum medium and subsequently stimulated with stimuli. The most common and inexpensive means to evaluate proliferation is by using hemocytometer in conjunction with cell-viability dye. An additional method based on the incorporation of DNA-binding dyes, such as BrdU, can also be used to visualize proliferation cells when cells are in S phase of the cell cycle. Metabolic

activity can also be correlated with cell proliferation and its activity can be examined using colorimetric assays. However, in some cases, an increase in metabolic demand doesn't always correlate with cell proliferation (128).

A commonly used in vitro angiogenic assay is tube formation on Matrigel in which endothelial cells are plated on a 2D surface of Matrigel, which is highly enriched in laminin (129). Quickly after 4-16hrs, endothelial cells organize into tube-like network on the Matrigel surface. Images can be taken in different areas of wells to quantify tube length, number of sprouts, number of branches, and number of ring structures. This assay can be used quickly to assess the potential therapeutic agents for angiogenesis. However, it is still under dispute whether these tube-like structures resemble capillaries with lumen in angiogenesis. Moreover, many other non-endothelial cell types such as fibroblast, vascular smooth muscle cells, and cancer cells may also form similar structures when plated on Matrigel, suggesting that this assay describes a competitive cell-cell versus cell-matrix interactions and hence, not specific to endothelial cells.

To mimic the fundamental properties of endothelial cells to form lumen in 3D matrices, other models have been employed but the most common one is the endothelial cell tubulogenesis model. Endothelial cells are seeded in 3D collagen or fibrin matrices (130, 131) to allow them to assemble and align over time to form lumenized tubes. Lumen can be demonstrated by cross-sections of cultures, confocal microscopy or transmission electron microscopy. Interestingly, this model also describes formation of tunnel spaces in the ECMs, vascular guidance channels, through MT1-MMP. These channels enable motility of endothelial cells, matrix remodeling, and recruitment of mural cells to the abluminal surface. Attachment of mural cells also increase basement membrane protein depositions interior of the guidance channels (34, 132, 133).

Even though tubulogenesis recapitulate some of the intrinsic properties of endothelial cells such as tubule, lumen formation and recruitment of pericytes, this model generally lacks the initial invasion of endothelial cells. Therefore, a common strategy to seed endothelial cells on a 2D collagen matrix and allows them to invade inwards into the gel under guidance of angiogenic factors

with or without pericytes (34). Aggregates of spheroids have also been embedded inside matrices to mimic sprouting angiogenesis. Alternatively, endothelial cells are also seeded to coat surface of carrier beads, which are embedded into fibrin gels with the presence of human lung fibroblasts to enable endothelial cells to migrate outward from the carrier beads to form 3D lumenized sprout structures (134). Endothelial cell migration, and dynamic sprouting can be monitored with bright field contrast in real time. Sprout length, branches, lumen formation, and anastomoses can be assessed under this model. However, one of the disadvantages of this model is the presence of thick collagen matrices that limits the capability to perform high resolution imaging.

A more recent advance of in vitro model of angiogenesis has been the utilization of microfluidic devices in which vascular sprouting occurs in the presence of fluid flow. Transparency of materials to make such microfluidic devices also enables higher resolution imaging. Though these microfluidic platforms are sophisticated, they are fabricated based on a simplistic design in which two square/rectangular channels are generated by casting off a mold. These rectangular channels are comprised of 3 sides made from inert polydimethylsiloxane (PDMS) whereas the 4<sup>th</sup> side is a collagen or fibrin matrix wall where endothelial cells adhere and spread to form a monolayer. The other rectangular channel is enriched with angiogenic factors to enable migration of the endothelial cells into the collagen or fibrin matrix (135). Interestingly, to support the hydrogel, additional structural PDMS posts are interspersed inside the hydrogel, which create artificial stiff surface and may influence the migration of endothelial cells.

#### **1.1.6 Rho GTPases as regulators for cell migration and cell-cell adhesion and angiogenesis**

Cells in multicellular animals not only migrate through the extracellular matrix but also on top of each other, between each other, and even through each other (136). There are various examples to illustrate such processes. For instance, immune cells migrate on endothelial cells, adhere and finally migrate through the endothelium to get to the inflamed tissues (137). In order to move, cells have to extend their protrusions and generate forces to advance their body forward.

Many different molecules and signaling pathways coordinate cell migration especially collective cell migration. Particularly important in cell migration is the role of actin cytoskeleton and regulators of actin dynamics. Angiogenic sprouting involves extensive remodeling and arrangement of actin cytoskeletons to enable a dynamic process between cell-cell within the multicellular sprout structures. Therefore, actin cytoskeleton and regulators of actin dynamics are expected to influence the morphogenetic processes of angiogenesis.

Among the regulators of actin dynamics are Rho GTPases. Mammalian Rho GTPases comprise a family of 20 molecules. Most Rho GTPases switch between an active GTP-bound state to an inactive GDP-bound state. The activation of Rho GTPases are controlled by three sets of proteins: guanine nucleotide-exchange factors (GEFs), GTPase-activating proteins (GAPs), and guanine nucleotide-dissociation inhibitors (GDIs) (138). GEFs catalyze the binding of GTP while GAPs deactivate the Rho GTPases. GDIs modulate Rho GTPases by sequestration of Rho GTPases in GDP-bound or GTP-bound states (139-141). Upon activation, Rho GTPases interact with their downstream targets to stimulate a variety of biological activities: cell migration, cell division, adhesion, vesicle transport, microtubule dynamics, morphogenesis, neuronal development, cell-cycle progression and gene expression (142).

Although there are many Rho GTPases, the three most studied members are RhoA, Rac1, and Cdc42. The most extensively studied RhoA effectors are the serine/threonine Rho-associated kinases (ROCKs), which are transported to the plasma membrane upon association with active RhoA (143). ROCKs is best known to regulate actomyosin contractility via phosphorylation of myosin light chain. The most well studied effector of Rac1 and Cdc42 is p21-activated kinase family of serine/threonine kinases.

Most studies within the context of RhoA signaling in angiogenesis have focused upstream of myosin through targeting RhoA and ROCK. Interestingly, these experiments obtain inconsistent results. For example, in studies of VEGF-induced, tumor-induced, or hypoxia-stimulated angiogenesis in vivo, RhoA/ROCK signaling appeared to enhance angiogenesis in some cases

(144, 145) but inhibit in others (146, 147). In agreement with in vivo studies, in vitro studies of RhoA/ROCK/Myosin II activity also exhibit inconsistent results. For instances, ROCK activity appeared to suppress invasion into 3D matrix (148) but it increased 2D migration and tube formation (149). This suggests the complicated role of RhoA to regulate angiogenesis. While RhoA regulates contractility, Rac proteins is most known to modulate lamellipodia and membrane ruffling formation (142). There are three Rac isoforms: Rac1, Rac2, and Rac3. Rac1 is probably the best studied among the three isoforms (138). Rac1 is ubiquitously expressed and involved in migration of pericytes, vascular smooth muscle cells, and macrophages (103, 150, 151), all of which can contribute to vessel development and angiogenesis (152, 153). In fact, conditional knockout of Rac1 suggest its crucial role for vascular development in the embryo. Interestingly and similarly to the RhoA, some study suggests the positive regulation of Rac1 (154) while some other study indicate the indispensable Rac1 in the context of tumor angiogenesis (155).

The role of Cdc42 in angiogenesis has not been well described as compared to the roles of RhoA and Rac1 in angiogenesis. Cdc42 protein was first identified in *Saccharomyces cerevisiae* as a cell-cycle mutant where loss of Cdc42 inhibits budding and mating (156). A myriad of genetic knockout studies of Cdc42 demonstrate the importance of Cdc42 during development. For example, Cdc42 global knockout is embryonic lethal while conditional knockout of Cdc42 under different specific promoters results into different effects in the organism development depending on the affected cell types: defect in homing and retention of hematopoietic cells in bone marrow under Mx1-Cre, disturbance fate determination of apical neural progenitor cells under Emx1-Cre, loss of polarity in telencephalic neuroepithelium under Foxg1-Cre, hair loss in keratinocytes under K5-Cre, defect in axonogenesis in the brain under Nestin-Cre, and carcinoma development in the hepatocytes under Alb-Cre (157-159). It plays an essential role to cellular polarity (156) both in yeast and mammalian cells. Many studies of cellular polarization have focused on the epithelial sheet formation during which cells polarize to form distinct apical and baso-lateral surfaces between cell-matrix and cell-cell contacts. This polarization is initialized by adhesion protein such as nectin and E-cadherin (160), whose engagement also induces Cdc42 activation (161-163). Additionally,

in the context of cell migration in chemotaxis, individual cells also polarize in response to chemotactic soluble factors to generate front and rear ends in order to migrate towards the higher concentration of chemotactic factors. Cdc42 is shown to regulate this polarizing axis during cell migration. Dominant-negative Cdc42 mutants in neutrophils disturb polarization of the cells through generating unstable pseudopods while constitutively active Cdc42 blocks any changes in morphology (164).

Another well-known biological activity of Cdc42 is to regulate formation of filopodia. Filopodia are finger-like actin-rich protrusions generated by the cells, often at the front of the cells during cell migration. They contain parallel bundles of filamentous actin and are thought to be important for probing the environment. More specifically, in angiogenesis, filopodia are present mostly in tip cells. In many cell types, both constitutively and dominant-negative Cdc42 affect the formation of highly dynamic filopodial extensions. Though it is important for cell migration, some study also suggests filopodia are dispensable for migrating tip cells in formation of intersomitic vessels in zebrafish model (165). Several downstream targets of Cdc42 in filopodia formations have been identified: Wiskott-Aldrich syndrome protein, actin-related protein-2/3, insulin-receptor substrate p53, and Diaphanous proteins (157, 166, 167).

In regard to angiogenesis, there have been fewer studies to address the role of Cdc42 in angiogenesis. However, there have been studies to address the role of Cdc42 in lumen formations in tubulogenesis which appears to capture vasculogenesis rather than angiogenesis. In these studies, endothelial cells form intracellular vacuoles through pinocytosis. These vacuoles coalesce to form the lumen between endothelial cells. This process is largely driven by Rac1 and Cdc42 as both Rac1 and Cdc42 localize to the vacuole membranes during formation of lumen. Silencing Rac1 or Cdc42 inhibits vacuole formation and thus lumen formation. Downstream signaling molecules include WASP, PAK, Par3, Par6, and protein kinase C (168). Assessing the roles of Cdc42 in angiogenesis in vivo has been challenging due to embryonic lethality before E6.5 which occurs before formation of the vasculature (169). A recent study attempts to address the

vasculature defect in a conditional knockout Cdc42 in Tie2-Cre mice. The authors demonstrate that lack of Cdc42 in endothelial cells impairs migration and survival of endothelial cells but not cell cycle progression and ultimately results in defects in the vasculature. Additionally, the role of ADAM17 to mediate VEGFR2 shedding is also linked to conditional knock out of Cdc42 in endothelial cells, suggesting the role of Cdc42 in mediating VEGF signal transduction in vivo (170).

## **1.2 Pathology of pancreatic cancer and vascular invasion in pancreatic cancer**

### **1.2.1 Pancreatic adenocarcinoma**

Pancreatic cancer is currently the fourth leading cause of death among all cancers in the United States. With a 5-year survival rate well below 7% and a median survival of less than 6 months, pancreatic cancer has become the most devastating cancer of all (171). In addition to that, due to a lack of unique symptoms and limitation in diagnosis, most patients are often diagnosed when they are in the advanced stages. Once diagnosed with pancreatic cancer, surgery and chemotherapy are possible options. However, for the 15-20% of patients who undergo potentially curative resection, 80% patients relapsed, resulting a 20% survival after 5 years (171). Improvement in survival has been minimal even when chemotherapy and/or radiotherapy are employed on patients who have had surgery due to the fact that the cancer itself is intensely resistant to chemotherapeutic drugs (172).

The normal pancreas is consisted of digestive enzyme-secreting acinar cells, bicarbonate-secreting ductal cells, centro-acinar that are located geographically at the transition between acinar and ductal cells, hormone-secreting endocrine islet cells, and relatively inactive stellate cells. However, the majority of malignant neoplasms of the pancreas are ductal adenocarcinomas. It has been thought that the origin of pancreatic cancer cells is from ductal cells (173). However, recent study pointed out that the Kras-mutated acinar cells were more capable of giving rise to pancreatic cancer as compared to Kras-mutated ductal cells and Kras-mutated centro-acinar cells (174).



Some less common pancreatic neoplasms include neuroendocrine tumors (arising from cells secreting insulin or glucagon), colloid carcinomas, pancreatoblastomas, and solid-pseudopapillary neoplasms (172).

Pancreatic cancer most frequently originates from pancreatic intraepithelial neoplasia (PanIN), but can also arise from larger precursor lesions such as intraductal papillary mucinous neoplasms (IPMNs) and mucinous cystic neoplasms. The molecular pathology of pancreatic cancer is dominated by constitutively active mutant Kras (>90%) (175). Additionally, inactivating mutations of TP53, CDKN2A, and SMAD4 are accounted for 50-80% of pancreatic cancers. Other genes such as ARID1A, MLL3, and TGF-BR2 are mutated in ~10% of all cases (176). In addition to the mutations acquired as the disease progresses, pancreatic cancers also display an aberrant autocrine and paracrine signaling cascades that ultimately support cancer cell proliferation, migration, invasion and metastasis. Some of which include TGF $\alpha$ , IGF1, FGFs, HGF, and their respective tyrosine kinase receptors EGFR, ERBB2, FGFRs, and HGFR. These signaling cascades are active in conjunction with anti-apoptotic and pro-survival pathway such as signal transducer and activator of transcription 3 (STAT3), nuclear factor-kB (NF-kB), and AKT (176).

Pancreatic cancers have also been characterized with an abundant and dense collagenous stroma (desmoplasia), resulting in a considerable hypoxic environment for tumor cells (177). The dense stroma of pancreatic cancer is comprised of many extracellular matrix proteins (ECMs), such as collagens, fibronectin, and laminins, as well as non-collagenous proteins such as glycoproteins, proteoglycan, and glycosaminoglycans (178). Tightly bound to the ECMs are factors together with osteopontin, periostin, and serine protein acidic and rich in cysteine that mediate interactions between the stromal cells and pancreatic cancer cells. Stromal cells include pancreatic stellate cells (believed to produce collagenous matrix and often been referred to as cancer-associated fibroblasts), infiltrating immune cells, endothelial cells, and neuronal cells. Immune cells within the tumors include T cells with majority being CD4+ regulatory T cells, myeloid-derived suppressor cells, macrophages and mast cells. Interestingly, the majority of infiltrating immune cells is

immunosuppressive phenotype even during earliest stages of the cancer (179). Because of the dense stromal environment, successful drugs delivery has been a challenge in both in vivo mouse models and in clinical settings. Although there has been substantial evidence of facilitatory role of stromal pancreatic stellate cells in tumor growth and metastasis, recent studies (using genetic techniques to deplete myofibroblasts numbers and functions) suggested stromal has a protective role in pancreatic cancer (180). These discrepancies indicate that the influence of stroma in pancreatic cancer might be context- and time-dependent.

Models of pancreatic cancer such as traditional cell lines, xenograft models, genetically engineered mouse models (GEMM), and organoid cultures have greatly advanced the knowledge and biology of pancreatic cancer (181). Traditional cell lines derived from human patients have been used together with the immunocompromised mouse in xenograft models remain widely used for initial screening of drugs or to understand the mechanisms in cell biology of pancreatic ductal adenocarcinoma cancer (PDAC). However, one of the key shortcomings of using cell lines and xenograft model is that the tumors from xenografts often lack the characteristics of the PDAC tumor environment such stromal cells and ECMs (181). To address many of the key weaknesses of the xenograft approach, GEMM was developed to recapitulate the tumor progression in PDAC. The most common GEMM is activating mutation in KRAS, followed by inactivating mutations in CDKN2A, TP53, and SMAD4 (182). The first successful engineering model that helped to launch the field was LSL-Kras<sup>G12D</sup> in combination of Cre recombinase technology to target the PDX promoter in pancreatic epithelial cells. KRas<sup>G12D</sup> mice (KC) bearing an activating Kras mutation appeared to have a median survival of 1 year and developed a spectrum of pre-invasive ductal lesions that mirror human PanIN. Upon aging, KC mice spontaneously develop primary and metastatic PDAC. However, not all KC mice develop PDAC. Therefore, to promote a rapid onset of PDAC, additional inactivating mutations in TP53, CDKN2A, or SMAD4 have been successfully implemented (183, 184). Among these, KC mice with mutated TP53 (KPC mice) possess properties that resemble human pancreatic cancer such as hypovascular, dense stroma, and chemo/radiotherapy-resistance (185, 186).

Interestingly, organoid cultures of human and mouse pancreatic cancer have been described. Inspired from previously reported techniques to culture intestinal, gastric, colon carcinoma, hepatic, pancreatic, and prostatic organoids, pancreatic cancer organoids can be readily established from small biopsy specimens to obtain tumor cells. These tumor fragments of ductal cells were then embedded in 3D Matrigel. The 3D culture conditions to culture patient-derived organoids enables personalized medicine and also serves as an important model to identify gene drivers and molecular pathways involved in PDAC progression (187).

### **1.2.2 TGF- $\beta$ signaling in cancer and in pancreatic cancer**

The transforming growth factor-beta (TGF- $\beta$ ) was first discovered in 1983 as it possessed the ability to transform rat fibroblast (188). It is an important cytokine that is implicated in an extraordinary range of biological processes. The nomenclature, structure, receptor types, ligand interactions, and variability in signaling molecules make TGF- $\beta$  and its partners an extremely complex group of proteins to study. TGF- $\beta$  is a member of a large family of structurally related polypeptide growth factors, with each cytokine capable of governing numerous cellular processes. The proteins in TGF- $\beta$  family are divided into 2 main branches: the BMP/GDF/MIS and TGF- $\beta$ /Activin/Nodal branches, based on their sequence homology and the specific signaling cascade that they participate in (189). In mammals, there are three distinct TGF- $\beta$  isoforms (TGF- $\beta$ 1, TGF- $\beta$ 2, and TGF- $\beta$ 3), Although, they are encoded by different genes and expressed in a tissue-specific and developmentally regulated manner, they signal through the same receptor-signaling systems. These isoforms are expressed in epithelial, endothelial, hematopoietic, and mesenchymal cells.

Among these isoforms, TGF- $\beta$ 1 is the most abundant and universally expressed across many tissues (189). TGF- $\beta$ 1 is secreted into the extracellular matrix as a 25kDa molecule which is subsequently bound to one of several latent TGF- $\beta$ 1-binding proteins (LTBPs) to constitute a complex comprising of a dimer of TGF- $\beta$  and LTBP (190, 191). The LTBP and TGF- $\beta$  complexes not only stabilize TGF- $\beta$ 1 but also sequester the molecule within the ECM. Though it is hypothesized that activation of TGF- $\beta$ 1 from the complexes require subsequent proteolytic

enzymes to release the bioactive TGF- $\beta$ 1, integrins have been shown to activate TGF- $\beta$ 1 from its complexes as well (192). Once released from the complexes, TGF- $\beta$ 1 dimers initiate its signaling via binding to its appropriate receptors.

There are two high affinity receptors for TGF- $\beta$  ligands: TGF- $\beta$  receptor type I, TGF- $\beta$  receptor type II. The mechanism of signaling for all the ligands is fundamentally the same. Each ligand requires two types of receptors (type I and type II). For some ligands, additional co-receptors are required for optimal binding. Once the ligands bound to the receptor complexes, the constitutively active type II receptor phosphorylates the type I receptor on several serines and threonines in a highly conserved glycine- and serine-rich domain, close to the membrane-spanning region. This phosphorylation then activates the type I receptor kinases and allows binding site for the downstream substrates (193), the receptor-regulated SMADs (R-SMADs).

Although SMAD proteins are not the only molecules that can transduce TGF- $\beta$  superfamily signals to the nucleus, they are the best understood. There are eight vertebrate SMADs: SMAD1 to SMAD8 (194), which are classified into 3 groups: R-SMAD (SMAD1, SMAD2, SMAD3, SMAD5, and SMAD8), co-SMAD (SMAD4), and I-SMADs (SMAD6, SMAD7). A traditional view of TGF- $\beta$  superfamily is that BMPs and GDFs signal through SMAD1, SMAD5, and SMAD8 whereas TGF- $\beta$ s, Activins, and NODAL signal through SMAD2 and SMAD3. However, TGF- $\beta$ s have also been shown to phosphorylate SMAD1 and SMAD5 in addition to SMAD2 and SMAD2 in many cell types depending on the context (195-198). The mechanism of signaling for all the TGF- $\beta$  family ligands is fundamentally similar.

Receptor-mediated phosphorylation allows R-SMADs to form heteromeric complexes with SMAD4. SMAD4 occupies a central position in the signaling pathways downstream of all the ligands. SMAD4 is required by many ligand-mediated responses but not all. The activated SMAD complexes are then transported into the nucleus to bind DNA and transcription factors to express multiple genes. In the nucleus, SMAD phosphatases also dephosphorylate activated R-SMADs to allow them to be exported into the cytoplasm. SMAD-pathways are also subject to numerous levels

of regulations. TGF- $\beta$  superfamily pathways are also modulated by other signaling pathways. For example, R-SMADs are activated by growth factors-mediated through MAPKs, glycogen synthase kinase 3b (GSK3b), and cyclin-dependent kinases (CDKs). Interestingly, the TGF- $\beta$  superfamily pathways are also known to antagonize each other – for example, GDF3 directly inhibits BMP signaling (199).

Although inhibition of cellular proliferation is one of the primary functions of TGF- $\beta$  signaling pathway, numerous other contributions have been identified such as embryogenesis, differentiation, apoptosis, angiogenesis, immunosuppression, and wound healing. Because TGF- $\beta$  regulates multiple biological processes, any aberration of its normal activities including its normal signaling partners in the TGF- $\beta$  signaling cascade can have a wide-range pathological consequences. In fact, pathogenesis and progression of many cancers such as pancreas, colon, breast, melanoma, prostate, gastric, neuroendocrine, gynecologic, skin and nervous system have been attributed to the disruption of normal TGF- $\beta$  signaling (200). Interestingly, though TGF- $\beta$  acts to inhibit proliferation, thus a tumor growth suppressor, some human malignancies can subvert TGF- $\beta$  for their own purposes. These cancers overexpress TGF- $\beta$  ligands, which eventually leads to loss of normal growth inhibitory response to TGF- $\beta$  and advances metastasis and decreased survival. Therefore, TGF- $\beta$  plays a paradoxical role as it is both classified as a tumor suppressor and as a tumor promoter in many cancers including pancreatic cancer (201).

In pancreatic cancers, tumor cells have lost their tumor suppressive effects of TGF- $\beta$ 1 and several mutations of the TGF- $\beta$  transduction pathway have been well described. The mutation or deletion of the common partner SMAD4 is probably the most well-characterized. SMAD4 or DPC4 was one of the first novel tumor suppressors identified in pancreatic carcinomas (202). Approximately 30% of all pancreatic cancers shows a homozygous deletion of DPC4. DPC4 is inactivated in another 20% of pancreatic cancers. Almost in 90% of pancreatic tumors, there is an allelic loss of DPC4 chromosome. Mutations in DPC4 are within either the MH1 or most commonly the MH2 domain of the SMAD4 protein. These mutations are consisted of missense, nonsense or

frameshift mutations. Some of the arginine mutations in the MH1 domain lead to rapid degradation of SMAD4 as compared to wild type. Approximately, 50-90% of patients have SMAD4 alterations that diminish cell cycle control (202).

Additionally, human TGF- $\beta$  receptors have also been found to have certain inactivating mutations in many cancers such as colon, gastric, liver, breast and pancreatic cancer. Although mutations in TGF- $\beta$ RII are observed in the majority (70-90%) of colorectal cancers, it is less frequently observed in pancreatic cancer, accounting for 4-7% of pancreatic cancers (203). Similarly, mutations in TGF- $\beta$ RI accounts for 5% of cases. Some pancreatic cancers acquire resistance to normal inhibitory-growth of TGF- $\beta$  by expressing low level of TGF- $\beta$ RI, which can be restored by transducing cells with functional TGF- $\beta$ RI (204).

### **1.2.3 Roles of other TGF- $\beta$ superfamily members in cancers**

The TGF- $\beta$  superfamily comprises the TGF- $\beta$ s, Activins, NODAL, bone morphogenetic proteins (BMPs), growth and differentiation factors (GDFs), and anti-Mullerian hormone (AMH). Over the past three decades, much emphasis has been given to the TGF- $\beta$ s in cancer. However, increasing evidence of other TGF- $\beta$ s superfamily members to contribute to cancer progression has upsurge in literature over the years. In particular, BMPs, Activins, NODAL, and GDFs (referred as BANGs) have now shown to participate in tumor development and dissemination (193).

The most prominent roles of BANGs have been well described during early vertebrate development in many studies in mice, fish, and frogs. The earlier role of NODAL in the mouse embryo is at the blastocyst state where it is responsible to maintain the pluripotency, such as Oct4 and Nanog (205). After implantation, a gradient of NODAL helps define the proximal-distal axis to establish the anterior-posterior axis of the embryo. In conjunction with BMP and WNT signaling, NODAL is essential for mesoderm and endoderm formation and patterning. At later stages, NODAL is also required for left-right axis patterning (206, 207). Similarly, the BMPs also act in a gradient in early embryos to establish the axis and the tissue patterns along them. BMP-induced patterning is molded by its secreted antagonists such as chordin and noggin (208). In later stages of

development, both BMPs and GDFs are required for the formation of many different organs such as for the regulation of teeth, limb, kidney, skin, muscle, vascular, hematopoietic and neural development (209, 210).

However, a recent surge of papers suggests that many of BANGs roles in cancer is merely a redeployment of their roles in early development. Because the central roles of BANGs are to regulate stem cell maintenance and expansion, normal tissue hierarchical organization of tissues, a disturbance in somatic stem cells may generate cancer stem cells (211), or break down the tissue architecture during tumorigenesis. In the colon, two polyposis syndromes are genetically linked to aberrant BMP signaling and altered stem cell dynamics. Patients with juvenile polyposis syndrome develop hamartomatous polyps in the intestine with an increasing risks of adenocarcinoma. Germline mutations in *ALK3* or *BMPR1A* are seen in 20-25% of JPS cases, with additional 15-20% of cases having mutations in *SMAD4* (212). Hamartomatous polyps are associated with stem cell expansion and crypt fission in the colon, reflecting an aberrant BMP-WNT signaling axis. In sporadic colorectal cancer, evidence points to the loss of BMP signaling in the transition stage between adenoma and carcinoma. About 70% of cases displays inactivating BMP signaling in *SMAD1*, *SMAD5*, and *SMAD8* (213). Cancer stem cells in 20% cases of human glioblastomas are rendered unresponsive to anti-proliferative and differentiation-inducing effects of BMPs by silencing of the *ALK6* promoter (214). In the skin, tumor-educated stroma can override the endogenous BMP signaling by secreting antagonists such as Gremlin 1. Gremlin 1 is highly expressed in basal cell carcinoma but not in normal skin tissue (215). Additionally, Gremlin 1 overexpression is also present in many breast, lung, colon, pancreatic, and esophageal tumors.

In contrast to BMPs and GDFs, which are both essential for adult tissue homeostasis and embryonic development, NODAL is not normally expressed in adult tissues with the exceptions of organs that undergo widespread remodeling such as the placenta, endometrium, and lactating mammary gland. NODAL expression in adult tissues is predominantly present in pathological contexts (216, 217). Pathological NODAL expression was first reported in melanoma, where the

amount of NODAL secretion correlated with tumor aggressiveness. Expression of NODAL enables melanoma to be less differentiated, more plastic and at the same time, NODAL signaling also allows aggressive melanomas to simultaneously express markers of multiple lineages (mesenchymal, epithelial, and endothelial). As a result, NODAL overexpression favors functional adaptation of melanoma cells to the hostile growth environment (218). Similarly, the phenomenon was also extended into prostate, breast and testicular tumors (219-221). In pancreatic cancer, NODAL signaling has similar roles as in embryonic development, that is to drive pluripotency and self-renewal of cancer stem cells (222). Overexpression of NODAL has been shown in multiple human pancreatic cancer cells and enhances metastasis to liver in a splenic xenograft model (223).

#### **1.2.4 Tumor-blood vessel interactions during tumor metastasis-cascade**

Regardless of successful techniques and advances in resecting primary tumors and adjuvant therapy to cure confined primary tumors, treatment of metastasis disease from tumor dissemination largely remain a clinical challenge to be addressed. Tumor metastasis has accounted for >90% of death in cancer patients. Metastasis of carcinomas is a complex and multi-step process: 1) abnormal tumor cells begin to outgrow and break the basement membrane protein, 2) tumor cells invade into the stromal environment and interact with stromal cells, 3) tumor cells gain access to the blood and lymphatic vessels to intravasate into the circulating blood/lymphatic vessels, 4) tumor cells survive rigorous transport in blood stream, 5) tumor cells are arrested at distant organ sites and extravasate out of the blood vessels, 6) tumor cells begin to colonize in tumor-supporting microenvironment of different distant organs and form secondary tumors (224).

One of the hallmarks of tumor growth is angiogenesis. In the early 1970s, Folkman postulated that tumors need to be vascularized to grow and that diffusible molecules regulate this process. Later, vascular endothelial cell growth factor (VEGF) was identified as one of many important factors to recruit blood vessel growth. However, tumor angiogenesis possibly involves multiple angiogenic factors besides VEGF as anti-angiogenesis targeting VEGF has been effective in some tumors but not others. Interestingly, many tumors develop in highly vascularized tissues,



such as brain, liver and lung. In these tissues, tumors can use other mechanism for vascularization named vessel cooption (225). Vessel co-option is a mechanism in which tumors obtain a blood supply by hijacking the existing vasculature and tumor cells migrate along the vessels of the host organ. In a rat glioma model, Holash et al. first observed the process of vessel-cooption, followed by vessel regression, tumor hypoxia and the stimulation of angiogenesis for further tumor growth. The process of vessel co-option was not just limited to gliomas, but also shown in rat mammary adenocarcinoma. In a zebrafish study by Zhao et al (226), vessel co-option and angiogenesis were thought to have distinct contributions at the earliest stage of microtumor initiation and metastasis. Vessel co-option served an alternative route to obtain nutrient and oxygen during early stage of tumor growth. However, angiogenesis played an essential role during the exponential growth during tumor progression (227). Interestingly, vessel co-option has also been suggested as a potential explanation for failure of anti-angiogenic therapy.

It has also been posited that tumor cells may also stay in the wall of blood vessels as they break into the blood vessels rather than staying outside the basement membrane in vessel co-options. Interestingly, Chang et al has shown that GFP-pre-labeled colon carcinoma cells could integrate into the blood vessels in both ectopic and orthotopic implantation models to form blood vessels with interspersed GFP-labeled tumor cells (228). These mosaic blood vessels were accounted for 4% of total vasculature surface. Interestingly, they also demonstrated that mosaic vessels are fully functional with perfused fluorescent lectin. These tumor cells were thought to be in a transition of intravasating in the blood vessels and stay temporarily in the capillary vessel walls. FGF-2 and VEGF-A activated MMP2 activity to increase the mosaic vessels.

Interestingly, tumor cells seem to adapt and utilize different mechanisms to vascularize their extremely demanding needs for nutrients. In fact, another different concept of tumor self-vascularized tissue was coined as vascular mimicry. Briefly, vascular mimicry (VM) is described as a functional plasticity of aggressive cancer cells to form de novo vascular networks to provide perfusion pathway for growing tumors. VM has been reported in multiple cancers including

melanoma, glioblastoma, carcinomas, breast, and sarcomas. Historically, vascular mimicry was proposed back in 1999 by Maniotis et al. In their study, using an aggressive uveal melanoma, they presented that the tumor was lined up with networks of channels interconnected by loops and visualized by periodic acid stain (PAS). Interestingly, these PAS positive networks were in close contact with the peripheral vascular vessels and partly stained by antibodies against Von Willebrand factors, CD34, VEGFR2, and lectin, which are markers for endothelial cells. Thin basement membrane was detected using electron microscopy in these networks but endothelial cells were not detected. These channels were also perfused with blood cells. Consistently with their observations in vivo, very aggressive uveal or cutaneous melanoma cells when cultured in 3D Matrigel or collagen matrix also formed architectural loops and network patterns that were lumenized and perfused by fluorescent dyes (229).

Among tumors, which are capable of VM, cancer cells exhibit a high degree of plasticity indicative of a multipotent phenotype similar in many respects to embryonic stem cells (230-232). Molecular profiling of these cells displays highly upregulation of genes associated with embryonic progenitors (CD133, Nodal), endothelial cells (Notch, VE-cadherin), matrix remodeling (MMP2, MMP14), and hypoxia (VEGF, HIF1a, HREs), and down regulation of genes associated with lineage-restriction of differentiation. VEGFR1, but not VEGFR2, mediates VEGF-A induced VM in melanoma cells and it has been proposed that VM is mediated through synergistic transduction of VEGFA/VEGFR1/PI3K/PKC $\alpha$  and integrin signaling pathways (233). Additionally, blocking of Nodal signaling has been shown to reduce VM activity of cancer cells (218, 234, 235).

### **1.2.5 Vascular invasion in pancreatic cancer and carcino-endothelialization**

Although pancreatic cancer is an aggressive and highly metastatic cancer, evidence of vascular mimicry has not been described. However, vascular invasion, a process where cancer cells break through the blood and lymphatic vessels, is evident in pancreatic cancer. At the time of diagnosis, only approximately 16% of patients are present at stage I where the tumor is confined within the pancreas while 85%-90% have unresectable tumors (236). Vascular invasion is an

important parameter to assess the resectability of pancreatic tumors. Because of the close proximity of the pancreas to different large caliber vessels such as the hepatic aorta and veins, mesentery aorta and veins, about 21%-64% of patients exhibits vascular invasion according to one report (236) at the time of diagnosis.

Interestingly, when patient samples from PDAC were examined, microscopy vascular invasion was observed in 65.1% of the cases (237). Among the vascular invasion cases, histological samples also revealed isolated solitary ductal units (ISDs) within the adipose tissue adjacent to the pancreatic tumor. These ISDs were detected mostly in human pancreatic cancer patients up to 69.1% in cases with vascular invasion but not in chronic pancreatitis (238). Astonishingly, these ISDs exhibited features of vascular structures with evidence of elastin smooth muscle layer. However, the endothelial cells with flat morphology were not detected. Instead, the ducts are lined with cuboidal epithelial cells that also exhibit intraneoplasia (Figure 1.2). This phenomenon of endothelial cell replacement is termed carcino-endothelialization (238).

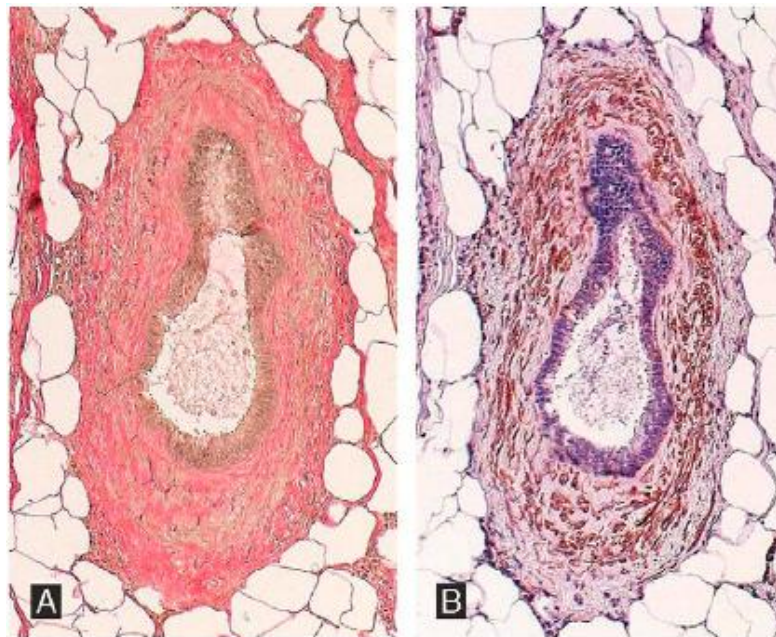


**Figure 1.2.** Carcino-endothelialization in the fibroadipose tissue covering the pancreas in patients with pancreatic ductal adenocarcinoma. Image was adapted from Bandyopadhyay S. *et al.* (*Am J Surg Pathol* 2009; 33:425-429). (A) The Elastic-Van Gieson stain to demonstrate the elastin layer

around carcino-endothelialization ducts. (B) Smooth muscle actin stain to demonstrate the presence of myofibroblastic cells, typically present in vascular wall.

## CHAPTER 2: ANGIOCHIP, A BIOMIMETIC MODEL TO RECONSTITUTE ANGIOGENIC SPROUTING MORPHOGENESIS IN VITRO

### 2.1 Abstract

Angiogenesis is a complex morphogenetic process whereby endothelial cells from existing vessels invade as multicellular sprouts to form new vessels. Here, we have engineered a novel organotypic model of angiogenic sprouting and neovessel formation that originates from pre-formed artificial vessels fully encapsulated within a 3D extracellular matrix. Using this model, we screened the effects of angiogenic factors and identified two distinct cocktails that promoted robust multicellular endothelial sprouting. The angiogenic sprouts in our system exhibited hallmark structural features of *in vivo* angiogenesis, including directed invasion of leading cells that developed filopodia-like protrusions characteristic of tip cells, following stalk cells exhibiting apical-basal polarity, and lumens and branches connecting back to the parent vessels. Ultimately, sprouts bridged between pre-formed channels and formed perfusable neovessels. Using this model, we investigated the effects of angiogenic inhibitors on sprouting morphogenesis. Interestingly, the ability of VEGFR2 inhibition to antagonize filopodia formation in tip cells was context dependent, suggesting a mechanism by which vessels might be able to toggle between VEGF-dependent and VEGF-independent modes of angiogenesis. Like VEGF, S1P also appeared to exert its pro-angiogenic effects by stimulating directional filopodial extension, whereas MMP inhibitors prevented sprout extension but had no impact on filopodial formation. Together, these results demonstrate an *in vitro* 3D biomimetic model that reconstitutes the morphogenetic steps of angiogenic sprouting, and highlight the potential utility of the model to elucidate the molecular mechanisms that coordinate the complex series of events involved in neovascularization.

## 2.2 Introduction

Angiogenesis, the process by which new capillary vessels sprout from existing vasculature, plays a critical role in embryonic development and wound healing, while its dysregulation can contribute to cancer progression as well as numerous inflammatory and ischemic diseases (54, 239) . Consequently, therapeutic strategies to suppress, enhance, or normalize angiogenesis are widely sought to treat a broad spectrum of diseases (54, 239) . The most mature amongst these approaches targets the activity of angiogenic growth factors, such as vascular endothelial growth factor (VEGF), to modulate relevant signaling pathways and control the angiogenesis process. Indeed, inhibitors of such pathways have emerged as a mainstay therapy for some cancers and diabetic retinopathy (117, 240, 241) . However, it is still unclear how the endothelial cells (ECs) lining blood vessels form new vessels, or how angiogenic factors regulate such a dynamic, multi-cellular process.

Examining the physical process of angiogenesis requires experimental systems in which the formation of new capillary vessels can be easily observed and manipulated. Commonly used *in vivo* models such as the mouse dorsal window chamber, chick chorioallantoic membrane, and mouse corneal micropocket assays provide important validation platforms (242, 243) , but are low-throughput and less suitable for identifying new cell biological mechanisms. In contrast, traditional cell culture models of angiogenesis bear little anatomical resemblance to the *in vivo* process. For instance, the tube formation assay involves the reorganization of ECs seeded onto the surface of Matrigel into multicellular cords that partially resemble vascular networks but lack important features observed in native angiogenesis, such as directional invasion of cells into a 3D extracellular matrix (ECM), proper polarization of the luminal and abluminal sides of ECs, lumen formation, and support of fluid flow (242, 244) . Assays involving sprouting of ECs from microcarrier beads or spheroids capture aspects of multicellular invasion, but the initial geometry of these systems requires cells to invade toward their apical domain, counter to the basally-directed invasion

in physiologic angiogenesis, and they also lack the continuous fluid flow known to fundamentally impact endothelial cell behavior (245).

In contrast, organotypic models that have faithfully captured biological structure have proven to be transformative for a field, as exemplified by studies of engineered skin or mammary epithelial morphogenesis (246-248) . Here, we demonstrate the use of endothelium-lined channels as a platform to recapitulate angiogenic sprouting *in vitro*. The system allowed us to screen combinations of angiogenic factors and identify cocktails that induced highly organized, directed multicellular sprouting into a surrounding ECM that appears to mimic key morphological aspects of *in vivo* angiogenesis not yet described by other *in vitro* models. Furthermore, we demonstrate the utility of this model by illustrating how pro- and anti-angiogenic agents impact the complex multicellular process of angiogenesis.

### 2.3 Materials and Methods

**Device Fabrication.** The device supporting the parallel channels consists of two layers of poly(dimethylsiloxane) (PDMS; Sylgard 184; Dow-Corning) bonded to each other and sealed against a glass substrate. The top PDMS layer was cast from a PDMS positive mold, previously replicated from a silicon wafer template. The bottom PDMS layer was cast off a silicon wafer template containing positive features illustrated in supplementary information (Figure 2.S3). Dimensions of important features in both layers are shown in Figure 2.1A. To assemble the device, the bottom layer was first reversibly sealed to a glass coverslip. The top and bottom layers were then separately treated with oxygen plasma, bonded together and cured at 110°C overnight. Upon removal from the oven, devices were treated with oxygen plasma to render the exposed PDMS surfaces hydrophilic. Hydrophilized devices were immediately treated with 0.1 mg/ml poly-L-lysine (Sigma) for 1 hour, followed by 1% glutaraldehyde (Sigma) for 1.5 hours. Devices were washed several times with H<sub>2</sub>O to remove residual glutaraldehyde, sterilized with UV light for 15 min, and soaked in 70% ethanol for 1 hour. To mold cylindrical channels, two acupuncture needles (Hwato),

400  $\mu\text{m}$  in diameter, were inserted into parallel grooves at the top of the bottom layer (Figure 2.S3). The needles were passed through the middle rectangular chamber of the device, resting approximately 200 $\mu\text{m}$  above the glass coverslip surface. Rat tail collagen I, at 2.5 mg/ml, was pipetted into the middle chamber and allowed to polymerize at 37°C for 30 minutes. Excess collagen was subsequently aspirated from the fluid reservoirs feeding from the middle chamber. Devices were then covered with EGM-2 (Lonza) for at least 4 hours before the needles were extracted as previously described. Devices were then covered in EGM-2 for at least two days prior to seeding with cells.

**Cell Culture and Seeding in Devices.** Human umbilical vein endothelial cells (HUVECs) (Lonza) were cultured in EGM-2. HUVECs, from passage seven to nine, were used in all experiments. HUVECs were concentrated at  $10^7$  cells/mL and seeded into one of the two channels. The device was inverted to allow HUVECs to adhere to the top surface of the channel for 10 minutes, and then flipped upright to allow cells to adhere to the bottom surface of the channel for another 10 minutes. Cells that adhered in the fluid reservoirs were scraped off with a pipette tip, and unattached cells in the channel were thoroughly flushed out with phosphate-buffered saline (PBS). EGM-2 was immediately added thereafter and the devices were placed on a platform rocker (BenchRocker, BR2000), oscillating at 0.1Hz and with a maximum tilt of 9.5° in order to generate gravity-driven flow across the channels. Cells were cultured in channels for 1-2 days before the experiment was initiated.

**Immunofluorescence Staining.** At designated time points, cells in the devices were fixed in situ with 3.7% formaldehyde for 45 minutes. For CD31 immunohistochemistry staining, cells were permeabilized with 0.1% Triton-X for 30 minutes, blocked in 3% BSA overnight at 4°C, washed 3 times with PBS and incubated with mouse monoclonal antibody against human CD31 (1:200, Dako). For Laminin and Podocalyxin immunohistochemistry staining, the cells were blocked with 3% BSA overnight at 4°C, washed 3 times with PBS and incubated with either rabbit polyclonal antibody against Laminin (1:100, Chemicon) or goat polyclonal anti-human podocalyxin (1:100,

R&D) overnight at 4°C. Before secondary antibody incubation, the devices were washed overnight with PBS at 4°C. All secondary antibodies (Invitrogen) were used at 1:500 dilution. In addition, cell nuclei were stained with DAPI (1:500, Sigma) and F-actin was stained with Alexa Fluor 488-conjugated Phalloidin (1:100, Sigma). Before imaging, all devices were completely submerged in PBS for 2-3 days to remove background staining.

**Image Acquisition and Processing.** Brightfield images of sprouts were acquired with a Nikon TE200 epifluorescence microscope (Nikon Instruments, Inc.) using 10x. Confocal immunofluorescence images were acquired with either 10x air objective or LD C-Apochromat 40x, 1.1 numerical aperture (N.A.) water immersion objective attached to either an Axiovert 200M inverted microscope (Zeiss) equipped with an CSU10 spinning disk confocal scan head (Yokogawa Electric Corporation), and an Evolve EMCCD camera (Photometrics) or an Olympus IX 81 microscope (Olympus America, Inc.) equipped with an CSU-X1 spinning disk confocal scan head (Yokogawa Electric Corporation), and an Andor iXon3 897 EMCCD camera (Andor Technology). ImageJ was used to merge channels, perform Z-projection for all confocal stacks, and generate longitudinal and transverse cross-sections. Custom MATLAB scripts and ImageJ were used to stitch images together.

**Screening of Angiogenic Factors.** In screening experiments, the endothelialized 'parent' vessel was perfused with EGM-2 while the adjacent source channel was perfused with EGM-2 enriched with angiogenic factors. Angiogenic factors include Vascular Endothelial Growth Factor (VEGF), Monocyte Chemotactic Protein-1 (MCP-1), Hepatocyte Growth Factor (HGF), and basic Fibroblast Growth Factor (bFGF), all purchased from R&D Systems. Sphingosine-1-Phosphate (S1P) and Phorbol Myristate Acetate (PMA) were purchased from Cayman Chemical and Sigma, respectively. VEGF, MCP-1, bFGF, HGF, and PMA were all used at 75ng/mL while S1P was used at 500nM. EGM-2 and enriched EGM-2 were refreshed daily for up to six days. Brightfield images were acquired daily for quantification.

**Bead Perfusion of Microvessels.** After neovessels bridged the two preformed channels in the device, a solution of CellTracker CM-Dil (Invitrogen) was delivered into the parent vessel to



stain live HUVECs and neovessels in situ. Fluorescent beads (Polysciences) of 3  $\mu\text{m}$  diameter were suspended in PBS and perfused into the parent vessel at a flow rate of 5  $\mu\text{L}/\text{min}$ . Images of flowing beads were acquired at 40 frames/sec using an Eclipse TE2000 inverted epifluorescence microscope equipped with a live cell incubator and an Evolve EMCCD camera. Frames of bead time-lapse movie were stacked and overlaid with image of Dil-stained neovessels using custom Matlab code. Bead-video samples were subsequently fixed and imaged with a 10x air objective attached to a Leica LSM 710 confocal microscope system.

**Inhibition of Angiogenic Sprouting.** The effects of inhibitors targeting VEGFR2 (Semaxanib, Cayman Chemical), S1P receptors (Fingolimod, Selleck Chemicals) and MMPs (Marimastat, Tocris Bioscience) were evaluated in a similar setup to the angiogenic factor screening experiments. HUVECs were cultured in the 'parent' vessel in either full EGM-2 (for Marimastat experiments) or incomplete EGM-2 lacking VEGF and bFGF (for Semaxanib and Fingolimod experiments). In all cases, the angiogenic source channel contained the same media as the 'parent' vessel supplemented with either the MVPS or HFMVS cocktails described in *Results*. In separate devices, Semaxanib or Fingolimod were administered into both channels at 14  $\mu\text{M}$  and 140 nM to yield effective concentrations of 10  $\mu\text{M}$  and 100 nM, respectively, due to the additional volume of the gel. Marimastat was administered only into the source channel at 0.6  $\mu\text{M}$ . All inhibitors were added daily at starting on concurrent with or three days after the initial addition of angiogenic cocktails. Media in both channels were refreshed daily. Brightfield images were acquired daily for quantification.

**Quantification of Sprout Length and Sprout Density.** Custom MATLAB code was written to measure the individual distances from the leading protrusions of tip cells to the wall of the parent vessel. Tip cells were additionally quantified as either attached to stalk cells extending from the endothelialized channel or as isolated single cells (Figure 2S1). Sprouting metrics were quantified for the screening experiment ( $n = 2$  samples per condition), the VEGFR2 and S1P inhibitor experiment ( $n = 5$  samples per condition), and the MMPs inhibitor experiment ( $n = 3$  samples per condition).

**Filopodia Quantification and Analysis.** Projections from z-resolved confocal stacks, which were taken using 25x water immersion objective attached to Axiovert 200M inverted microscope (Zeiss) with spinning disk confocal scan head, were used to analyze filopodia length and number. A custom MATLAB code was used to determine the distance from the tips of filopodia to the center of cell nuclei and count the number of filopodia. The number and length of filopodia were averaged over the number of cells across 3 samples per condition.

**Statistical Analysis.** Sample populations were compared using unpaired, two-tailed Student's t-test.  $P < 0.05$  was the threshold for statistical significance. Data points on the graphs represent mean values and error bars depict SEM.

## 2.4 Results

### **A microengineered platform that supports angiogenic sprouting and neovessel formation *in vitro***

To study the process of angiogenic invasion and sprouting from an existing vessel, we designed a device in which an endothelium lining a cylindrical channel was fully surrounded by matrix and exposed to a gradient of angiogenic factors emanating from a parallel source channel (Figure 2.1A). The device was assembled by casting Type I collagen into a PDMS mold/gasket with two parallel needles held across the casting chamber. Upon collagen polymerization, the needles were extracted to create hollow cylindrical channels in the collagen matrix (Figure 2.1A). Endothelial cells (ECs) were then injected into one of the channels, allowing them to attach on the interior wall and form a confluent endothelium or "parent vessel" (Figure 2.1B). Flow was maintained through both channels for the duration of the experiments and media containing angiogenic factors was subsequently added to the second channel to establish a gradient across the collagen matrix to the endothelium (Figure 2.1B). Thus, the device design provided a means to promote and visualize endothelial sprouting that might emulate early angiogenic processes.

Using this device, we first examined how various pro-angiogenic factors might impact directed invasion and sprouting from the parent vessel. Six common factors associated with angiogenesis in the literature were selected: basic fibroblast growth factor (bFGF) (249) , hepatocyte growth factor (HGF) (250) , vascular endothelial growth factor (VEGF) (58, 251), monocyte chemoattractant protein-1 (MCP-1) (85), sphingosine-1-phosphate (S1P) (252), and Phorbol 12-myristate 13-acetate (PMA) (253). After these factors were added individually to the non-endothelialized source channel, phase-contrast and confocal microscopy were used to assess the organization and development of EC invasion over four days. We found that VEGF, MCP-1, HGF or bFGF alone did not induce significant invasion into the matrix, while S1P and PMA resulted in substantial directed invasion (Figure 2.S1). This invasion was oriented directly toward the source channel, despite the fact that cell migration from the endothelium was not artificially constrained in any direction by our system design (Figure 2.1C).

Interestingly, S1P and PMA stimulated markedly different modes of cell migration. S1P drove chemotactic migration primarily of single cells from the endothelialized channel, whereas PMA triggered collective cell migration that manifested itself in the form of sparse, long, multicellular sprouts into the matrix (Figure 2.1Ci,ii). Progressively more complex combinations of the six factors yielded more substantial multicellular sprout-like structures, especially in the case of two distinct combinations that drove robust sprouting – HGF, bFGF, MCP-1, VEGF, and S1P (HFMVS) and MCP-1, VEGF, PMA, and S1P (MVPS) (Figure 2.S1). HFMVS-guided invasion exhibited numerous sprout-like structures that extended hundreds of micrometers from the endothelialized parent vessel as well as large numbers of solitary cells migrating into the matrix (Figure 2.1C iii,iv). The MVPS cocktail induced an even greater multicellular sprouting response with less single cell migration (Figure 2.1Cv). In both cases, the sprouts continued to invade toward the source channel as long as the gradient was maintained.

Remarkably, when the tips of these sprouts reached the source channel (typically after one week), they breached into the source channel, forming what appeared to be new microvessels

connecting the two parallel channels (Figure 2.1D). To test whether these “neovessels” possessed functional, perfusable lumens, 3µm fluorescent beads were added to the media flowing into the endothelialized parent channel. Beads traveled through the neovessels to the source channel with no leakage into the interstitial space, indicating fully developed lumens lined by a continuous endothelium. Overlaying frames of the time-lapse images demonstrated the path of the beads through these occasionally branching neovessels (Figure 2.1D).

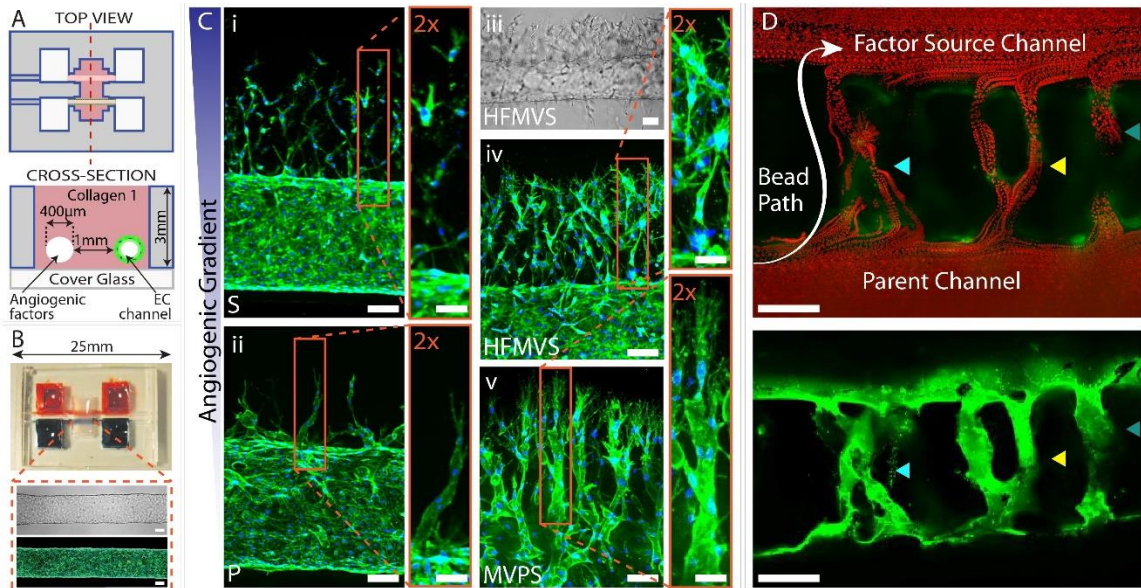


**Figure 2.1.** 3D formation of endothelial sprouts and neovessels in a microfluidic device. (A) Device schematic. Parallel cylindrical channels are encased in 3D collagen matrix within a microfabricated PDMS gasket and connected to fluid reservoirs. One channel is coated with ECs and perfused with medium while the other channel is perfused with medium enriched with angiogenic factors. (B) Photograph of the device. Zoom shows phase (top) and fluorescent (bottom) micrographs of an endothelialized channel. F-actin and nuclei are labeled with phalloidin (green) and DAPI (blue), respectively. (C) Representative confocal immunofluorescence images of sprouting and migrating ECs in response to gradients of different pro-angiogenic factors: S (i), P (ii), HFMVS cocktail (iv), and MVPS cocktail (v). Panel iii shows a phase image of directed sprouting induced by HFMVS. F-actin and nuclei are labeled with phalloidin (green) and DAPI (blue), respectively. (D) Neovessels in the device are shown in (i) a merged image of a time-lapse movie tracking the position of 3µm red fluorescent beads perfused through the large channels and neovessels and (ii) a z-projection confocal image of the same vessels. Beads were added to the left end of the parent vessel and flowed through neovessels to the factor source channel. In both images ECs (green) are labeled with Dil. Scale bars of 2x zoom-in insets in (C) are 50 µm. All other scale bars are 100 µm. Abbreviations: F=bFGF, H=HGF, M=MCP-1, P=PMA, S=S1P, V=VEGF.

### **Sprouts exhibit morphologic features of *in vivo* angiogenesis**

Because this experimental model allows us to monitor the detailed structural events of sprouting, we next proceeded to examine the changes in cellular organization during early stages of invasion. For this purpose, we focused on the MVPS cocktail, which promoted the greatest sprouting response with minimal single cell migration. Prior to stimulation, cells in the endothelialized channel exhibited the expected apical-basal polarity as demonstrated by the localization of CD34 apical marker podocalyxin to the luminal face (254). On the basolateral side of the endothelium we observed laminin deposition. Upon stimulation, occasional single ECs began invading into the matrix and extending filopodia-like protrusions in the direction of the angiogenic gradient (Figure 2.2A). During initial invasion, we observed interruptions in laminin immunofluorescence, consistent with focal degradation of the basement membrane (Figure 2.2B). These leading tip cells were replete with filopodia-like protrusions, morphologically recapitulating *in vivo* sprout tips (50). As these tip cells migrated deeper into the matrix, neighboring cells followed while maintaining cell-cell contacts along the length of the sprout, as shown by PECAM-1 staining (Figure 2.2C). Thus, the sprouting process from the parent endothelium into the matrix involved collective cell migration that supported a contiguous structure between the sprout and parent vessel. Even at this early stage of 2-3 cells per sprout, evidence of lumen formation was detected in 3D reconstructions of confocal images (Figure 2.2D). Moreover, apical-basal polarity appeared intact in the sprouts as evidenced by apically targeted podocalyxin staining (Figure 2.2Di,iii).

As the sprouts continued to invade and extend into the matrix, they became longer, contained progressively more cells, and began to branch (Figure 2.2E-G). Stereotypical sprouting morphology was evident in these mature sprouts, with cells at the sprout tip developing numerous thin filopodia-like protrusions, in contrast to cells in the stalk containing few filopodia protrusions (Figure 2.2E-G). Lumens developed in both early and late sprouts that often extended from the parent vessel up to, but never within, the tip cell (Figure 2.2D,E). Partial lumens occasionally were evident behind the tip cell that were not connected to the parent vessel, suggestive of spontaneous,

focal cord-hollowing or lumenization (Figure 2.2Fiv). Staining confirmed that the sprout tip cells lacked specific localization of podocalyxin, while stalk cells demonstrated localization of podocalyxin to the luminal space (Figure 2.2E). We observed laminin deposition in the mature sprouts (Figure 2.2F) and found that PECAM-1-positive cell-cell junctions were generally intact throughout the sprouts (Figure 2.2G). In addition to primary sprouts, maturation of secondary branches also occurred in our system. Different stages of secondary branching were evidenced by stalk cells occasionally marked by direct filopodia-like protrusions suggesting early branch initiation (Blue arrow, Figure 2.2F), whole cells extending out from the stalk of the sprout (Blue arrow, Figure 2.2E), and finally as full multicellular branches with their own new tip cells extending toward the angiogenic gradient (Figure 2.2G).

Upon formation of neovessels spanning the two channels, non-perfused filopodial protrusions notably disappeared (Figure 2.2Hi). The neovessels were lumenized end-to-end (Figure 2.2Hii, iii), and cells were aligned with flow as in the parent vessel, demonstrated by actin stress fiber alignment (Figure 2.2Hiv). Further examination revealed the deposition of laminin around the neovessels (Figure 2.2I), localization of podocalyxin to the luminal domains (Figure 2.2J), and PECAM-1 staining reflective of intact cell-cell junctions (Figure 2.2K).

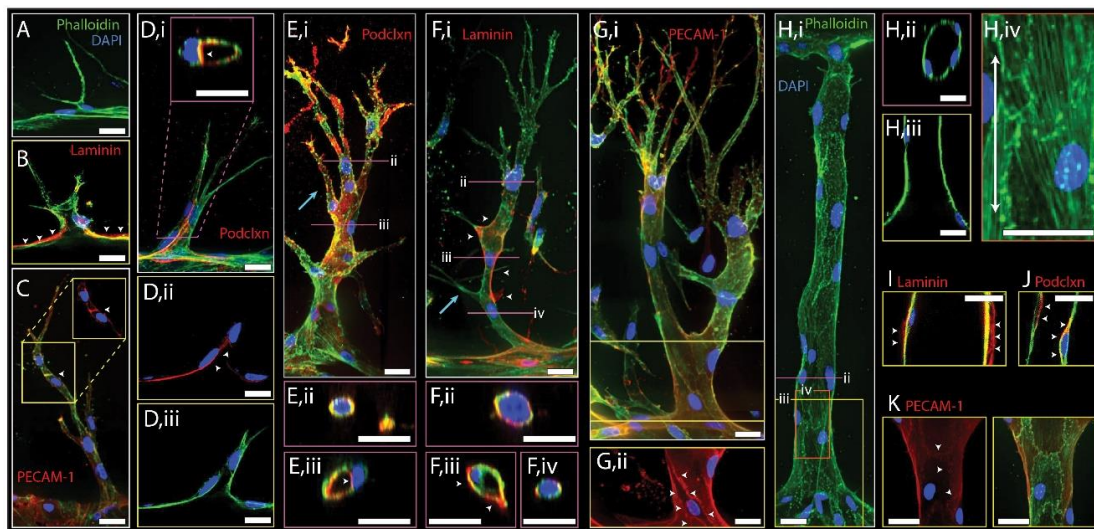


**Figure 2.2** Characterization of early and late sprouts and neovessels. Representative confocal immunofluorescence images of early (A-D) and late (E-G) sprouts and neovessels (H-K). For all

images F-actin and nuclei are labeled with phalloidin (green) and DAPI (blue), respectively. Staining for laminin (B, F, I), PECAM-1 (C, G, K), and podocalyxin (podclxn; D, E, and J) are shown in red. (A) Micrograph of an EC extending processes into the matrix towards the source channel. (B) Laminin immunofluorescence (red) is marked by white arrowheads on the abluminal side of the parent vessel. Fluorescence is interrupted by early sprout invasion. (C) Image of an early multicellular sprout stained for F-actin (green) and PECAM-1 (red). White arrowheads point to PECAM-1 staining at cell-cell junctions. Inset: z-projection of back half of sprout showing only red channel (PECAM-1). (D) Early sprout stained for podocalyxin (red) shown in z-projection (i), and single slice (ii, iii). White arrowheads mark podocalyxin at luminal side of sprout shown by transverse (inset, i) and in-plane (ii) sections. (E) Mature sprout stained for podocalyxin (red) shown in z-projection (i) with blue arrow marking cell invading out from sprout stalk, and in cross-sections of tip cell (ii) showing no lumen or spatial podocalyxin localization in the cell, and stalk (iii) with white arrowheads marking podocalyxin staining at apical side of lumenized stalk cells. (F) Mature sprout stained for laminin (red) shown in z-projection (i) with blue arrow marking stalk cell filopodia, and in cross-sections of sprout tip cell (ii) that contains no lumen and shows presence of laminin staining, in lumen-containing stalk cell (iii) with white arrowheads marking laminin staining at basal side, and stalk cell that contains no lumen (iv) showing laminin immunofluorescence. (G) Mature sprout stained for PECAM-1 (red) shown in full z-projection (i) and z-projection of back half of sprout (ii). White arrowheads in (ii) mark PECAM-1 staining at cell junctions. (H) Neovessel shown in z-projection (i), cross-section (ii), and in-plane slice (iii). F-actin (iv) shows actin fiber alignment with direction of flow indicated by double-arrow line. (I) Neovessel exhibits laminin staining (red) at its basal side (white arrowheads). (J) Neovessel exhibits podocalyxin staining (red) at its luminal side (white arrowheads). (K) Neovessels express PECAM-1 staining (red) at cell junctions (white arrowheads). Yellow, pink, orange boxes indicate longitudinal slice or partial stack, transverse cross-section, and zoom-in, respectively. Scale bars are 25  $\mu\text{m}$ .

### **VEGF drives directed filopodia formation and sprout extension in a context dependent manner**

While the structural similarities between angiogenic sprouts observed in our system and those found *in vivo* were broadly encouraging, it was also important to explore whether our angiogenic sprouts responded physiologically to agents known to perturb the angiogenic process. To address this question, we investigated whether anti-angiogenic agents could impact sprouting in our system. First, a VEGF receptor 2 (VEGFR2) inhibitor Semaxanib (255, 256) was added with the HFMVS angiogenic cocktail. If added from the outset, the inhibitor abrogated sprout initiation (Figure 2.3A). Because angiogenic inhibitors are also thought to lead to regression of pre-existing sprouts (257), we also tested the effects of adding Semaxanib to the source channel after 3 days of uninhibited sprouting. We found that further progression of sprouts was arrested, but obvious regression of the sprouts did not occur (Figure 2.3A). Closer inspection of VEGFR2-inhibited sprout architectures revealed a near complete loss of the many filopodia-like protrusions normally present in the tip cells, with a decrease in the number and length of protrusions (Figure 2.3B,C).



Surprisingly, we observed that sprouting induced by the MVPS cocktail, while slowed, appeared to proceed despite VEGFR2 inhibition (Figure 2.3D). Confocal images revealed that the filopodia-like protrusions in these sprouts were largely unaffected by Semaxanib, whether added at Day 0 or Day 3 (Figure 2.3F). Quantitative analysis showed that the number of filopodial extensions was unchanged and their length was unaffected (Figure 2.3E). Importantly, these results demonstrate that the angiogenic process modeled by our system can respond to physiologically relevant anti-angiogenic therapeutics. Moreover, this system offers insights into the mechanism by which Semaxanib may antagonize angiogenesis, by arresting the formation of cellular protrusions that are critical to the initiation and growth of angiogenic sprouts. Interestingly, in contexts containing factors that can promote protrusive activity in a VEGF-independent manner, angiogenic sprouts become refractory to Semaxanib.

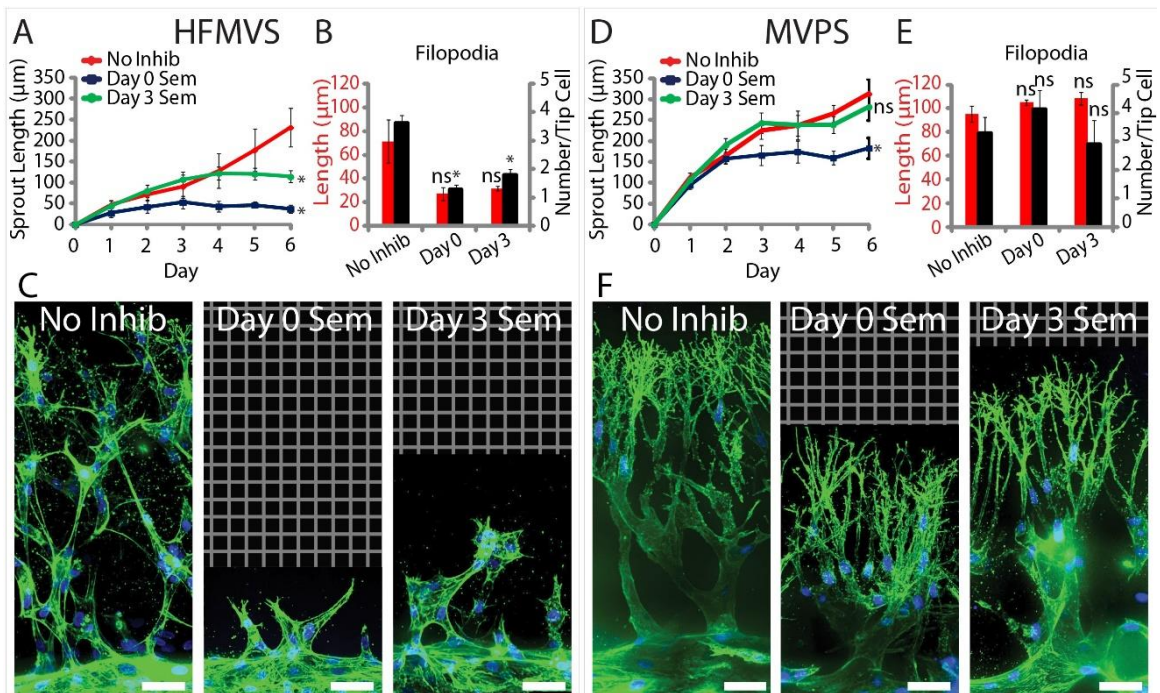


**Figure 2.3.** Effects of VEGFR2 inhibition on angiogenic sprouting. (A, D) Plot of sprout length driven by HFMVS (A) or MVPS (D) in response to Semaxanib treatment over time. Pro-angiogenic cocktail was initiated at Day 0 and Semaxanib treatment was initiated at either Day 0 (Day 0 Sem), Day 3 (Day 3 Sem), or never (No Inhib). (B,E) Quantification of filopodia length and number in sprouting for inhibitor treatment versus no-inhibitor control. (C,F) Representative confocal immunofluorescence images of indicated conditions at Day 6. F-actin and nuclei are labeled with phalloidin (green) and DAPI (blue), respectively. Grid indicates no detectable signal so no data was acquired. Scale bars are 50 µm. Error bars are SEM. \* represents significant difference from control



( $p < 0.05$ ). ns represents no significant difference from control. N = 5 samples for sprout length quantification, N = 3 samples for filopodia quantification. All filopodia quantifications performed on data from Day 6 of experiment.

### **S1P and MMP inhibition demonstrate independent steps for angiogenic invasion**

To further investigate the morphogenetic responses to anti-angiogenic factors, we examined the effects of perturbing S1P signaling, which acts as a strong chemoattractant through a G-protein coupled receptor (S1PR) and is known to regulate angiogenesis (258, 259). Exposing cells to the S1PR inhibitor Fingolimod (260) resulted in abrogation of sprout initiation when introduced at Day 0, and inhibited further sprout extension when given at Day 3 (Figure 2.4). Interestingly, these effects were independent of which angiogenic cocktail (HFMVS or MVPS) was employed (Figure 2.4A,D). Quantification of the remaining sprout structures revealed nearly complete loss of filopodia-like protrusions, with cells appearing less elongated and organized (Figure 2.4B,C,E,F). These data suggest that S1P signaling also regulates angiogenic sprouting, and that multiple pathways in addition to VEGF signaling may contribute specifically to the directional protrusions necessary for sprout extension. However, though necessary, we would anticipate that filopodial protrusions are only one of several key cellular processes required for sprout extension. In support of this, we observed that the broad spectrum MMP-inhibitor, Marimastat (261, 262), also blocked sprout invasion and extension (Figure 2.S2), but had no effect on directed filopodial extension.

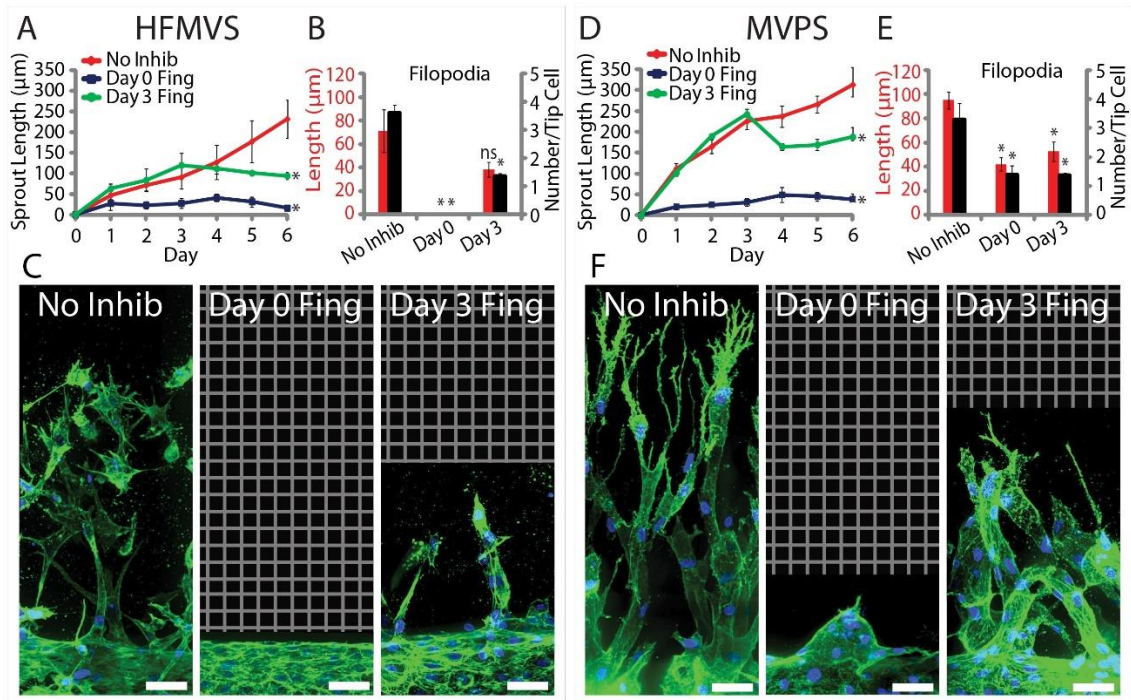


**Figure 2.4.** Effects of S1P receptor inhibition on angiogenic sprouting. (A, D) Plot of sprout length driven by HFMVS (A) or MVPS (D) in response to Fingolimod treatment over time. Pro-angiogenic cocktail was initiated at Day 0 and Fingolimod treatment was initiated at either Day 0 (Day 0 Fing), Day 3 (Day 3 Fing), or never (No Inhib). (B,E) Quantification of filopodia length and number in sprouting for inhibitor treatment versus no-inhibitor control. (C,F) Representative confocal immunofluorescence images of indicated conditions at Day 6. F-actin and nuclei are labeled with phalloidin (green) and DAPI (blue), respectively. Grid indicates no detectable signal so no data was acquired. Scale bars are 50 µm. Error bars are SEM. \* represents significant difference from control ( $p < 0.05$ ). ns represents no significant difference from control.  $N = 5$  samples for sprout length quantification,  $N = 3$  samples for filopodia quantification. All filopodia quantifications performed on data from Day 6 of experiment.

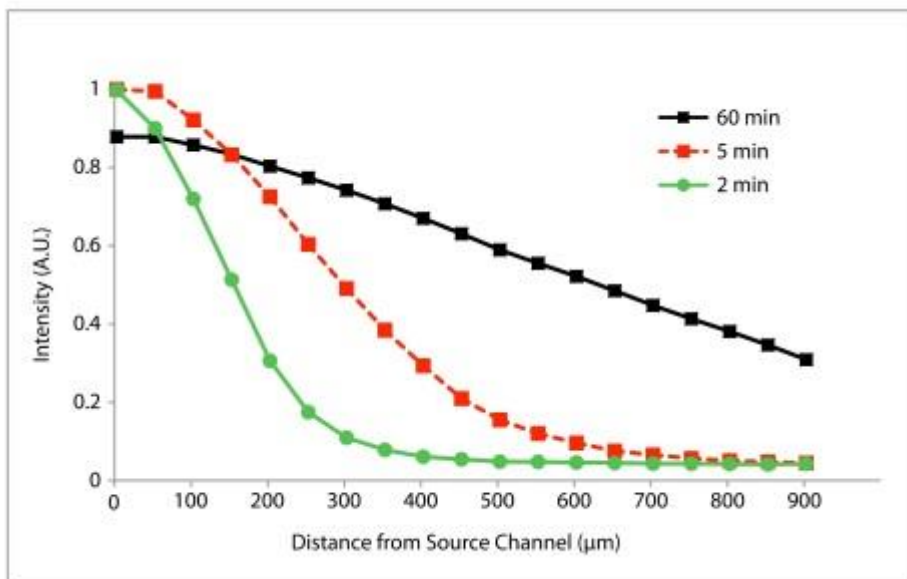


**Figure 2.S1.** Characterization of gradient between parent vessel and source channel. Relative intensity profile at 2, 5, and 60 min after addition of 20kDa fluorescently tagged dextran. A 1D solution to Fick's Law using data acquired at 2 min after introduction of the dextran provided an estimate for the diffusion coefficient of  $1.80 \times 10^{-6} \text{ cm}^2/\text{s}$

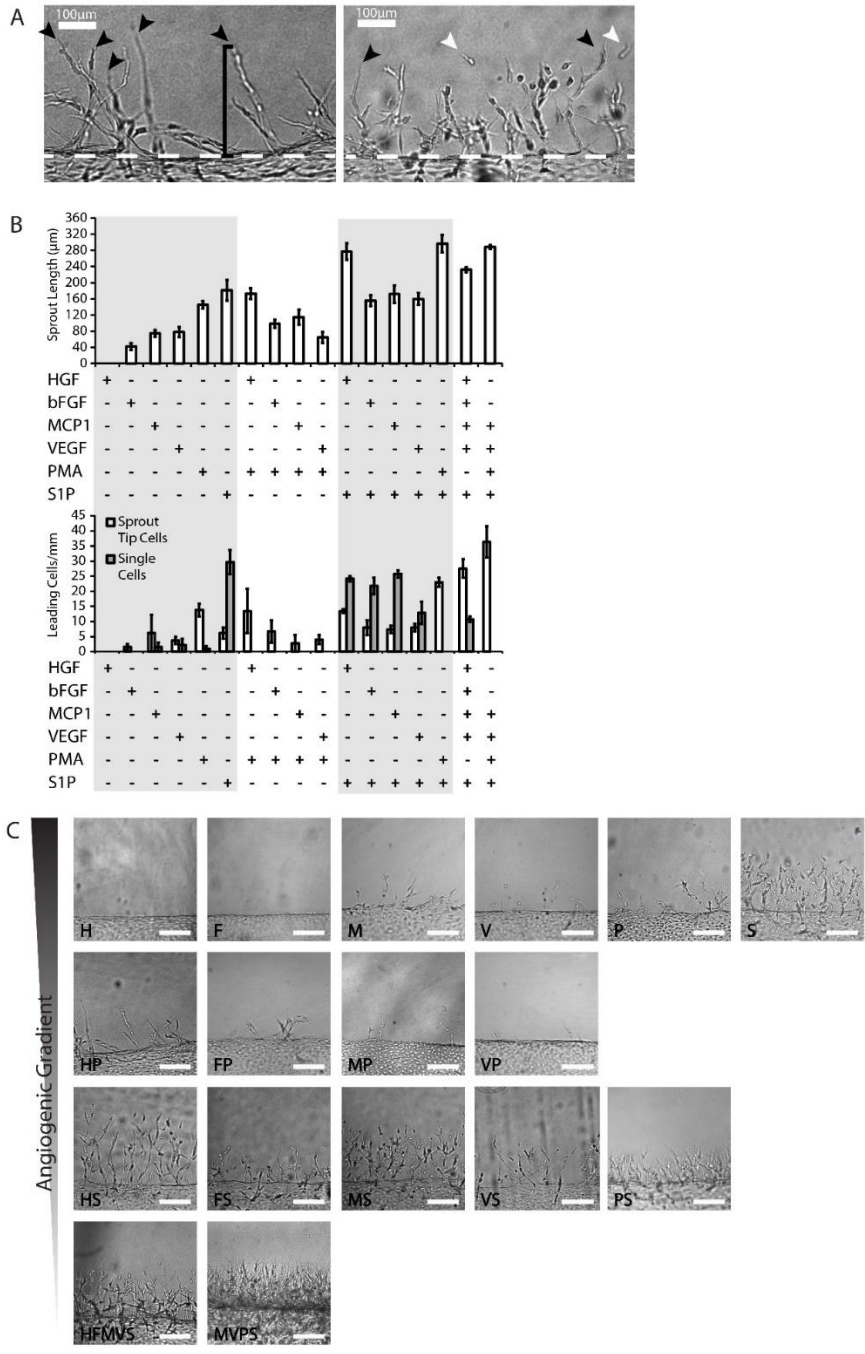


**Figure 2.S2.** Quantitative metrics for scoring number and length of sprouts and single cell migration. (A) Leading cells are categorized as sprout tip cells (black arrowheads) when in contact with stalk cells connected to the parent vessel (dashed white line), or as isolated, single cells (white arrowheads). Sprout length was measured as the distance between leading protrusions of sprout tip cells and the nearest point along the parent vessel. Scale bars are 100  $\mu\text{m}$ . (B) Plot of sprout length and the number of sprout tip cells and single cells after 4 days of exposure to indicated factor(s).  $N = 2$  samples per condition. (C) Representative phase images of each condition after 4

days of exposure to indicated factor(s). Scale bars are 200  $\mu\text{m}$ . Abbreviations: F=bFGF, H=HGF, M=MCP-1, P=PMA, S=S1P, V=VEGF.

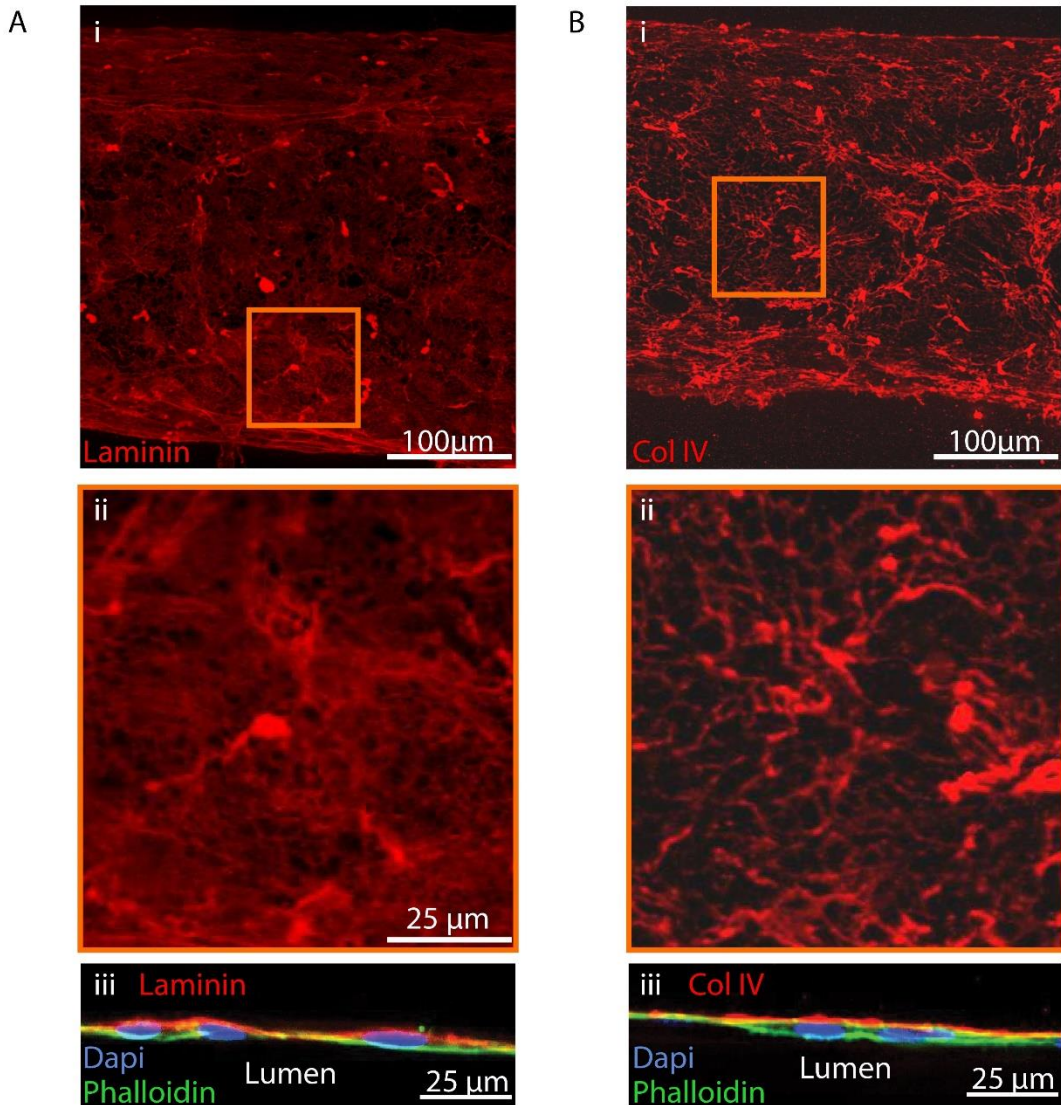


**Figure 2.S3.** Characterization of cell-deposited extracellular matrices by the endothelium. (A) Laminin immunofluorescence (red) is shown in a z-resolved confocal stack en face projection of a parent vessel (i), with zoomed-in view (ii). Radial slice (iii) indicating localization of laminin at the basal side. (B) Collagen IV immunofluorescence (red) is shown in a z-resolved confocal stack projection of a parent vessel (i), with zoomed-in view (ii). Radial slice (iii) indicating localization of collagen IV at the basal side. F-actin and nuclei are labeled with phalloidin (green) and DAPI (blue).

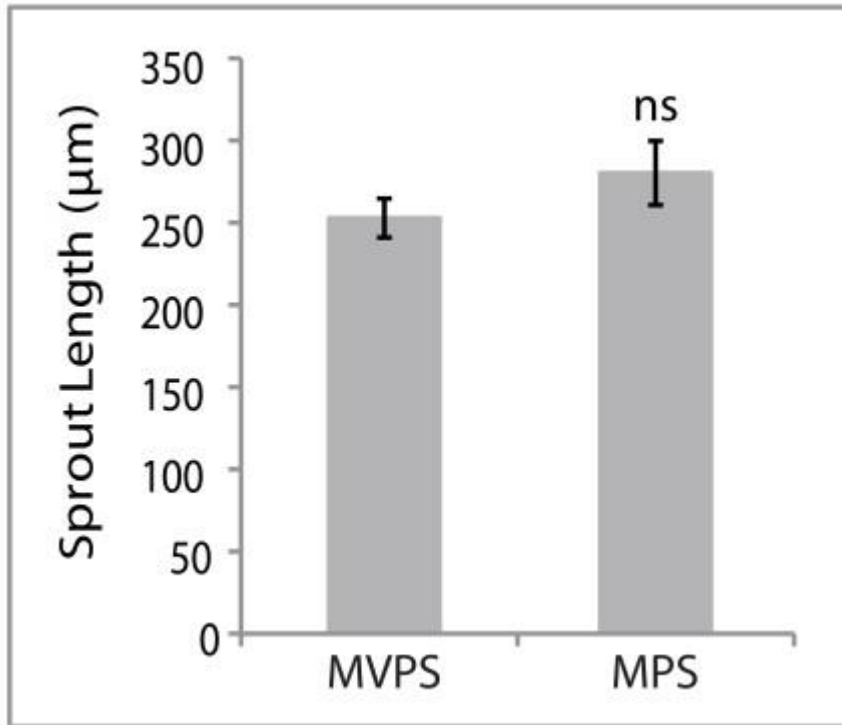


**Figure 2.S4.** Quantification of sprout length for the MVPS and MPS cocktails at day 4. MVPS and MPS cocktails were only added to the source channel. Error bars are SEM. Ns, no significant difference from MVPS control ( $P \geq 0.05$ ).

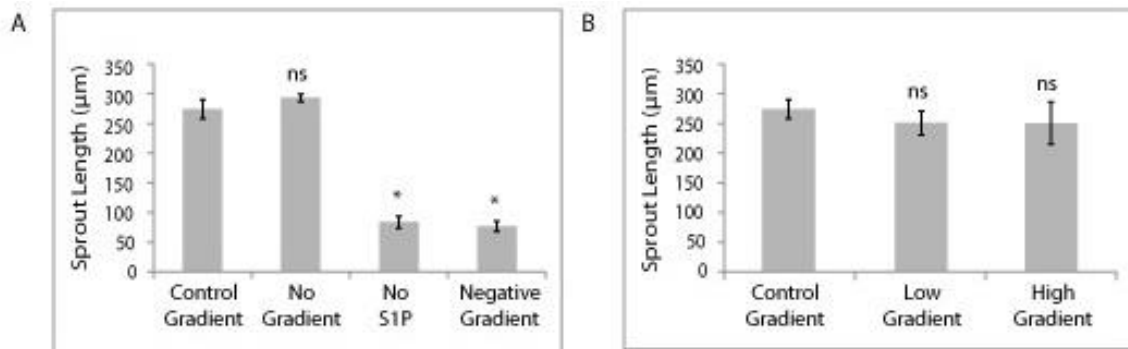


**Figure 2.S5.** Quantification of sprout length for different S1P gradients. (A) Plot of sprout length at day 4 for the MVPS cocktail in source channel (control gradient), MVPS in source channel plus S1P in parent vessel (no gradient), MVP in source channel plus S1P in parent channel (negative gradient), and MVP in source channel (no S1P). (B) Plot of sprout length at day 4 for the MVPS cocktail in source channel with different concentrations of S1P: 250nM (low gradient), 500nM (control gradient), and 1µM (high gradient). \* Significant difference from the MVPS (control gradient) ( $P \geq 0.05$ ); ns, no significant difference from MVPS (control gradient) control.



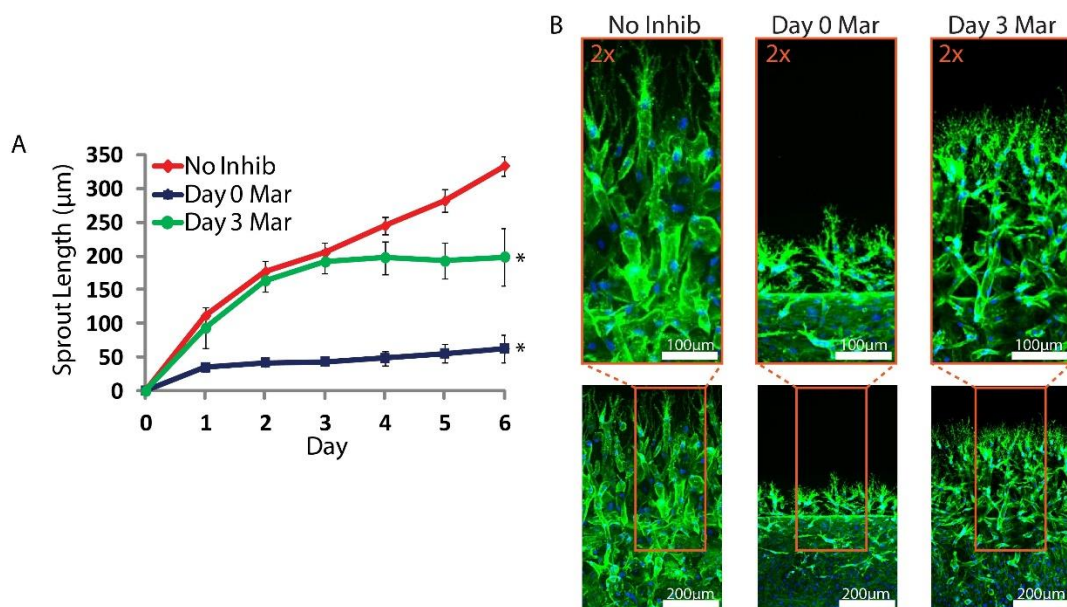


**Figure 2.S6.** Effects of MMP inhibition on angiogenic sprouting. (A) Plot of sprout length driven by MVPS in response to Marimastat treatment over time. Pro-angiogenic cocktail was initiated at Day 0 and Marimastat treatment was initiated at either Day 0 (Day 0 Mar), Day 3 (Day 3 Mar), or never (No Inhib). (B) Representative confocal immunofluorescence images of indicated conditions at Day 6. F-actin and nuclei are labeled with phalloidin (green) and DAPI (blue), respectively. Scale bars are 50 µm. Error bars are SEM. \* represents significant difference from control ( $p < 0.05$ ).  $N = 3$  samples for sprout length quantification.

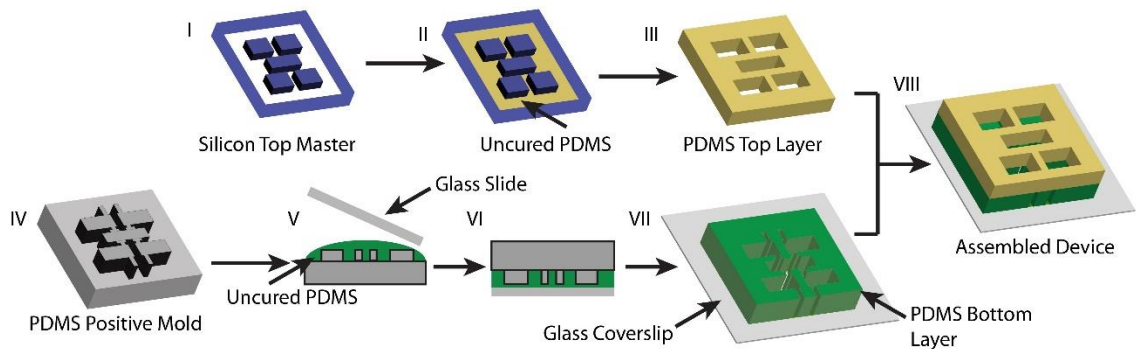


**Figure 2.S7.** Schematic of the device manufacturing process. A silicon template (blue and white) containing four rectangular features for the top layer of the device was made using UV lithography (I). Uncured PDMS (beige) was cast onto silicon template (II). After curing at 80 °C, PDMS top layer (beige) was cast off the template (III). A silicon template containing four linked rectangular features was used to make a bottom positive PDMS mold (grey) (IV). Uncured PDMS (green) was cast onto positive PDMS mold and a glass slide was applied to trap the PDMS between the mold and glass (V). System was inverted (VI). After curing at 110 °C, PDMS bottom layer (green) was cast off the PDMS mold and adhered to a glass coverslip (VII). Following oxygen plasma treatment, top and bottom PDMS layers were aligned and sealed and placed in a 110 °C oven overnight.

## 2.5 Discussion

Although central to angiogenesis, the morphogenetic process of endothelial invasion and sprout extension has been difficult to observe *in vivo* and models of sprouting *in vitro* have largely ignored the key initial conditions in which sprouts emanate from ECs lining a perfused vessel. Several tissue engineering approaches have been developed recently in which endothelial cells can be seeded into a channel within extracellular matrix to form a primitive vasculature (263-265). Here, we built on this concept with a device that allows angiogenic factors to trigger directed invasion and sprouting from such vessels, and used it to examine sprouting events. Other designs have been presented for studying sprouting that use channels with square rather than circular cross-sections in which endothelium lines a planar sidewall of matrix and expose cells to contact with silicone or glass on top and bottom walls (135, 266, 267). Although the close proximity of cells to the glass and silicone walls likely prevents cells from forming fully developed sprouts, the simplicity of such devices are an attractive alternative for more focused modeling of cellular invasion. In contrast, the system presented here allows cells to emanate outwards from the vessel wall in all directions without introducing such physical constraints, and thus provides a new avenue for studying multicellular, morphogenetic aspects of angiogenesis.

The ability to assess the organization of invading cells was a critical feature that enabled us to begin to characterize and isolate factors that support the many steps involved in angiogenic sprouting. In our system, VEGF alone had negligible effect on sprouting while S1P only triggered single cell migration. Instead, only in the presence of a more complex cocktail of multiple factors could we observe robust multicellular sprout-like invasion where a morphologically distinct leading tip cell was trailed by a multicellular stalk. Interestingly, our results suggest that different combinations of factors can be similarly potent. In line with these findings, one recent study reported that a combination of factors secreted by stromal fibroblasts was necessary to induce sprouting (268). Another study suggested that exposure to a combination of hematopoietic chemokines, VEGF, and FGF led to a marked enhancement in tubulogenesis and sprouting (269). The



recognition that multiple combinations of factors can drive angiogenesis, likely through different mechanisms, further underscores an important role for model systems that allow for the rapid characterization of factor combinations.

With the appropriate stimuli in place, sprout formation and extension in our system proceeded through a well-defined progression that mirrored major steps of *in vivo* angiogenesis, including directed tip cell invasion, multicellular stalk formation, lumen formation, and neovessel perfusion. These steps are consistent with seminal observations of *in vivo* angiogenesis showing the emergence of tip cells from an existing vessel, and stalk cells that establish apical/basal polarity and form a lumen that excludes the tip cell (50, 254, 270). VEGF has been shown to be important in triggering such tip cells to extend thin, actin-rich protrusions and in guiding stalk cells to form elongated multi-cellular sprouts (50, 117). Here, we showed that both VEGF and S1P signaling appear to drive these filopodia-like protrusions and sprouting, consistent with mechanistic studies suggesting that multiple angiogenic factors can activate Cdc42, a key GTPase for filopodia formation. Interestingly, the effect of VEGFR2 inhibition on sprouting depended on the composition of the angiogenic cocktail, and may explain why some anti-VEGF inhibitors block angiogenesis in some instances but not others.

Many distinct mechanisms have been described for *in vivo* lumen formation (271). In our system, we observed fully developed lumens formed by stalk cells lining a tunnel left behind the leading tip cell. In other instances, the lumen was present only just behind the tip cell, not yet extending contiguously back to the base of the stalk, suggesting spontaneous lumen formation by the stalk cells. These observations are consistent with mechanisms for lumenization observed *in vivo*. Finally, in addition to the simple coordination of tip and stalk cells to form linear vessels, our system also seems to support higher-order events such as branching, a key mechanism to the patterning of sprouts controlled by the dynamic interconversion of stalk cells and filopodia-containing tip cells (50, 272-275), as well as loss of filopodial activity and regression upon eventual perfusion of the neovessel, a critical component of microvascular pruning and remodeling (276).

The basis for this type of pruning could be explained by recent studies reporting that shear stress could suppress VEGF-induced invasion (266). Thus, the system introduced here faithfully recapitulates key features of in vivo angiogenesis and provides the ability to link specific stimuli to defined morphogenetic processes, further illustrating the power of such a model.

Loss-of-function in vivo models remain the mainstay for studying both physiologic and pathologic processes, including those involving angiogenesis (242, 277). However, organotypic models that are able to capture basic features of these processes in an in vitro setting undeniably offer additional levels of control and analysis that are critical to gaining mechanistic insights (248). The model system presented here highlights that the field of angiogenesis has matured sufficiently to enable reconstitution of the complex morphogenetic changes within endothelial cells as they invade to form multicellular sprouts and newly perfused vessels. Even so, it represents merely a first step toward establishing a new platform for investigating vascular remodeling. Indeed, the introduction of additional cell types, including stromal, parenchymal, and circulatory cells, could open the door to establishing a deeper understanding of how different microenvironmental, genetic, organ-specific, and pathologic factors could contribute to the different forms of angiogenesis. This study adds to recent developments (278, 279) that together highlight the importance of engineered experimental models as a new approach to studying biological processes.

## CHAPTER 3: THE ROLE OF CDC42 IN BRANCHING MORPHOGENESIS

### 3.1 Abstract

Angiogenesis is a highly dynamic process where endothelial cells extensively rearrange their cytoskeletal structures to migrate and coordinate between tip and stalk cells in a collective manner. The Rho family of GTPases has been shown to be important regulators of cytoskeletal rearrangement during cell migration. However, the roles of Rho GTPases in angiogenesis remains unclear. Particularly, conditional knockout of Cdc42 in endothelial cells resulted in lethality in mouse embryos and defects in formation of vasculature, which makes it challenging to understand the roles of Cdc42 in the morphogenetic processes of angiogenesis. In vitro manipulations of Cdc42 indicated the role of Cdc42 in lumen formation in 3D tubulogenesis. But its role in other morphogenetic processes of angiogenesis such as formation of branching is largely unknown. Here, using a previously developed 3D biomimetic model of angiogenesis, we examine the roles of Cdc42 in branching morphogenesis of angiogenic sprouting. We find that inhibition of Cdc42 though reduces migration speed has minimal effect on directional migration of 3D sprouting. Disturbance of Cdc42 activity leads to less branching in angiogenesis but has no effect on the length of branches. We also observe the role of Cdc42 to regulate collective migration. Interestingly, we also find that Cdc42 negatively regulates filopodia formation. Taken all together, our study reveals the many aspects of Cdc42 to mediate different morphogenetic processes of angiogenic sprouting.

### 3.2 Introduction

Angiogenesis is a process where new blood vessels form from existing vasculature. During endothelial cell sprouting, endothelial cells from the blood vessels detect and respond to angiogenic cues. The endothelial cells then probe the environment using their filopodia protrusions, and digest the vascular basement membrane to extend their bodies into the interstitial tissue to form tip cells

with following stalk cells (50). Tip cells and stalk cells form multicellular sprouts, which ultimately develop into mature perfusable blood vessels with hierarchical structures (168). To establish these ordered vessel networks, sprouts have to extensively form multiple branching structures and undergo changes such as pruning to remodel the structures. Such processes require dynamic changes in cytoskeleton of endothelial cells.

Rho GTPase proteins are known to regulate actin cytoskeleton dynamics in cell migration during organ development and tissue morphogenesis (138). Among Rho GTPase proteins, Cdc42 has a conserved role to regulate cellular polarity, cell cycle division and actin cytoskeleton dynamics. More importantly, Cdc42 has been shown to regulate the formation of filopodia in different cell types including fibroblasts, immune cells, and endothelial cells in 2D culture (138). In neuronal cells, deletion of Cdc42 led to reduction in branching of growth cones (158, 159, 280). In vivo deletion of Cdc42 whether global or endothelial-cell-specific knockout, has resulted in similar defects in vascular formation in both fetal and adult vasculatures. More specifically, formation of the vascular tree lack branching structures in the trunk and heart of mice with genetic knockout of Cdc42 (170). However, as both vasculogenesis and angiogenesis concomitantly occur during embryonic development to form the branching network of the vasculature, it is a challenge to decipher the role of Cdc42 in the morphogenetic processes of angiogenesis.

Despite the implication of Cdc42 in mediating branching morphogenesis in angiogenesis, traditional culture of endothelial cells on Matrigel has attempted to answer the formation of branching network but the assay does not fully capture the 3D microenvironment where angiogenesis typically occurs within eukaryotic organs (242). Additionally, studies of Cdc42 in 3D culture relies on embedding endothelial cells within 3D collagen matrix to allow the cells to form a vascular network, which resembles the process of vasculogenesis during embryonic development rather than the process of angiogenesis (116). Therefore, the role of Cdc42 to mediate branching morphogenesis in angiogenesis remains to be explored. Here, using a previously developed Angiochip (281), where endothelial cells are triggered to sprout from a biomimetic blood vessel, we sought to investigate the effects of Cdc42 on the morphogenesis of angiogenesis. Unlike other studies of tubulogenesis

and Matrigel assays, where endothelial cell network formation occurred in a uniform distribution of biochemical stimuli, which makes it challenging to address biological significance of Cdc42 on chemotactic migration in angiogenesis, our AngioChip employed a biochemical gradient not only to stimulate formation of multicellular sprout structures but it also allows us to unveil the effects of Cdc42 in the context of chemotactic migration in angiogenic sprouting. Additionally, we were able to tune the amount of Cdc42 pharmacological inhibitor to investigate a more complex role of Cdc42 within cytoskeleton dynamics. We observed the many facets of Cdc42 to mediate the morphogenetic processes of angiogenesis in our study.

### **3.3 Materials and Methods**

**Device Fabrication.** As previously reported, devices were fabricated from two layers of poly(dimethylsiloxane) (PDMS; Sylgard 184; Dow-Corning) (281). They were treated with plasma etcher, bonded together and adhered to a 25mm square glass coverslip. After treatment with 0.1mg/ml poly-L-lysine (Sigma) for 1hr, they were treated with 1% glutaraldehyde for 1hr and washed several times with H<sub>2</sub>O. Rat tail collagen 1 (2.5mg/ml, Corning) was pipetted into the devices with two 400µm diameter acupuncture needles. Upon gelation, the needles were extracted leaving two hollow cylindrical channels within the collagen matrix.

**Cell Culture.** Human umbilical vein endothelial cells (HUVECs) (Lonza) were cultured in EGM-2. HUVECs were seeded into the channel at  $3 \times 10^6$  cells/mL as previously described. After seeding was complete, devices were immediately placed on a platform rocker (BenchRocker, BR2000).

**Angiogenic Sprouting Assay.** A combination of angiogenic factors including vascular endothelial growth factor (VEGF, 75ng/ml, R&D), monocyte chemotactic protein-1 (MCP-1, 75ng/ml, R&D), sphingosine-1-phosphate (S1P, 500nM, Cayman Chemical) and Phorbol Myristate acetate (PMA, 10ng/ml, Sigma) were administered the next day after cell seeding. The cocktail of angiogenic factors was refreshed daily as previously described.

**Inhibition of Cdc42 Experiment.** The next day after cell seeding, Cdc42 inhibitor (ML141, 15 $\mu$ M, Millipore) was added on the same day that sprouting was started. ML141 was administered in both the biomimetic blood vessel and in the angiogenic source channel. Devices were either treated with DMSO as control or ML141 over a course of 4 days before they were fixed and stained for confocal imaging. Devices were always placed on rocker to provide shear forces in the channels over the entire course of experiments. For filopodia experiment, 22.5 $\mu$ M ML141 was added for 4 hours before they were fixed for quantification (N=4 samples per conditions).

**Immunofluorescence and Confocal Image Acquisition.** After fixation, devices were permeated with 0.1% Triton-X (Sigma) for 30min and proceeded to incubation with Phalloidin Alexa 488 (1:200, Invitrogen) overnight in the cold room. Devices were washed several times with 1xPBS till fluorescent background was negligible before image acquisition. Confocal images were acquired with 40x water immersion objective, Axiovert 200M inverted microscope (Zeiss), and spinning disk confocal scan head. Images were acquired in a tiling mode and later stitched using ImageJ.

**Quantification of Sprout Length, Sprout Density, Sprout Angle, and number of Invading Cells.** To quantify sprout length and density, custom MATLAB code was written to measure the individual distances from the leading protrusions of tip cells to the wall of the parent vessel, and to count the number of sprouts. Sprout angle was determined as the angle from which the sprout deviates from the vertical direction of the gradient between the two channels. ImageJ was used to count the number of cell nuclei from projection of z-resolved confocal stacks. (N = 4 samples per condition).

**Quantification of Branches and Intersegmental Branches.** Adopting the custom MATLAB code from quantification of sprouts, we quantified number of branches and intersegmental branches and their respective lengths. A branch length was defined as the distance from the tip of the branch to the end of the branch on the sprout trunk whereas intersegmental branch length was defined as the distance connecting the two ends of the intersegmental branch on two separate sprouts.

**Filopodia Quantification.** A custom MATLAB code was used to determine the distance from the tips of filopodia to where it originates on the cell body from projections of z-resolved confocal stacks. The number and length of filopodia were averaged over the number of tip cells in each sample. Filopodia angle was measured as the angles in which filopodia deviate from the vertically perpendicular line between the 2 channels. (N=4 samples per condition).

**Statistical Analysis.** Sample populations were compared using unpaired, two-tailed Student's t-test or two-sided Wilcoxon rank sum test. \*P < 0.05 was the threshold for statistical significance. Data points on the graphs represent average values and error bars depict SEM. \* indicates P<0.05; \*\*\* indicates P < 0.001.

### 3.4 Results

#### **Inhibition of cdc42 reduced migration speed**

To elucidate the role of Cdc42 in angiogenesis, we employed a biomimetic angiogenic model or the AngioChip, which was previously published in our lab (Figure 3.1A). In brief, the AngioChip was comprised of two hollow cylindrical channels embedded within a 3D collagen matrix. In one of the channels, we seeded endothelial cells and allow them to form an endothelium. In the second channel, we administered a cocktail of angiogenic factors, which established an angiogenic gradient to trigger sprouting into the 3D collagen matrix (281). To inhibit Cdc42 activity, we used a pharmacological inhibitor ML141 (282, 283). We observed that complete inhibition of Cdc42 led to cell death. However, sprouting morphogenesis typically occurred over a course of 3-4 days in our AngioChip. Therefore, to observe the function of Cdc42 in morphogenesis, we targeted a 50% decrease in Cdc42 activity (Figure 3.1B). We administered the inhibitor at the beginning of cocktail addition in order to investigate the effects of Cdc42 from the onset of sprouting till formation of multicellular sprouts. Partial inhibition of Cdc42 activity significantly decreased the invasion depth of sprout tip cells into the interstitial matrix (Figure 3.1C). Cell migration speed was subsequently diminished (Figure 3.1D). Interestingly, the appearance of angiogenic sprouts appeared similarly

between DMSO control and in Cdc42 inhibition under phase contrast images over a course of 4 days (Figure 3.1E).

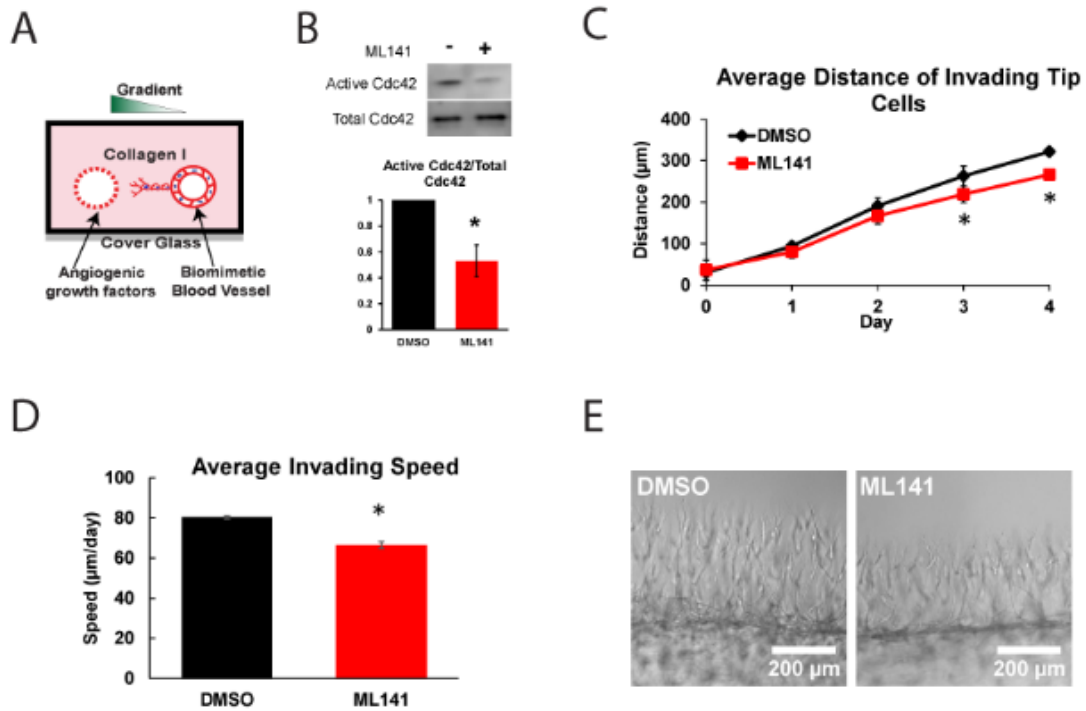


**Figure 3.1.** Inhibition of Cdc42 in AngioChip. (A) Device schematic. 2 channels fully embedded inside 2.5mg/ml Collagen gel. (B) Cdc42 activity was reduced in half with Cdc42 inhibitor ML141. (C) Average invading distance of tip cells into matrix guided by a gradient of angiogenic cocktail including MCP-1, VEGF, PMA, and S1P. (D) Average invading speed of tip cells over 4 days. (E) Representative images of sprouts at Day 4 for control DMSO and Cdc42-inhibited devices. N=4; \* indicates significant difference ( $P \leq 0.05$ ); ns indicates no significant difference.

### Inhibiting Cdc42 diminished sprout density and sprout length

To further characterize the changes in the morphogenesis of angiogenesis upon Cdc42 inhibition, we utilized confocal microscopy to capture high resolution images of sprouting and quantify the number of sprouts and average sprout length. Partial inhibition of Cdc42 =slightly decreased the number of sprouts per unit area (Figure 3.2A). However, the average sprout length was significantly reduced in half (Figure 3.2B).

Cdc42 has been shown to regulate cell polarity, one of the many important aspects of cell migration (156). Thus, inhibition of Cdc42 results in non-persistent migration in 2D (282). Our



previous results also showed a slight decrease in migration distance and speed, which may be a result of non-persistent migration. To verify this, we decided to measure the average sprout angle. We postulated that tip cells with non-persistent migration may continuously change directions as they migrate towards the source and thus the angle of sprout (Figure 3.2D) may be larger. To our surprise, average sprout angle remained unchanged, which revealed that inhibition of Cdc42 didn't affect chemotactic migration towards a gradient of angiogenic cocktails in our biomimetic model of angiogenic sprouting but rather directly affected the invasion speed.

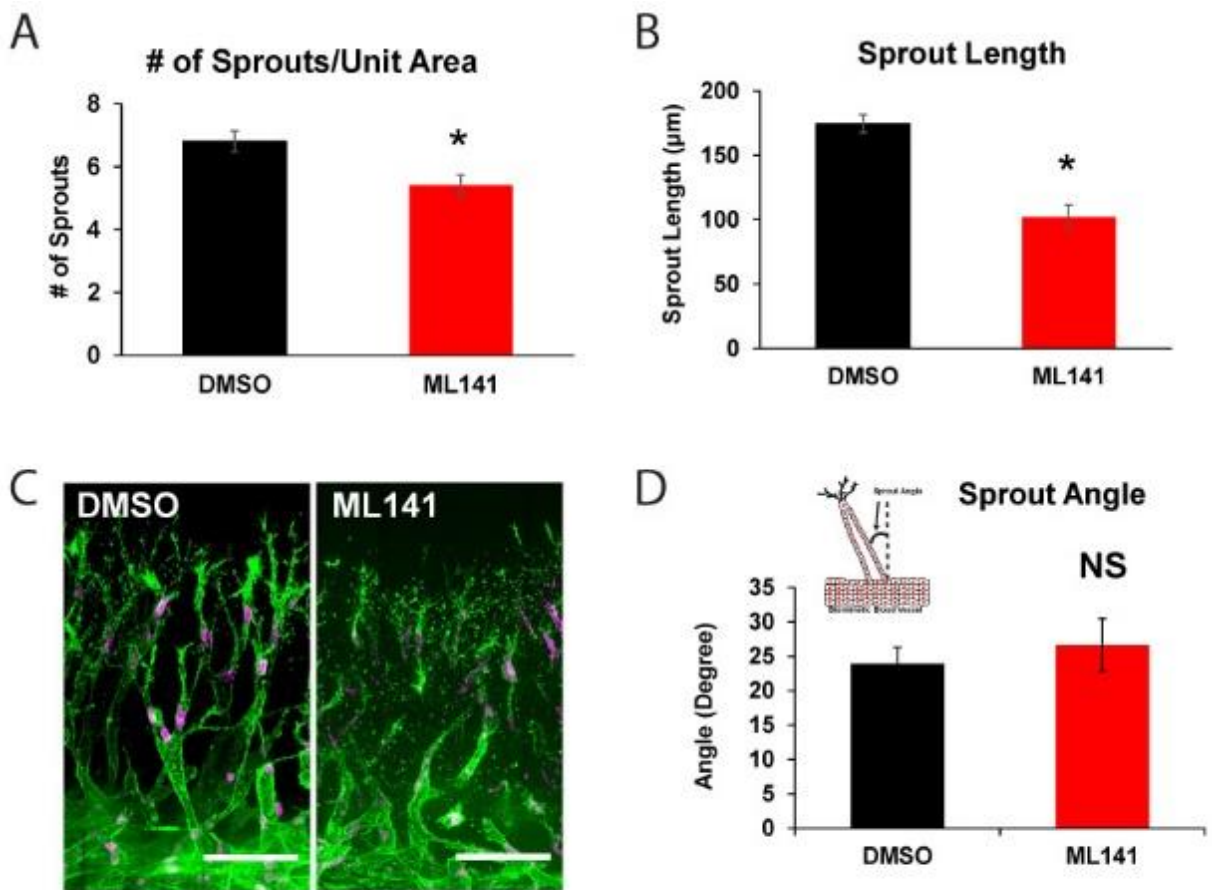


**Figure 3.2.** The effects of Cdc42 on sprout length and density during angiogenesis sprouting. (A) Quantification of sprout density between control DMSO and Cdc42 inhibition. ML141 was initiated at onset of sprouting for 4 days. (B) Sprout length was quantified at day 4. (C) Representative confocal images of sprouting in DMSO and ML141 devices at day 4. (D) Average sprout angle was

quantified between DMSO and ML141 devices. N=4; \* indicates significant difference ( $P \leq 0.05$ ); ns indicates no significant difference.

### Inhibition of Cdc42 decreased collective cell migration

To our surprise, the fact that inhibition of Cdc42 activity had a stronger effect on sprout length but less so on the invasion depth prompted us to further investigate the extent of cellular invasion. From our previous work, different invasion modes (single cell and collective cell migration) were observed in our system. Therefore, we characterized the extent of single and collective cell migration. We observed the presence of more single cells at the invading front when we inhibited Cdc42 activity (Figure 3.3A,B). We also observed a significant reduction in the number of invading cells into the 3D interstitial collagen matrix (Figure 3.3C). Interestingly, among these migrating cells, we found a significant elevation in the number of single cell migration (Figure 3.3D). Taking together, this unveiled that inhibition of Cdc42 activity reduces the extent of cellular invasion and collective cell migration of angiogenic sprouting.

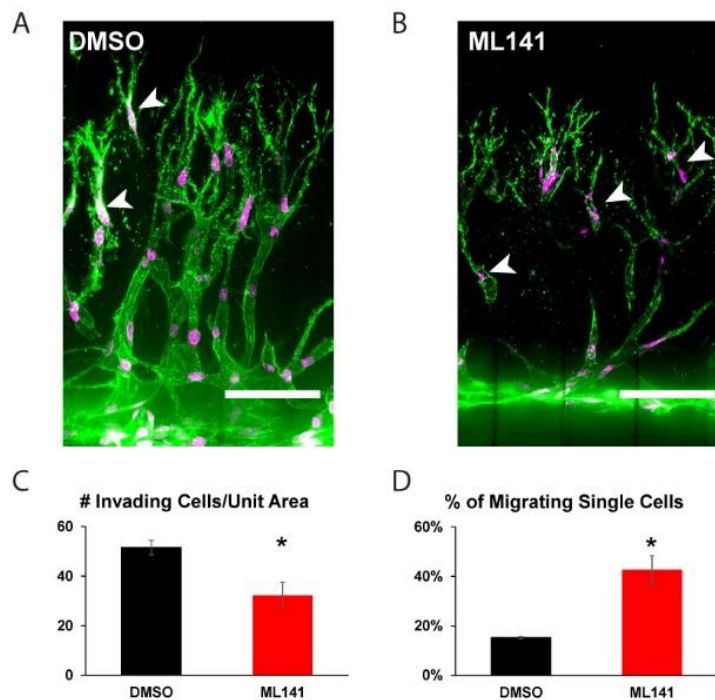


**Figure 3.3.** The effects of Cdc42 on collective migration of endothelial cell sprouting. (A) Representative image of cellular invasion in control DMSO device at day 4. (B) Representative image of cellular invasion in Cdc42-inhibited device at day 4. (C) The number of invading cells

quantified at day 4 between DMSO and Cdc42-inhibited conditions. (D) The percentage of single migrating cells quantified at day 4 between DMSO and Cdc42-inhibited conditions. N=4; \* indicates significant difference ( $P \leq 0.05$ ).

### **Cdc42 regulates branching morphogenesis of angiogenic sprouting**

One of the many important morphogenetic processes of angiogenesis is the formation of vessel branches (168, 273). As previously reported, branching was evidenced in our AngioChip (281). To further identify the morphogenetic differences of sprouts during angiogenic sprouting upon inhibition of Cdc42 activity, we quantified the formation of branches with confocal images. Occasionally, we also observed tip cells that fuse to another multicellular sprout structure from the parent vessel as demonstrated in the schematic (Figure 3.4A). In our model, a majority of sprouts exhibited formation of one single branch (Figure 3.4B). Inhibition of Cdc42 significantly reduced the number of branches in sprouts (Figure 3.4C). Occasionally, we also observed intersegmental branches that connect two individual sprouts through a multicellular tubular structures, which we called intersegmental branches. These intersegmental branches appeared to be significantly less as Cdc42 was inhibited (Figure 3.4E). Surprisingly, the length of both branches and intersegmental branches remained to be unaffected upon inhibition of Cdc42 activity (Figure 3.4D,F).

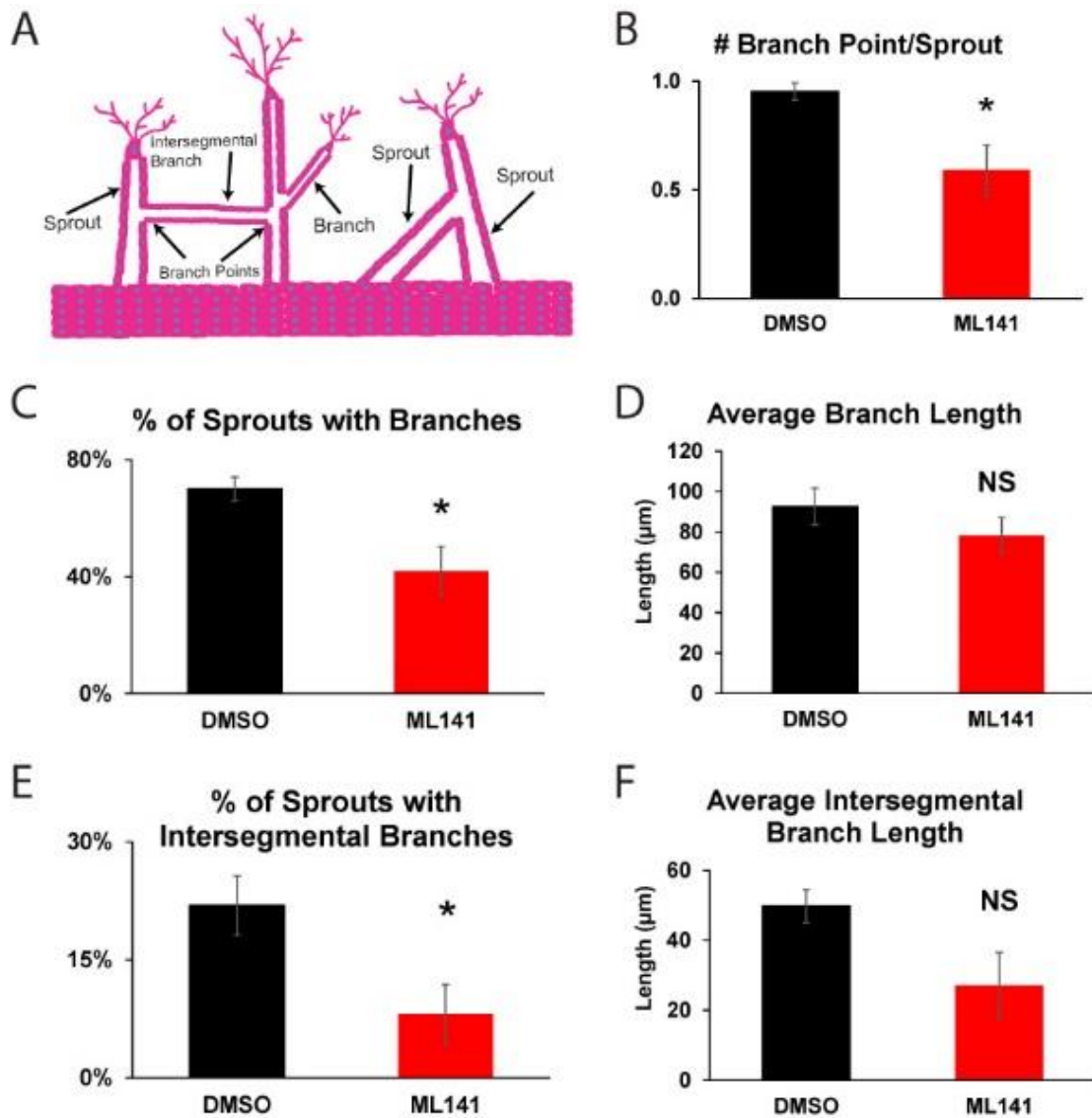


**Figure 3.4.** The effects of inhibiting Cdc42 on branching morphogenesis of angiogenic sprouting. (A) A schematic of difference branching structures and sprout morphology observed in angiogenic sprouting in the AngioChip guided by a cocktail of MCP-1, VEGF, PMA, and S1P. (B) Number of branch points is quantified for DMSO vs ML141 conditions. (C) The number of sprouts with branches between DMSO and ML141 conditions. (D) Average branch length for DMSO and ML141 conditions. (E) Percentage of intersegmental branches for DMSO and ML141 conditions. (F) Average length of intersegmental branches in DMSO and ML141 conditions. N=4; \* indicates significant difference ( $P \leq 0.05$ ); ns indicates no significant difference.

### Effects of Cdc42 inhibition on filopodia formation

To further understand the role of Cdc42 to significantly abate the formation of branches, we carefully studied the formation of filopodial extensions as Cdc42 has been demonstrated to

regulate the formation of filopodia formation in other cell types including fibroblasts, and neuronal cells (284-286). Filopodia are protrusive extensions predominantly present in leading tip cells of branch tip and sprout tip cells. We treated Day 3 multicellular sprout structures with defined tip cells (Figure 3.5A,i) for a short and acute dose of inhibitor ML141. Short and acute treatment of Cdc42 inhibitor on invading angiogenic sprouts with multiple extensions in tip cells revealed changes in filopodia appearance (Figure 3.5A,i and ii). Surprisingly, acute exposure to Cdc42 inhibitor didn't affect the angle of filopodial extensions (Figure 3.5B). Unexpectedly, inhibition of Cdc42 doubled the number of filopodial extensions in tip cells (Figure 3.5C). The distribution of filopodia number per tip cells appeared to maintain a similar distribution between control DMSO and Cdc42 inhibition conditions but shifted to where there was higher filopodia number/tip cell (Figure 3.5D). Additionally, we observed an increase in the percentage of filopodia smaller than 10 $\mu$ m (Figure 3.5F) whereas there was no noticeable change in filopodia-like protrusions larger than 10 $\mu$ m. This ultimately led to a significantly smaller average length of filopodia in tip cells as Cdc42 activity was inhibited (Figure 3.5E).

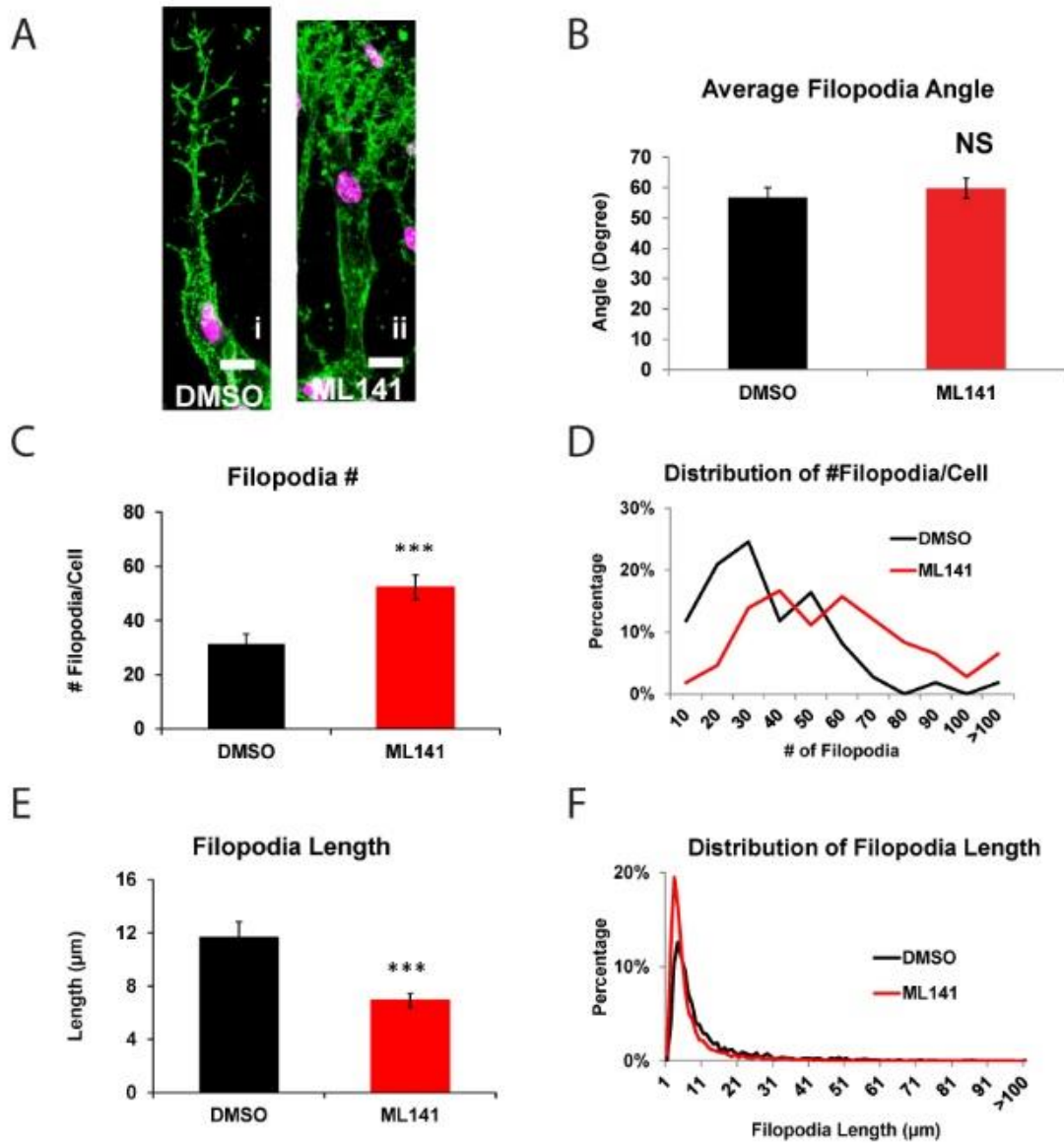


**Figure 3.5.** Filopodia formation of endothelial cell sprouting upon Cdc42 inhibition. (A) Representative confocal images of phalloidin-stained sprout tip cells showing filopodial extensions in DMSO and ML141 conditions. Sprouting was initiated for 3 days before 22.5 $\mu$ M ML141 was added for 4hrs before fixation. (B) Average angle of filopodia of sprout tip cells was quantified for DMSO vs ML141 conditions. (C) The number of filopodial extensions per sprout tip cells for DMSO and ML141 conditions. (D) Histogram of filopodial extension numbers per sprout tip cells for DMSO and ML141 conditions. (E) Average length of filopodial extensions is quantified for DMSO and ML141 conditions. (F) Histogram of filopodial extension length for DMSO and ML141 conditions. N=4; \* and \*\*\* indicate significant difference  $P \leq 0.05$  and  $P < 0.001$ , respectively.

### 3.5 Discussion

While Cdc42 has been identified as an important regulator of many cellular processes such as control of cell division, establishment of cellular polarity, and formation of filopodia in 2D cell culture (156, 287), its role in endothelial cells, especially, in 3D settings has only been explored in details at the initiation and formation of lumen during tubulogenesis (288, 289). Using our biomimetic blood vessels where endothelial cells were triggered to sprout by a defined chemical gradient, our study suggests that inhibition of Cdc42 also affects the formation of branches of endothelial cell sprouts.

It has been shown that Cdc42 is an important regulator of chemotaxis. Though the role of Cdc42 in chemotaxis is possibly cell-type dependent. For example, mouse embryonic fibroblasts and hematopoietic stem cells without Cdc42 failed in directed migration, whereas directed migration was unaffected in Cdc42-null fibroblastoid cells (290). In our study, inhibition of Cdc42 had a mild effect on migration speed but appeared to be unaffected in chemotactic migration. In fact, persistency of migration as quantified through sprout angles remained unchanged when Cdc42 was inhibited. This suggested that Cdc42 inhibition appeared to impair migration speed rather than chemotaxis. This observation is in agreement with a previous report where Cdc42 and Rac regulate migration speed but not direction of migration towards a gradient of PDGF (291). In addition to the role of Cdc42 effect on cell migration, we also observed that its activity also contributed to cytoskeletal arrangement ultimately leading to extension of sprouts and extension of filopodial protrusions.

During lung development, Cdc42 directly regulates polarity and its activity is heightened at the active budding sides (292). Consequently, disruption of Cdc42 by genetic knockout causes abnormal Cdc42 activity on the epithelial cell layer and ultimately reduces epithelial cell budding during lung morphogenesis (292). Similarly, in endothelial cell sprouting from an endothelium, quiescent endothelial cells first need to reverse polarity to become tip cells (293). As a result, a disruption of polarity signaling may potentiate abnormal morphogenesis. Our result demonstrated that inhibition of Cdc42 caused a reduction in sprout density, which may suggest a role of Cdc42

to contribute to the initiation of tip cells from the endothelium. Similarly, the number of branches, where stalk cells have to emerge from sprouts to become tip cells, is also reduced. These results indicate that Cdc42 may act through cellular polarity to positively regulate the initiation of tip cell formation within an endothelium and within the stalk cells in the trunk of endothelial sprouts. As a result, disruption of Cdc42 signaling caused a reduction in the formation of sprouts and branches in angiogenic sprouting in our AngioChip.

Interestingly, if Cdc42 positively mediates the formation of sprout and branches, its activity appeared to negatively regulate the initiation of filopodia formation. In our organotypic model, inhibition of Cdc42 significantly upsurged the number of filopodia in tip cells. This result appeared to contradict other reports in which inhibition of Cdc42 prevented formation of filopodia in fibroblasts, and neurons (156, 285). This suggests that Cdc42-driven filopodia formation may be cell type-specific. Additionally, most studies often examine a particular biochemical stimulus to activate Cdc42 for filopodia bursts in endothelial tip cells. For example, a previous study in caudal migration of endothelial cells in zebrafish indicated the role of Bmp signaling to mediate filopodia outgrowth (294) whereas another study suggested the function of ECM to induce activation of Cdc42 to promote filopodia formation through VEGF-independent NRP1 signaling in zebrafish and angiogenesis in mouse retina (295). In contrast, our biomimetic model employed a cocktail of different angiogenic factors to trigger sprouting, which may be a factor contributing to the discrepancy.

During angiogenic sprouting events, endothelial cells need to establish apical-basal domains to mature into a lumenized blood vessels. At the same time, they need to maintain cell-cell junction between tip-stalk and stalk-stalk cells to form multicellular structures. In 3D endothelial cell tubulogenesis, a previous study has reported the role of Cdc42 to mediate lumen formation through Par3, Par6 and PKC complexes (289). Here, in our model, we observed a role of Cdc42 to regulate collective cell migration. Disruption of Cdc42 encouraged migration of single cells. This suggests another important role of Cdc42 to not only regulate the cellular polarity during lumen



formation but also to target and maintain the junctional complexes between cell-cell during angiogenic sprouting.

In conclusion, using an organotypic model of angiogenesis in which sprouting emanate from an endothelium under a defined biochemical gradient, we characterized the effects of Cdc42 on angiogenic sprouting. In our angiogenic model, Cdc42 appeared to regulate migration speed, branching morphogenesis, and filopodia formation. Interestingly, we also observed the many facets of Cdc42 activity depending on the morphogenetic processes that Cdc42 targets. For example, Cdc42 positively initiates sprout formation but negatively mediates filopodial initiation. In addition, it contributes to the extension of sprout length but appears to have no effect on branch length. Further studies need to address its activity to mediate and maintain vascular junction to support collective cell migration.

## **CHAPTER 4: A PRECLINICAL ORGANOTYPIC MODEL TO EXAMINE VASCULAR INVASION AND VASCULAR REPLACEMENT IN PANCREATIC DUCTAL ADENOCARCINOMA**

### **4.1 Abstract**

Pancreatic ductal adenocarcinoma (PDAC) is often not detected until it has already spread significantly into surrounding tissues and metastasized to distant sites (296). However, it remains unclear how the PDAC cells interact with the blood vessel during vascular invasion to metastasize. Here, we describe a preclinical organotypic PDAC-on-a-chip to examine the vascular invasion of PDAC. [Need a sentence that actually describes the model – something like “Tumor cells are seeded in a 3D matrix wherein an engineered endothelialized lumen is juxtaposed>” In this model, we reveal a striking phenomenon where PDAC cells invaded into the blood vessel, induced apoptosis in the endothelial cells and replaced the endothelial cells in blood vessels. This phenomenon was confirmed in a model of ectopic tumor growth. We further identified ALK7 as a critical mediator of vascular replacement in PDAC. Blocking ALK7 diminished tumor cell proliferation and ultimately inhibited vascular replacement. Our study unveils ALK7 as a potential therapeutic target to prevent vascular replacement during vascular invasion in PDAC.

### **4.2 Introduction**

Although the detection and treatment of cancer in its earliest stages has significantly improved outcomes in many confined tumors, survival rates for tumors that have spread to distant sites remains dismal (297). As such, the vast majority of cancer mortalities stem from metastasis and its complications (298, 299). Metastasis is a final product of a chain of complex multiple steps including local spread of cancer cells at primary sites of origin, invasive entry into nearby

vasculature (intravasation), and dissemination and growth at distant organ sites (224, 300). The interactions between tumor cells and blood vessels in particular are poorly understood, despite the importance of these interactions to many steps of the metastasis cascade.

In part, the lack of detailed understanding of these tumor-vessel interactions is because it is difficult to observe these interactions in models of tumor invasion. In vivo studies of tumor growth in mice have made important observations of tumors near vascular structures, based on histologic evidence, and a few studies have attempted to observe these events through intravital microscopy. For instance, metastatic breast cancer to the brain after extravasation remained closely adhered to the vessels to avoid apoptosis induced by astrocyte-secreted serpin proteins (301). Recent attempts to use in vitro cultures to model these interactions have suggested the importance of juxtaposing tumor cells with vessel-like structures such as endothelial cell-lined lumens in order to model processes such as extravasation or intravasation (302, 303). Here, we apply such engineered 3D models of vessels to study the interactions of such vascular structures with pancreatic ductal adenocarcinomas. These tumors are reportedly highly avascular, with a paucity of endothelial cells within these tumors (185, 304).

Pancreatic ductal adenocarcinoma (PDAC) is a highly metastatic cancer whose cancer cells have been shown to escape the tumor and enter into the circulation at very early stage of the tumor progression (296, 305, 306). One of the hallmarks of advanced PDAC is local invasion of the tumor onto the nearby hepatic veins, arteries, and mesentery blood vessels (307). Vascular invasion is an important parameter to determine resectability of the tumor (236). It also contributes to the dismal 5-year survival rate below 7% of PDAC (307). It is also an initial step to enable entry of tumor cells into the circulation, resulting in circulating tumor cells that are present in the blood stream before lesions are detectable in PDAC (305). Yet, these tumors are reportedly highly avascular, with a paucity of capillary vessels within these tumors (185, 304). Thus, it appears that PDAC exhibits unusual yet important features in its interactions with vessels. Here, we describe a model system in which a biomimetic ductal channel containing PDAC cells is juxtaposed to an

engineered rudimentary blood vessel consisting of an endothelialized, perfused lumen. Using this model, we investigated PDAC invasion and interactions at the blood vessel interface. Our model revealed a striking phenomenon where blood vessels were replaced by the PDAC cells. We also provided a mechanistic study to unveil Nodal/Activin-mediated signaling through ALK7 receptor to enhance PDAC proliferation to permit de-endothelialization of blood vessel during vascular invasion.

### 4.3 Materials and Methods

**Cell culture.** Primary murine pancreatic cancer cells (a gift from Dr. Stanger, University of Pennsylvania) were isolated from primary tumors of GEMM (Kras-G12D p53<sup>-/-</sup> YFP) and cultured in DMEM + 10% fetal bovine serum + L-glutamine + Gentamycin. Human pancreatic cancer cell lines, Panc-1 (a gift from Dr. Faller, Boston University) and BxPC-3 (a gift from Dr. Stanger, University of Pennsylvania) were cultured in DMEM + 10% FBS + 1% Pen/strep and RPMI1640 + 10% FBS + 1% Pen/Strep respectively. HUVECs were cultured in EGM-2 (Lonza). EGM2 was used in all coculture experiment unless indicated otherwise.

**Device fabrication and 3D organotypic PDAC experiments.** Devices were fabricated as previously described (281). Briefly, our organotypic PDAC on a chip was comprised of 2 polydimethylsiloxane (PDMS) gaskets cast from silicon wafer masters. The gaskets were bonded after plasma etching and treated with 0.1mg/ml poly-L-lysine (Sigma) overnight and subsequently treated with 1% glutaraldehyde (EMS) as previously described. 2.5mg/ml rat tail collagen I (Corning) was pipetted into the devices after 2 acupuncture needles were placed in the gaskets. Needles are either 1mm or 500 $\mu$ m apart. PDAC cells were seeded at  $2 \times 10^6$  cells/ml in EBM2 (Lonza) and HUVECs were seeded at  $3 \times 10^6$  cells/ml in EGM-2 (Lonza) as previously described (281). Devices were plated on platform rocker. Media in blood vessel channel containing an additional 10%FBS + EGM2 was added into blood vessel channel to induce migration of PDAC

cells. PDAC channel was cultured in EBM2. All media was refreshed daily. SB431542 (Tocris) was used at 5 $\mu$ M concentration and added into both channels.

**Immunofluorescence staining in 2D cultures.** Samples were fixed with 4%PFA and permeated with 0.1% Triton-X. Samples were blocked with 3%BSA and subsequently incubated with primary antibodies: anti-CD31 (Dako, 1:200), anti-GFP (Abcam, 1:500), anti-cleaved caspase 3 (Cell Signaling, 1:500) and DAPI (Sigma, 1:500). All secondary antibodies (Invitrogen) were used at 1:1000.

**Cell imaging and quantification in 3D devices.** Migration of PDAC in 3D organotypic model was captured using bright field. Invasion distance was measured using a custom Matlab code to determine the distance from the tip of the invasive front to the biomimetic PDAC duct. For quantification of PDAC invasion area on biomimetic blood vessel, devices were fixed with 4%PFA, permeated and blocked with 3%BSA overnight. Primary antibodies for anti-CD31 (Dako, 1:200), anti-GFP (Abcam, 1:500), anti-cleaved caspase 3 (Cell Signaling, 1:500), and Dapi (Sigma, 1:500) were all incubated overnight at 4°C. Primary antibodies were washed overnight. Secondary antibodies (Invitrogen, 1:500) were incubated overnight and devices were washed over a few days to remove background before confocal microscopy. Confocal images were acquired with spinning disk confocal microscope. Z projection of image stack was used to quantify the area of blood vessel replaced by PDAC.

**2D co-culture experiment for apoptosis.** HUVECs were seeded into 96 well plate at 17000cells/well overnight to obtain a confluent monolayer. PDAC cells were seeded at 4200 cells/well over HUVECs. Apoptosis was determined via active caspase activity quantified by apoptosis bioluminescence kit (Promega), following the manufacturer's instruction. Bioluminescence intensity of activate caspase was acquired using SpectraMax5. Tumor-conditioned media were collected from coculture of 500000 HUVECs and 130000 PD7591 overnight in 1.5ml EGM2 in wells of 6 well plate and immediately used in experiment. Neutralizing antibodies for TNF $\alpha$ , FasL, Trail and their respective control antibodies were used at 25 $\mu$ g/ml.

Neutralizing antibody for pan-TGF $\beta$  (R&D) and its respective antibody control (R&D) were both used at 100ug/ml

**PDAC vascular invasion in 2D heterotypic patterning coculture.** Annulus rings were cut out by using biopsy hole punches (2mm and 3.5mm diameter) from a PDMS slab. Annulus rings were placed in the center of wells in 24 well plate. 10000 PDAC cells were seeded inside the annulus ring while HUVECs were subsequently seeded at 150000 cells outside the annulus rings overnight. Annulus rings were peeled off the next day and cells were allowed to grow into contact for 2-3 days after removal of annulus rings. Multiple overlapping images of YFP PDAC cell islands were imaged using TE200 microscope (Nikon). Overlapping images were stitched using ImageJ and PDAC areas were quantified using ImageJ.

**Tumor xenograft model.** Under anesthesia (standard isoflurane inhalation) pancreatic cancer cell line (PD7591) was subcutaneously inoculated into the dorsal area of the athymic nude mouse (NCR-nu/nu, 4-5 week, female) by using regular insulin syringes. The cancer cells were resuspended in 1:1 mixture of cancer cell growth medium and Matrigel (high protein concentrated form) kept in ice. Two million cancer cells in 100  $\mu$ L mixed solution were rapidly injected per animal. Mice were monitored daily after the tumor injection and the size of growing tumors was measured with a caliper every two days. The tumor volume was calculated with an equation:  $0.52 \times (A \times B^2)$ , where 'A' is a long axis and 'B' is a short axis of the tumor. Tumors were allowed to grow to a maximum volume of 2000 mm<sup>3</sup> in all cases as consideration for the animals' welfare. All procedures were performed in the sterile environment of a laminar flow cabinet housed in the animal facilities area in Charles River Campus (CRC) animal facility at Boston University. When the tumors reach a certain size, the tumors were excised to examine tumor microenvironment and tumor invasion to blood vessels. The animals were sacrificed using the standard carbon dioxide euthanizing method or the secondary physical (cervical dislocation) method.

**Tumor tissue processing and immunofluorescence staining.** Excised tumors were rinsed in PBS, and fixed in 4% formalin for 18 hours at room temperature, then stored in 100%

methanol at -20°C. For immunofluorescence, the fixed tumors were placed in 30% sucrose solution in PBS, incubated overnight at 4°C, and frozen in the Tissue-Tek Optimal Cutting Temperature (O.C.T.) compound (Sakura, Tokyo, Japan). Sections of 10-µm thickness were cut at -20°C. Some other cases, we cut small pieces of tumors using blades for whole mount staining. After blocking with 5% normal goat serum (Jackson ImmunoResearch, West Grove, PA) in PBST (1X PBS with 0.3% Triton) overnight at 4°C, the sections were treated with one or more of the following primary antibodies overnight at 4°C: rabbit anti-cleaved caspase 3 (1:100, Cell Signaling), rat anti-mouse CD31 (1:100, BD Pharmingen), rat anti-TER119 (1:100, Santa Cruz) antibodies. After rinses with PBS overnight at 4°C, sections or whole mount tumor pieces were incubated overnight at 4°C with one or more of the secondary antibodies: fluorescein isothiocyanate (FITC)-conjugated goat anti-GFP antibody, rhodamine-conjugated goat anti-rat antibody, Alexa 647-conjugated goat anti-rabbit antibody (1:500, all three from Jackson ImmunoResearch). DAPI (4',6-diamidino-2-phenylindole, 1:10,000, Roche, Indianapolis, IN) was also included in the secondary antibody solution. Rinsed samples were mounted with the ProLong Gold anti-fade reagent (Invitrogen, Carlsbad, CA). Fluorescent signals were visualized and digital images were obtained, using a LEICA confocal microscope.

**Statistical Analysis.** Sample populations were compared using unpaired, two-tailed Student's t-test. \*P < 0.05 was the threshold for statistical significance. Data points on the graphs represent average values and error bars depict SEM.

## 4.4 Results

### **A model of PDAC on a chip reveals 3D invasion and vascular replacement**

To examine the process of PDAC invasion toward engineered blood vessels, we engineered an organotypic model of pancreatic ductal adenocarcinoma (PDAC) on a chip building on a previously developed vessel on a chip (281). Briefly, our PDAC organotypic model is

composed of two hollow cylindrical channels, which are completely embedded into collagen matrix (Figure 4.1A). In one of the channels, we seeded endothelial cells to form a biomimetic blood vessel as previously discussed (281). In a parallel channel, we seeded pancreatic cancer cells and allowed them to adhere to form a monolayer of epithelial cells to mimic a ductal compartment of pancreatic duct. In order to observe the interactions of pancreatic ductal adenocarcinoma with the blood vessels, we stimulated migration of the pancreatic cancer cells with a gradient of 10% FBS, a commonly used method to investigate migration of cancer cells. FBS was administered into the endothelium channel and refreshed daily.

Upon stimulation with FBS, the pancreatic adenocarcinoma cells in the biomimetic ductal channel began to proliferate and lost their polarity and pile on top of one another to form a multilayer of cells. By day 4, PDAC cells began to invade into the matrix towards endothelial lumen. The invasion was collective with epithelial cells remaining in contact with each other with branched structure reminiscent of epithelial morphogenesis (Figure 4.1B). As we maintained the FBS gradient, the pancreatic cancer cells continued to approach the engineered blood vessel. Upon contact with the biomimetic blood vessel, they wrapped around the blood vessel and spread along the length of the blood vessel (Figure 4.1C). Intriguingly, during PDAC invasion, we observed part of the blood vessel was de-endothelialized and replaced by the PDAC cells (Figure 4.1D). We first observed de-endothelialization of blood vessel in primary mouse PDAC cell line PD7591 but later also identified 3 additional primary mouse PDAC cell lines and human pancreatic cancer cell line producing the same result (Supplementary Figure 4S1).

Close examination of the interface between PDAC and endothelium on the luminal surface of the vessel, we observed dying endothelial cells, marked by active caspase-3 in proximity to the area where pancreatic cancer cells have invaded onto the blood vessel (Figure 4.1E). To investigate whether our model has revealed an *in vivo* process that occurs in the pancreatic tumor environment, we subcutaneously inoculated the same tumor cells into nude mice. After the tumor reached 400mm<sup>3</sup>, we sacrificed the mice and resected the tumor including the adjacent area around



the tumor. Interestingly, we also observed a scarcity of blood vessels in the vicinity of the tumor region (Figure 4.1F), consistent with observations reported in genetically engineered mouse models and human pancreatic tumors (185). Among the small number of intratumoral blood vessels, a majority of endothelial cells were positive for active caspase-3, and some adjacent blood vessels near the peripheral tumor were also positive for active caspase 3 (Figure 4.1F).

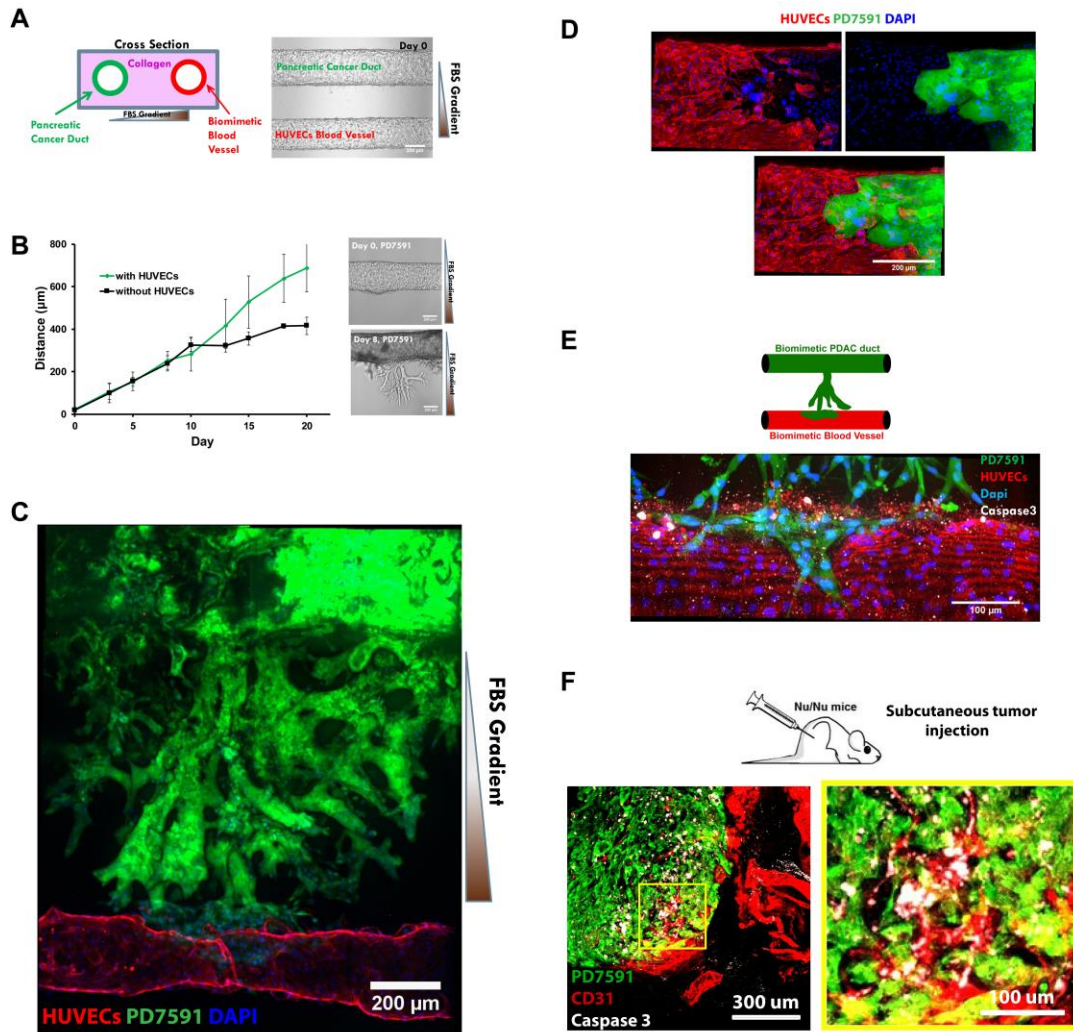


**Figure 4.1.** Preclinical organotypic model for PDAC-on-a-chip to capture vascular invasion and vascular replacement. (A) Schematic of PDAC-on-a-chip with a biomimetic blood vessel and a pancreatic cancer duct. Phase image shows cells seeding after 1 day in culture (B) Average invasion distance of PDAC cell line PD7591 towards a gradient of FBS with and without HUVECs. Addition of HUVECs increases migration speed of PD7591. (C) PD7591 invaded towards blood vessel, migrated along the vessel and wrapped around the blood vessel. (D) Confocal image of a section of the blood vessel invaded by PD7591 showed that part of the blood vessel was de-endothelialized. (E) PDAC caused apoptosis in endothelial cells in the blood vessels in PDAC 3D

organotypic model. (F) Endothelial cells were also apoptotic in the tumor in a xenograft model in vivo

### **PDAC vascular invasion induces endothelial cell apoptosis through TGF- $\beta$ signaling.**

We next sought to identify which signaling pathways that caused endothelial apoptosis. We employed a 2D heterotypic co-culture of PDAC cells and endothelial cells by interspersing PDAC cells on top of a monolayer of endothelial cells (Figure 4.2A). Overnight incubation revealed a significant number of apoptotic endothelial cells in proximity to the pancreatic cancer cells while pancreatic cancer cells were all negative for active caspase 3 (Figure 4.2A), which is also consistent with our organotypic model and in vivo xenograft model. TGF- $\beta$ , TNF- $\alpha$ , FasL, and Trail have been shown to induce apoptosis in different cell types (308-312). We sought to identify which of these apoptotic pathways may be involved in endothelial apoptosis in 2D heterotypic coculture with PDAC cells. After PDAC cells were plated for 24hrs with or without inhibitor of each of these four common apoptotic pathways, we quantified the active caspase activity. Blocking Trail, FasL, or TNF- $\alpha$  signaling with neutralizing antibodies didn't prevent apoptosis. However, inhibition of TGF- $\beta$  signaling with SB431542 (313) significantly prevented apoptosis of endothelial cells in 2D heterotypic co-culture with PDAC cells (Figure 4.2B).

To examine the effectiveness of blocking TGF- $\beta$  signaling to prevent de-endothelialization in our 3D organotypic PDAC on-a-chip model, we allowed pancreatic cancer cells from the pancreatic cancer duct to invade to the engineered blood vessel. Once the pancreatic cancer cells landed on the blood vessels, we started 5 $\mu$ M SB431542 treatment for a duration of 7 days. Interestingly, we also found that blocking TGF- $\beta$  signaling significantly prevented pancreatic cancer cells to de-endothelialize our biomimetic blood vessel (Figure 4.2C).

We further investigated whether inhibition of TGF- $\beta$  signaling also led to less vascular apoptosis in vivo by subcutaneously injecting the same pancreatic cancer cell line PD7591 into mice. By day 9, when the tumor reached 100mm<sup>3</sup>, we started to administer SB431542 and control

vehicle into two groups of mice through peritoneal injection daily for 1 week. Interestingly, tumor growth didn't decelerate in response to SB431542 (Figure 4.2D), in agreement with previous studies (222, 223). Remarkably, mice treated with SB431542 for 1 week had less apoptotic endothelial cells. Subsequently, these tumors acquired a higher vessel density within the tumor microenvironment (Figure 4.2E). This mirrors what we uncovered using our preclinical organotypic PDAC-on-a-chip.

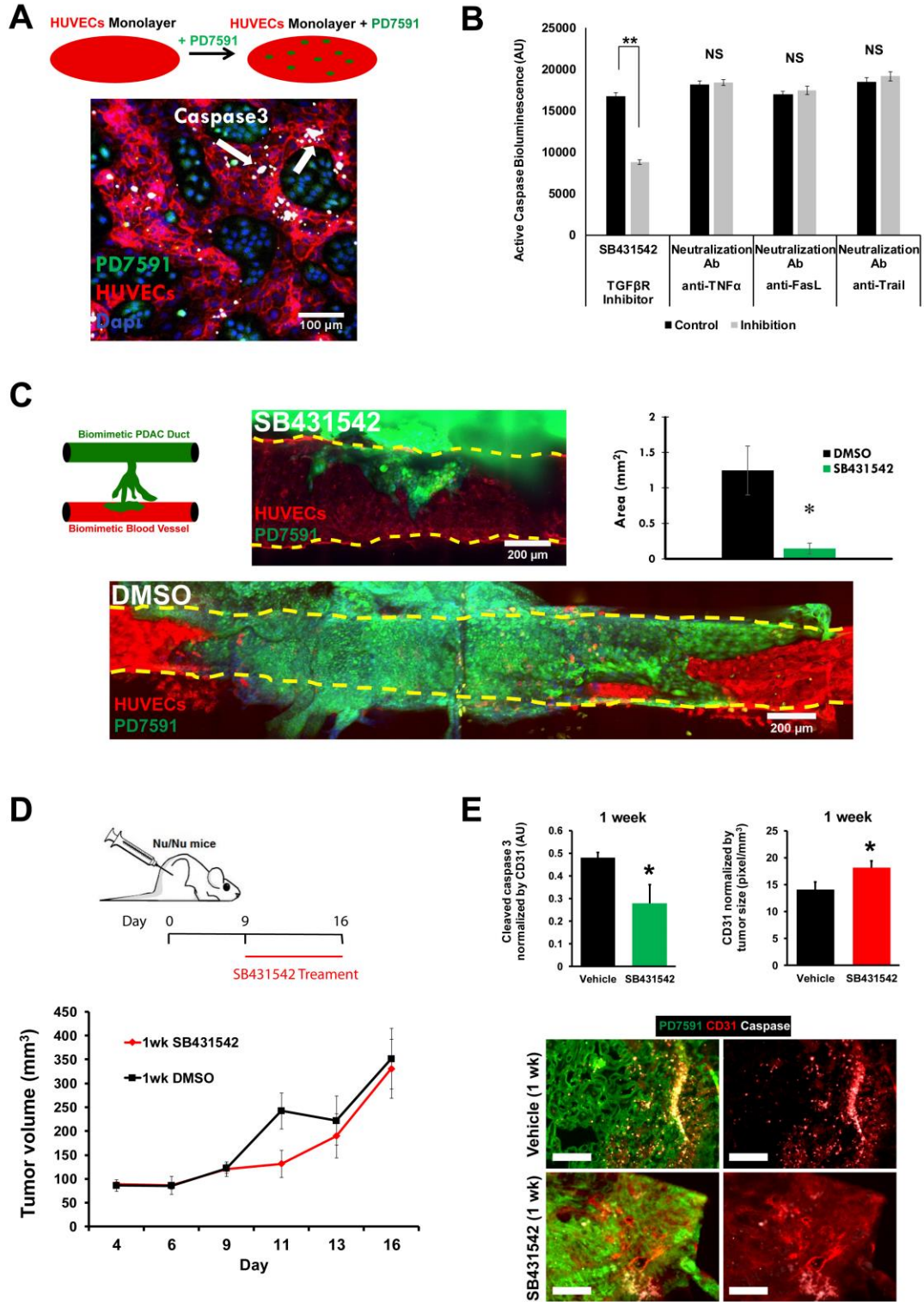


**Figure 4.2.** Inhibition of TGF- $\beta$  signaling prohibited vascular apoptosis and vascular replacement. (A) Endothelial cells were apoptotic, shown by active caspase 3 staining (white), near the invading

pancreatic cancer cells PD7591 in 2D heterotypic coculture. (B) Screening for apoptosis pathways revealed TGF- $\beta$ -mediated apoptosis in endothelial cells. (C) Inhibition of TGF- $\beta$  signaling with SB431542 prohibited vascular replacement in 3D organotypic model. (D) Inhibition of TGF- $\beta$  signaling with SB431542 in tumor xenograft model. Tumor growth didn't decelerate. (E) Quantification of vascular apoptosis and vascular density revealed a significant reduction in endothelial cell apoptosis and significantly higher vessel density within the tumor in the xenograft model. NS indicates non statistical significance ( $p>0.05$ ). \* and \*\* indicate statistical significance,  $p<0.05$  and  $p<0.01$  respectively.

### **Vascular replacement is driven through invasion and endothelial displacement by PDAC cells.**

To closely examine cellular interactions during vascular replacement, we designed a 2D heterotypic pattern coculture to enable careful observation of cell-cell interactions at the interface between endothelial cells and PDAC cells. Pancreatic cancer cells were plated inside an annulus while endothelial cells were plated outside the annulus ring. Retrieval of the annulus revealed a circular pattern of pancreatic cancer cells surrounded by a monolayer of endothelial cells (Figure 4.3A). Over a period of 6 days, pancreatic cancer cells began to invade outward and took over the endothelial cells (Figure 4.3A). When cultured alone, pancreatic cancer cells expanded quickly to cover the surface. However, as endothelial cells were present outside, the extent of tumor cell invasion dropped drastically, which suggested that pancreatic cancer cells first need to break through the barrier of endothelial cell in order to invade outward. Notably, when the co-culture pattern was treated with 5  $\mu$ M SB431542 to inhibit TGF- $\beta$  signaling, we observed an even more significant reduction in the extent of tumor cell invasion, suggesting that SB431542 was effective to prevent vascular replacement in our 2D heterotypic pattern coculture. This 2D heterotypic pattern coculture appeared to capture the replacement of endothelial cells during invasion of PDAC cells. Similarly, we also observed the efficiency of SB431542 to prevent vascular replacement of human pancreatic cancer cell lines BxPC-3, and Panc-1 over several days in 2D heterotypic pattern coculture (Supplementary Figure 4S2).

Interestingly, we also observed that there was a significantly high signal of active caspase-3 in endothelial cells at the interface between endothelial cells and PDAC cells. Treatment with

SB431542 significantly reduced the active caspase-3 staining in endothelial cells closely in contact with PDAC cells (Figure 4.2B). This observation prompted us to carefully examine the cellular dynamics at the interface between PDAC cells and endothelial cells through time lapse movie. Remarkably, the PDAC cells appeared to invade and push the endothelial cell front line backward, causing the endothelial cells to round up and undergo apoptotic (Supplementary Movie S1). Addition of SB431542 to the culture media during time lapse halted the physical invasion of pancreatic cancer cells (Supplementary Movie S2).

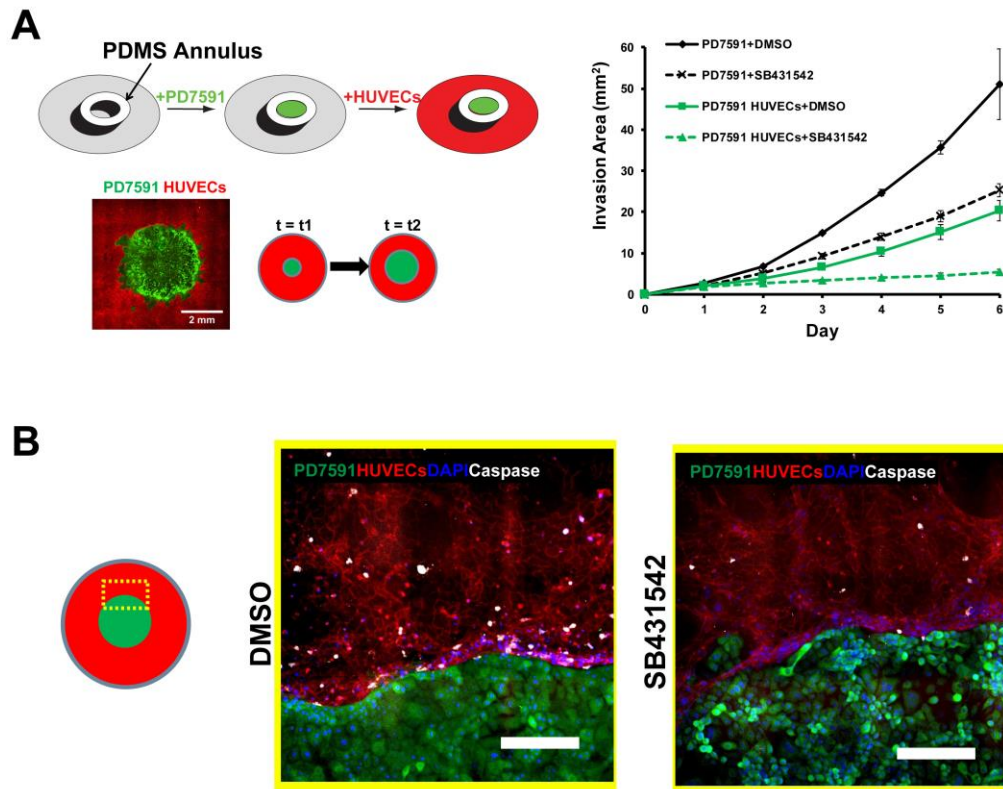


**Figure 4.3.** Vascular replacement is driven through invasion and endothelial displacement by PDAC cells. (A) Heterotypic pattern coculture of PD7591 and HUVECs. PD7591 was patterned inside the annulus while HUVECs were seeded outside the annulus. PD7591 was allowed to invade and replace the vascular cells in the presence of DMSO or SB431542. Invasion area of PD7591 was quantified over 6 days and revealed the effectiveness of inhibition of TGF $\beta$  signaling to prevent vascular replacement. (B) Apoptotic endothelial cells were more pronounced at the interface between pancreatic cancer cells and endothelial cells. SB431542 diminished apoptotic endothelial cells in proximity of pancreatic cancer cells. Scale bar is 200  $\mu$ m. \* indicates statistical significance ( $p < 0.05$ ).



**Vascular replacement of PDAC was driven through ALK7-mediated proliferation of PDAC cells.**

Since SB431542 has previously been reported as an inhibitor for ALK4/ALK5/ALK7 (313), we sought to determine which receptors in each of the cell types contributed to vascular replacement. In endothelial cells, treatment with SB431542 significantly reduced the apoptosis of endothelial cells (Figure 4.4A). We also knocked out ALK5 in endothelial cells via CRISPR/Cas9 and observed a similar reduction in apoptosis in endothelial cells (Figure 4.4B). This demonstrated that ALK5 was the receptor that regulated endothelial cell apoptosis. To investigate whether ALK5 KO endothelial cells impede vascular invasion, we plated wild type PD7591 and ALK5 KO HUVECs in 2D heterotypic pattern coculture. Interestingly, the quantified invasion area of PD7591 showed no difference between ALK5 KO vs scramble HUVECs condition (Figure 4.4C). This suggested that although ALK5 regulated endothelial cell apoptosis, inhibition of ALK5 signaling in endothelial cells contributed minimally to PDAC invasion and vascular replacement.

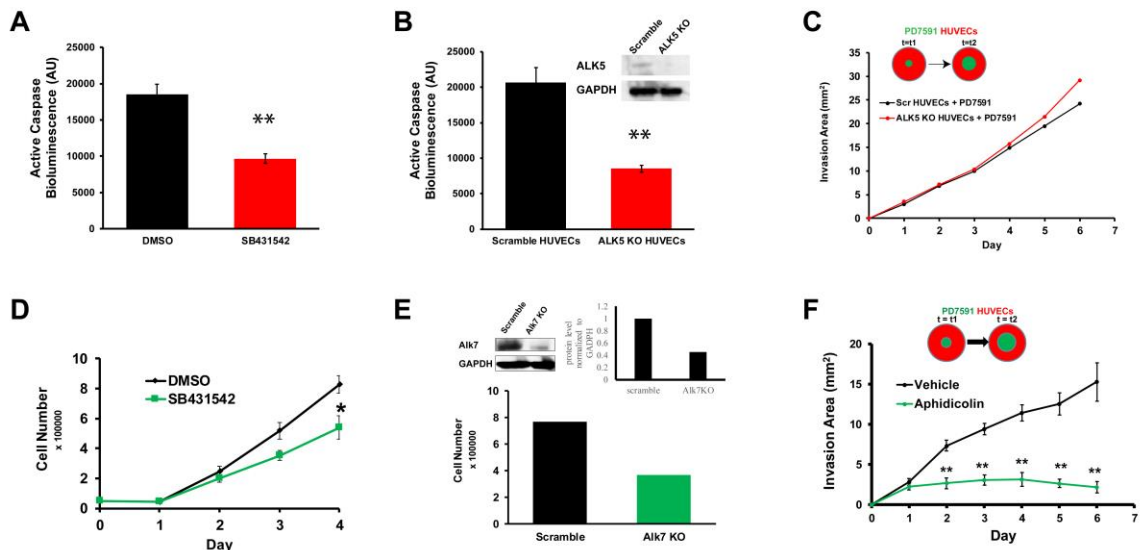


**Figure 4.** Vascular replacement of PDAC was driven through ALK7-mediated proliferation of PDAC cells. (A) SB431542 inhibited apoptosis of endothelial cells (n=3 individual experiments). (B) Knocking out ALK5 receptor in endothelial cells suppressed apoptosis of endothelial cells reflecting the similar effect of SB431542 (n=3 individual experiments). (C) ALK5 KO HUVECs didn't decelerate PD7591 invasion suggesting that ALK5-mediated apoptosis contributed minimally to the vascular replacement in PDAC (n=2 individual experiments). (D) SB431542 reduced proliferation of PD7591 (n=3 individual experiments). (E) Knocking out ALK7 receptor in PD7591 suppressed proliferation of PD7591 mirroring the similar effect of SB431542 (n=2 individual experiments). (F)

Blocking proliferation using 5 $\mu$ g/ml Aphidicolin halted vascular invasion and vascular replacement in 2D heterotypic pattern coculture (n=3 individual experiments). \* and \*\* indicate statistical significance, p<0.05 and p<0.01, respectively.

On the other hand, SB431542 reduced proliferation of PD7591 (Figure 4.4D). Noticeably, using CRISPR-mediated knockout of ALK7 receptor in PD7591, we observed a similar reduction in proliferation of PD7591 (Figure 4.4E). This suggested that ALK7 mediated proliferation of PD7591. To verify that proliferation is the main contributor of vascular replacement, we employed the 2D heterotypic pattern coculture and compared the invasion area of PD7591 with and without Aphidicolin, a proliferation inhibitor. Noticeably, we observed a significant reduction in invasion area of PD7591 cells when cell proliferation was inhibited (Figure 4.4F). This confirmed our hypothesis that ALK7-mediated proliferation of PDAC plays a particularly prominent role to vascular invasion and endothelial cell replacement in PDAC.

#### **4.5 Discussion**

In contrast to most tumors, which are hyperangiogenic, human PDAC is poorly vascularized (185, 304). Previous studies, using genetically engineered mouse model (GEMM), have shown that PDAC is also hypovascular and the tumor has a paucity of vessels with diameter larger than 10  $\mu$ m (185, 304). Interestingly, pancreatic cancer cells are also known to express and secrete a plethora of pro-angiogenic factors (314), which raises the question of how these tumors end up hypovascularized. Our studies suggest that the lack of intratumoral vasculature in PDAC is not a result of reduced angiogenesis per se, but instead a result of endothelial cell apoptosis triggered by the invading tumor cells. The ability of these tumors to rapidly invade into the vessel lumen and displace the endothelial cells has been observed in human PDAC samples but not with chronic pancreatitis (237, 238), and could explain the high rate of CTC and metastatic load of PDAC in general. Reportedly, 69.1% of cases of human PDAC with vascular invasion exhibits vascular replacement as examined through histological sections of patient samples (238). Similarly, a recent



study reported that when ovarian cancer spheroids were plated on a monolayer of endometrium, they spread on the surface of the endometrium and displaced the endometrial cells (322). This study together with ours demonstrate that tumor cells acquire an efficient capability to clear stromal components as they continue to invade and engross the stromal environment.

Apart from discovering a mechanism to explain hypovascularity in PDAC, our study unveils the crucial role of ALK7 signaling to contribute to hypovascularity in PDAC. ALK7 is a receptor for both Activin and Nodal (193). The roles of Activin and Nodal are well characterized during embryogenesis and especially they also play a role in pancreas development (217). However, its pathological activities in diseases, such as in pancreatic cancer have been elusive. A recent study has linked Nodal but not Activin to the formation of pancreatic cancer stem cells (222). In addition, besides stimulating formation of a rare population of pancreatic cancer stem cells, Nodal has also been found to re-express in many human pancreatic cancer cell lines while it is absent in normal adult pancreatic epithelial cells. Blocking Nodal diminished liver metastasis in an in vivo liver metastasis model of pancreatic cancer (223). Here, we discovered that ALK7 activation stimulates proliferation of PDAC cells, likely mediated by Activin and Nodal ligands. CRISPR-mediated knockout of ALK7 in the tumor cells abrogated the invasion and replacement of endothelial cells in blood vessels. Interestingly, Nodal has also been linked to mediate formation of microvascular channels by aggressive and genetically deregulated tumor cells in melanoma (218, 315). These findings together with our study suggested that Nodal/Activin-ALK7 is an important signaling to promote tumor-blood vessel interactions and inhibiting Nodal/Activin-ALK7 signaling is a potential avenue to block vascular invasion and vascular replacement in PDAC.

Endothelial cells can be induced to undergo apoptosis via many previously identified soluble pro-apoptotic signals such as FasL, TNF $\alpha$ , TGF $\beta$ , and Trail to trigger caspase-dependent apoptosis. However, the apoptosis of endothelial cells induced by PDAC invasion may be triggered through an alternative mechanism that requires proximal physical contact and differential proliferation rates between the tumor cells and endothelial cells. Specifically, highly proliferative

tumor cells physically invaded and displaced slowly proliferative endothelial cells, leading to endothelial cell apoptosis and vascular replacement. Such a phenomenon resonates with a classical concept of cell-cell competition, which describes the existence of 'winner cells' and 'loser cells' based on their fitness within the local environment such as their cellular division potential (316). For instance, during *Drosophila* development, *Minutes* mutated cells experienced slow growth rate and were cleared by wild type cells through apoptosis induction (317). These effects are not unique to PDAC, as previous studies also observed mammary tumor lines can induce apoptosis in HUVECs while normal mammary epithelial cells, fibroblasts, or leukocytes did not (318).

Here, using our 3D organotypic model, we demonstrate that tumor-endothelial cell interactions are not restricted only to intravasation and extravasation, but involve more complex processes such as endothelial displacement within the blood vessels. Our simple model of PDAC and blood vessels provided sufficient complexity to reveal this process, yet allowed us to introduce genetic and spatiotemporal control to isolate receptor pathways involved for each cell type. Going forward, such models could be used to capture the behavior of other tumor types as well as additional features of tumor progression, such as specific stromal components (ECMs, stromal cells, blood vessel components) and immune cells. Although existing *in vivo* mouse models provide great opportunities to capture the progression of cancer, dissecting the molecular mechanisms and cell-cell interactions is often difficult due to the complexity of *in vivo* models. Thus, as demonstrated here, 3D organotypic models provide an important complement to understand these complex cellular interactions with more mechanistic insight (319).

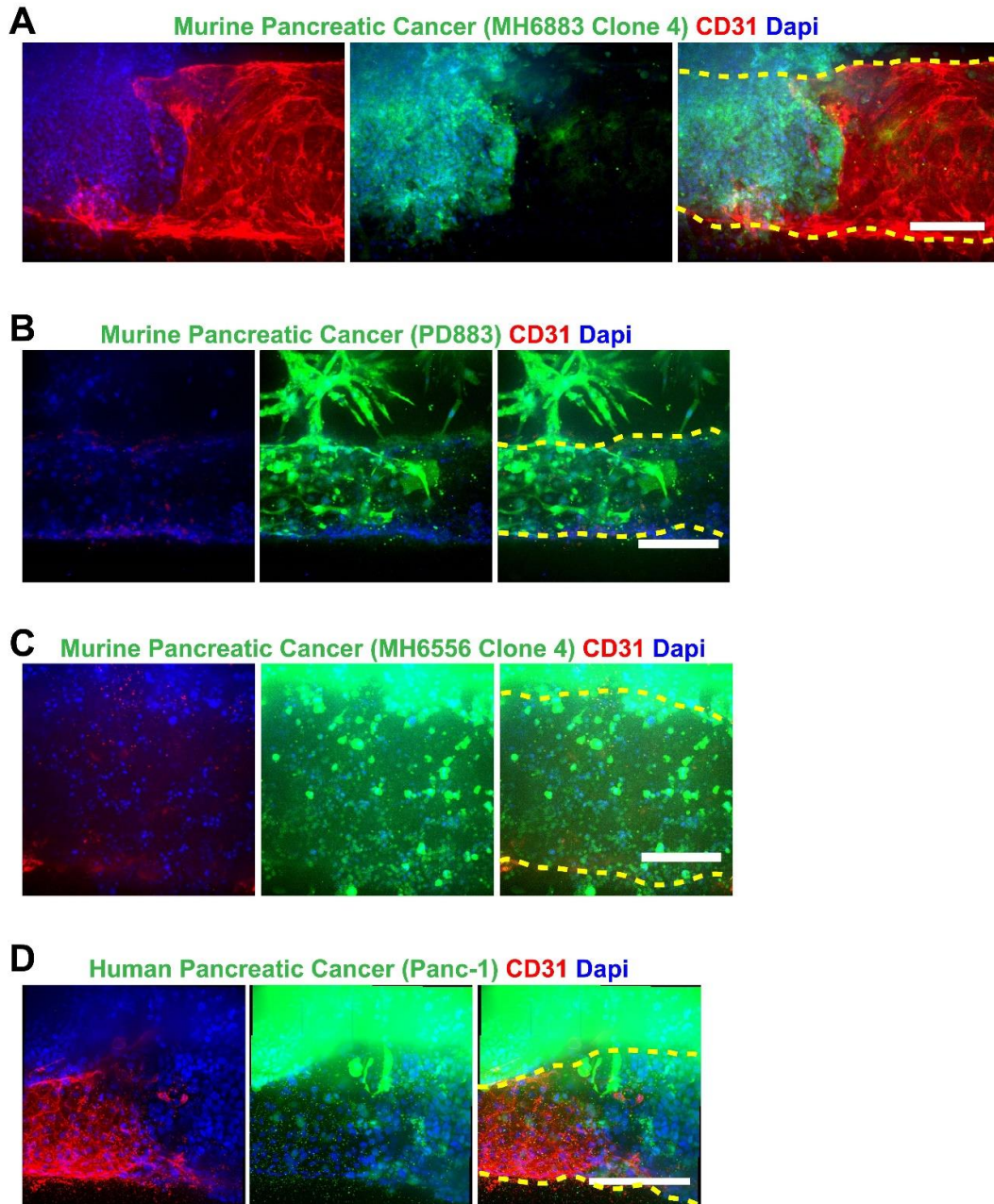


**Figure 4.S1.** Vascular invasion and replacement were also observed in other murine primary PDAC cell lines and human pancreatic cancer cell line in our 3D biomimetic PDAC-on-a-chip model. (A) Murine primary pancreatic cancer cell line (MH6883 Clone 4) invaded and de-endothelialized the blood vessels. (B) Murine primary pancreatic cancer cell line (PD883) invaded and de-endothelialized the blood vessels. (C) Murine primary pancreatic cancer cell line (MH6556 Clone 4) invaded and de-endothelialized the blood vessels. (D) Human pancreatic cancer cell line (Panc-1) invaded and de-endothelialized the blood vessels. In all images, pancreatic cancer cells are in green, HUVECs stained with CD31 in red, and cell nuclei stained with DAPI in blue. Scale bar is 200 $\mu$ m. Blood vessels were outlined in yellow dash lines.

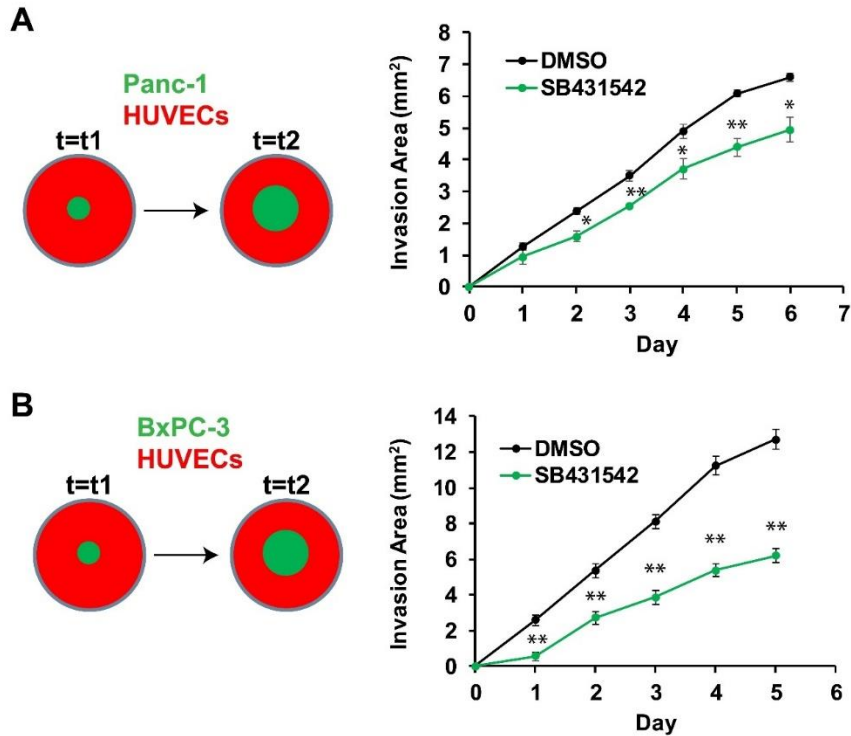


**Figure 4.S2.** Vascular invasion and replacement of human pancreatic cancer cell lines in 2D heterotypic patterning coculture. (A) Human pancreatic cancer cell line Panc-1 and HUVECs were patterned in 2D heterotypic coculture with or without 5 $\mu$ M SB431542. SB431542 effectively reduced vascular replacement of Panc-1 (n=3 individual experiments). (B) Human pancreatic cancer cell line BxPC-3 and HUVECs were patterned in 2D heterotypic coculture with or without 5 $\mu$ M SB431542. SB431542 effectively reduced vascular replacement of BcPC-3 (n=3 individual experiments). \* indicates statistical significance ( $p < 0.05$ ), \*\* indicates statistical significance ( $p < 0.01$ ).

**Table 4.1. Primers for qPCR.**

<b>Primers (5'-3')</b>	
Human ALK5 (Forward)	<i>GCTGTGAAGCCTTGAGAGTA</i>
Human ALK5 (Reverse)	<i>ATGCCTTCCTGTTGACTGAG</i>
Human TGFβ2 (Forward)	<i>TCCTCGTGAAGAACGACCTA</i>
Human TGFβ2 (Reverse)	<i>TAGGACTTCTGGAGCCATGT</i>
Human TGFβ1 (Forward)	<i>CTGTGGCTACTGGTGCTGAC</i>
Human TGFβ1 (Reverse)	<i>GCAGCTTGGACAGGATCTGG</i>
Human TGFβ2 (Forward)	<i>CTGCAGCACACTCGATATGG</i>
Human TGFβ2 (Reverse)	<i>TACTCTTCGTCGCTCCTCTC</i>
Human TGFβ3 (Forward)	<i>TTCCGCTTCAATGTGTCTCTC</i>
Human TGFβ3 (Reverse)	<i>TCCTCTGCTCATTCCGCTTA</i>
Mouse TGFβ1 (Forward)	<i>GAGCTGCGCTTGCAGAGATT</i>
Mouse TGFβ1 (Reverse)	<i>ACAGCCACTCAGGCGTATCA</i>
Mouse TGFβ2 (Forward)	<i>CGAGCAGCGGATTGAACTGT</i>
Mouse TGFβ2 (Reverse)	<i>ACAGCGTCTGTCACGTCGAA</i>
Mouse TGFβ3 (Forward)	<i>CACGGTGCTTGGACTATACA</i>
Mouse TGFβ3 (Reverse)	<i>GCTGCACTTACACGACTTCA</i>

**Table 4.2. Oligo sequences for CRISPR.**

gRNA oligos (5'-3')	
Human ALK5 oligos	<i>CACCGCATACAAACGGCCTATCTCG</i>
	<i>AAACCGAGATAGGCCGTTTGTATGC</i>
Human ALK7 oligos	<i>CACCGTGTGAAGCAGCATTTCGGTTT</i>
	<i>AAACAAACCGAATGCTGCTTCACAC</i>
Mouse ALK5 oligos	<i>CACCGTCCGCAGCTCCTCATCGTGT</i>
	<i>AAACACACGATGAGGAGCTGCGGAC</i>
Mouse ALK7 oligos	<i>CACCGCGGTTTGGGGAAGTGTGGCA</i>
	<i>AAACTGCCACACTTCCCCAAACCGC</i>
Scramble	<i>CACCGGCACTACCAGAGCTAACTCA</i>
	<i>AAACTGAGTTAGCTCTGGTAGTGCC</i>

## CHAPTER 5: CONCLUSION AND FUTURE WORK

Culture systems to study angiogenesis have evolved from traditional 2D systems to 3D systems and to microfluidic platforms to model angiogenesis. Standard 2D culture was first used to study endothelial cell migration in wound healing context in 2D. Tube formation on 2D Matrigel was also employed to study the network formation of endothelial cells. These assays, however, are unable to capture 3D invasion in in vivo angiogenic sprouting (242, 281). Perhaps, one of the most robust 3D culture systems for angiogenic sprouting is the microcarrier bead sprouting assay where endothelial cells are coated on a microcarrier bead and invade in a 3D manner into the interstitial matrix under the guidance of VEGF and additional cues provided by fibroblasts. Although microcarrier bead model quite accurately capture the angiogenic invasion in 3D, it is fundamentally lacking fluid shear stress, which endothelial cells are constantly under exposure (281). Thus, microfluidic platforms for angiogenesis have gained popularity as they not only introduce fluid shear forces but also enable better control of shear stress levels. Such a microfluidic platform is typically fabricated using standard photo lithography. A microfluidic angiogenesis on a chip fabricated from lithography is often comprised of 3 compartments. Two compartments are square rectangular channels, located at two sides of a middle compartment where extracellular matrix proteins are introduced. Endothelial cells are seeded into one of the square rectangular channels where endothelial cells are in contact with ECM proteins on just one vertical wall of the channel and with PDMS on the other 3 walls (48, 320-322). By introducing biochemical signals into the non-endothelialized channel, endothelial cells begin to invade into the interstitial compartment and organize into 3D multicellular sprout structures.

Our AngioChip device also has 3-compartment system that is capable of generating a gradient to induce angiogenic sprouting. However, our model has several distinct features that enable the study of morphogenetic processes of angiogenesis that might not be accessible by using other microfluidic platforms. First, the usage of acupuncture needles permits the creation of circular channels that resemble structural features of blood vessels. In contrast, in other microfluidic

devices, endothelial cells only sit on a vertical wall of extracellular matrix proteins, which may limit studies of how other non-endothelial cell types interact with the blood vessels. For instance, study of tumor cell migration along and around the blood vessels, which have been observed in vivo, may be challenging in such systems. Secondly, the biomimetic blood vessel in our device is completely surrounded by extracellular matrix proteins while other microfluidic devices may contain structural supports made from PDMS or glass coverslips. These mechanically stiff structures may alter cell behaviors as they begin to migrate into the environment with different stiffnesses (281, 319). Those described distinct features, thus, highlight the suitability of the AngioChip to study the morphogenetic processes of angiogenesis in vitro. However, similarly to other microfluidic devices, the Angiochip also exhibits limitations. For example, retrieval of cells for subsequent biochemical assays is possible but not straightforward when a large number of cells are required. In addition, the current design of the AngioChip does not enable study of various levels of shear stress as shear stress is dictated by a limited number of settings of the platform rocker. Additional modifications are thus required to incorporate microfluidic pump to enable studies of different shear stress levels.

Besides, the field of angiogenesis, we also observe a rapid adaptation of cell culture from 2D to 3D and to microfluidic platforms in different biological systems. Traditional 2D culture has been utilized to expand, culture and, study cellular signaling pathways. Despite their valuable contribution in biomedical research, they often fail to recapitulate in vivo tissue functions of many cell types or accurately predict drug activities (323). 3D models such as organoids, cell-embedded into matrices have provided an additional complexity of tissue organizations to better model disease states and drug responsiveness (324-327). Nonetheless, the 3D models also have limitations such as incapability to introduce fluid flow and tissue-tissue interfaces, which are crucial for many organs. As a results, microfluidic platforms offer the possibility of overcoming these limitations. In recent years, we have especially experienced a plethora of more complicated microfluidic-based culture platforms that model better disease states and functions of organs. For example, a simplified kidney model in a PDMS microfluidic device under physiologically relevant levels of shear forces greatly enhanced tissue polarization and induced formation of differentiated and polarized kidney



epithelium (328). A living model of human alveolar-capillary interface was created by microfabricating a flexible PDMS device. Human alveolar epithelial cells were cultured on one side of the porous membrane and exposed to air while human lung capillary endothelial cells were culture on the opposite side of the same membrane and exposed to flowing medium. Stretching of the flexible PDMS gaskets apply mechanical forces on both the human alveolar epithelial cells and endothelial cells to mimic better in vivo functions of lung (329). Moreover, a human blood-brain-barrier on a chip was developed by lining a porous, fibronectin-coated polycarbonate membrane with human brain microvascular endothelium on one side and human astrocytes on the other side (330). This device also included embedded microelectrodes to measure trans-epithelial electrical resistance across the barrier and demonstrated approximately 25% barrier of living brain, which is superior to standard 2D cultures. Our biomimetic model of angiogenesis also demonstrated its capability to capture in vivo-like features of sprouting angiogenesis such as digestion of basement membrane at initial invasion, formation of tip-stalk cells in multicellular sprout structures, lumen formation within sprouts, formation of perfusable neovessels. It can also serve as a screening platform to identify the effects of angiogenic factors and the efficacy of angiogenic inhibitors in different contexts (281) . Taken together, the microfluidic culture systems including our AngioChip provide strong evidence that microfluidic culture systems are capable of reproducing human organ physiology. With separate compartmental designs and introduction of fluid flow and mechanical cues, they also provide flexibility to dissect the biomolecular and mechanical contributors to tissue and organ function, as well as disease development (331).

In this thesis, I described the fabrication of a microfluidic platform, the AngioChip, to study angiogenic morphogenesis and also examined the role of Cdc42 in branching morphogenesis of angiogenesis using the AngioChip. In the study of Cdc42, I showed that inhibition of Cdc42 disrupted formation of multicellular structures. However, a detailed mechanism of how Cdc42 regulates collective cell migration in angiogenesis has not been described. Because angiogenesis is a dynamic process that involves different cytoskeletal regulators, further studies can focus on the effects of different cytoskeletal regulators such as Rac, RhoA, and their GEFs and GAPs to

coordinate the dynamics of cellular organization in sprouts. Rho GTPases exhibited spatial and temporal activity during cell migration in 2D. However, how Rho GTPases activity is distributed in 3D angiogenic sprouts remains to be explored. Molecular constructs that enable spatial and temporal activation of Rho GTPases have been described in literature (332). These molecular constructs may be employed in the AngioChip platform to explore the spatial and temporal regulation of Rho GTPases in angiogenesis.

Moreover, the physical forces that are generated by tip and stalk cells during sprouting angiogenesis can be realized in AngioChip with high resolution imaging and sophisticated algorithm of tracking forces. Notch and DLL signaling has been linked to formation of tip and stalk cell (50). Since tip and stalk cells undergo dynamic shuffling during sprout formation, a hypothesis that Notch and DLL may regulate cytoskeletal proteins or vice versa during shuffling is possible. Endothelial cells with knock down or over activation of Notch and DLL can be seeded into the AngioChip to elucidate their contributions to cytoskeletal rearrangement during sprouting. Angiogenesis is not only regulated by soluble biochemical cues in the environment, it is also regulated by the mechanical cues such as substrate stiffness, topography of the extracellular matrix proteins (32, 333). Thus, incorporating mechanically tunable synthetic materials in the AngioChip will enable such studies. Stromal cells in the interstitial tissue also participate in regulating angiogenesis. For example, macrophages have been described to enable fusion between vascular tip cells during zebrafish development (334). Addition of other cell types such as immune cells, pericytes, fibroblasts into the interstitial matrix of the AngioChip will permit studies of cell-cell interactions during angiogenesis.

In this thesis, I also described a development of a pancreatic cancer on a chip by introducing a biomimetic pancreatic ductal cancer channel in parallel to the biomimetic blood vessel. This study unveils a surprising phenomenon where tumor cells can replace endothelial cells from the blood vessels. I also dissected the molecular mechanism that enable endothelial cell replacement in PDAC. However, additional experiments are required to further dissect the

molecular mechanisms. For instance, we have shown that Alk7 KO PDAC cells are less proliferative while ALK5 KO HUVECs are less apoptotic. A heterotypic patterning coculture for these two cells are necessary to confirm the effects of Alk7 on PDAC cells and ALK5 on endothelial cells to prevent vascular replacement. Additionally, we propose to perform in vivo experiments to identify the effect of SB431542 on vascular replacement. Similarly, we also propose to implanted Alk7 KO cells into athymic mice to confirm their vascular replacement potential in vivo. It is also essential to perform histological section or whole mount confocal imaging of tumor samples to identify vessels that are replaced by PDAC in a xenograft model.

This study on vascular replacement also raises additional questions that need to be addressed in future studies. For example, we observed that in the presence of endothelial cells in the blood vessels, PDAC appeared to migrate more quickly towards the blood vessels in response of the gradient of FBS. This suggests that endothelial cells may secrete angiocrine factors to modulate migration of PDAC. What angiocrine factors that are involved in this process remain to be explored. Interestingly, we consistently observed collective migration of primary PDAC cell line PD7591. These collective structures contain a tip-like cell at the front and following stalk cells at the rear. Since PD7591 is derived from mice with heterozygous knockout of p53 protein, which regulates genomic stability, it is important to verify the collective migration capability of different clones of primary PDAC cell lines besides PD7591. One can also ask the question whether tip-stalk formation in PDAC collective migration is also regulated by Notch and DLL signaling as in endothelial cells. Will tip and stalk cells shuffle in PDAC collective migration?

Our study on vascular invasion specifically focused on the de-endothelialization process where PDAC cells have already undergone multiple steps to break into the blood vessels. Thus, we have largely neglected the preceding steps of vascular invasion before the de-endothelialization process. In particular, since endothelial cells have been shown to deposit a layer of basement membrane proteins surrounding the endothelium (281), it is unclear how PDAC cells are able to interact with the basement membrane proteins (e.g.: what integrins or MMPs are required to

engage tumor cells to the basement membrane and enable disruption of this barrier to allow tumor cells to gain access into the interior of the blood vessels). Will inhibiting TGF $\beta$  signaling with SB431542 block the entry of tumor cells into the blood vessels or the migration of tumor cells in 3D interstitial matrix? Additional questions in cellular polarity during invasion of the pancreatic cancer cells may also be explored with the PDAC-on-a-chip. For instance, what disturbed cellular polarity signaling enables tumor cells to form multiple layer of cells in the biomimetic ductal channel and whether invasion into the interstitial matrix occurs before or after formation of multilayer of cells. Interestingly, as the cancer cell transition from a surface of ducts into 3D tissue or from 3D tissue onto a curved surface of vasculature, they need to switch from a defined basal-apical polarization on 2D curved surfaces into a non-defined basal-apical polarization in 3D migration. Understanding the molecular mechanisms that regulate this polarization switch may provide strategies to block tumor cell migration.

## REFERENCES:

1. Friedl P & Gilmour D (2009) Collective cell migration in morphogenesis, regeneration and cancer. *Nat Rev Mol Cell Biol* 10(7):445-457.
2. Clark AG & Vignjevic DM (2015) Modes of cancer cell invasion and the role of the microenvironment. *Curr Opin Cell Biol* 36:13-22.
3. Friedl P & Alexander S (2011) Cancer invasion and the microenvironment: plasticity and reciprocity. *Cell* 147(5):992-1009.
4. Alexander S, Weigelin B, Winkler F, & Friedl P (2013) Preclinical intravital microscopy of the tumour-stroma interface: invasion, metastasis, and therapy response. *Curr Opin Cell Biol* 25(5):659-671.
5. Weigelin B, Bakker G-J, Friedl P (2012) Intravital third harmonic generation microscopy of collective melanoma cell invasion. *Intravital* 1:32-43.
6. Haas P & Gilmour D (2006) Chemokine signaling mediates self-organizing tissue migration in the zebrafish lateral line. *Dev Cell* 10(5):673-680.
7. Prasad M & Montell DJ (2007) Cellular and molecular mechanisms of border cell migration analyzed using time-lapse live-cell imaging. *Dev Cell* 12(6):997-1005.
8. Caussinus E, Colombelli J, & Affolter M (2008) Tip-cell migration controls stalk-cell intercalation during Drosophila tracheal tube elongation. *Curr Biol* 18(22):1727-1734.
9. Lauffenburger DA & Horwitz AF (1996) Cell migration: a physically integrated molecular process. *Cell* 84(3):359-369.
10. Hegerfeldt Y, Tusch M, Brocker EB, & Friedl P (2002) Collective cell movement in primary melanoma explants: plasticity of cell-cell interaction, beta1-integrin function, and migration strategies. *Cancer Res* 62(7):2125-2130.
11. Trinkaus JP, Trinkaus M, & Fink RD (1992) On the convergent cell movements of gastrulation in Fundulus. *J Exp Zool* 261(1):40-61.
12. Zegers MM, O'Brien LE, Yu W, Datta A, & Mostov KE (2003) Epithelial polarity and tubulogenesis in vitro. *Trends Cell Biol* 13(4):169-176.
13. Hilfer SR, Marrero L, & Sheffield JB (1990) Patterns of cell movement in early organ primordia of the chick embryo. *Anat Rec* 227(4):508-517.
14. Keller R (2002) Shaping the vertebrate body plan by polarized embryonic cell movements. *Science* 298(5600):1950-1954.
15. Tahinci E & Symes K (2003) Distinct functions of Rho and Rac are required for convergent extension during Xenopus gastrulation. *Dev Biol* 259(2):318-335.
16. Hutson MS, et al. (2003) Forces for morphogenesis investigated with laser microsurgery and quantitative modeling. *Science* 300(5616):145-149.
17. Grose R, et al. (2002) A crucial role of beta 1 integrins for keratinocyte migration in vitro and during cutaneous wound repair. *Development* 129(9):2303-2315.
18. Korff T & Augustin HG (1999) Tensional forces in fibrillar extracellular matrices control directional capillary sprouting. *J Cell Sci* 112 ( Pt 19):3249-3258.
19. Bell CD & Waizbard E (1986) Variability of cell size in primary and metastatic human breast carcinoma. *Invasion Metastasis* 6(1):11-20.
20. de Castro J, et al. (2000) beta-catenin expression pattern in primary oesophageal squamous cell carcinoma. Relationship with clinicopathologic features and clinical outcome. *Virchows Arch* 437(6):599-604.

21. Day CL, Jr., *et al.* (1981) Malignant melanoma. Prognostic significance of "microscopic satellites" in the reticular dermis and subcutaneous fat. *Ann Surg* 194(1):108-112.
22. Friedl P, *et al.* (1995) Migration of coordinated cell clusters in mesenchymal and epithelial cancer explants in vitro. *Cancer Res* 55(20):4557-4560.
23. Nabeshima K, Inoue T, Shimao Y, Kataoka H, & Koono M (1999) Cohort migration of carcinoma cells: differentiated colorectal carcinoma cells move as coherent cell clusters or sheets. *Histol Histopathol* 14(4):1183-1197.
24. Byers SW, Sommers CL, Hoxter B, Mercurio AM, & Tozeren A (1995) Role of E-cadherin in the response of tumor cell aggregates to lymphatic, venous and arterial flow: measurement of cell-cell adhesion strength. *J Cell Sci* 108 ( Pt 5):2053-2064.
25. Hashizume R, Koizumi H, Ihara A, Ohta T, & Uchikoshi T (1996) Expression of beta-catenin in normal breast tissue and breast carcinoma: a comparative study with epithelial cadherin and alpha-catenin. *Histopathology* 29(2):139-146.
26. Madhavan M, *et al.* (2001) Cadherins as predictive markers of nodal metastasis in breast cancer. *Mod Pathol* 14(5):423-427.
27. Khalil AA & Friedl P (2015) Determinants of leader cells in collective cell migration. *Integr Biol (Camb)* 2(11-12):568-574.
28. Riahi R, *et al.* (2015) Notch1-Dll4 signalling and mechanical force regulate leader cell formation during collective cell migration. *Nat Commun* 6:6556.
29. Weavers H & Skaer H (2014) Tip cells: master regulators of tubulogenesis? *Semin Cell Dev Biol* 31:91-99.
30. Dickinson RB, Guido S, & Tranquillo RT (1994) Biased cell migration of fibroblasts exhibiting contact guidance in oriented collagen gels. *Ann Biomed Eng* 22(4):342-356.
31. Gritsenko PG, Iliina O, & Friedl P (2012) Interstitial guidance of cancer invasion. *J Pathol* 226(2):185-199.
32. Bauer AL, Jackson TL, & Jiang Y (2009) Topography of extracellular matrix mediates vascular morphogenesis and migration speeds in angiogenesis. *PLoS Comput Biol* 5(7):e1000445.
33. Chan KT, *et al.* (2014) LKB1 loss in melanoma disrupts directional migration toward extracellular matrix cues. *J Cell Biol* 207(2):299-315.
34. Stratman AN & Davis GE (2012) Endothelial cell-pericyte interactions stimulate basement membrane matrix assembly: influence on vascular tube remodeling, maturation, and stabilization. *Microsc Microanal* 18(1):68-80.
35. Beaune G, *et al.* (2014) How cells flow in the spreading of cellular aggregates. *Proc Natl Acad Sci U S A* 111(22):6.
36. Shamloo A (2014) Cell-cell interactions mediate cytoskeleton organization and collective endothelial cell chemotaxis. *Cytoskeleton (Hoboken)* 71(9):501-512.
37. Insall RH (2010) Understanding eukaryotic chemotaxis: a pseudopod-centred view. *Nat Rev Mol Cell Biol* 11(6):453-458.
38. Garcia GL, Rericha EC, Heger CD, Goldsmith PK, & Parent CA (2009) The group migration of Dictyostelium cells is regulated by extracellular chemoattractant degradation. *Mol Biol Cell* 20(14):3295-3304.
39. Cai D & Montell DJ (2014) Diverse and dynamic sources and sinks in gradient formation and directed migration. *Curr Opin Cell Biol* 30:91-98.

40. Dona E, *et al.* (2013) Directional tissue migration through a self-generated chemokine gradient. *Nature* 503(7475):285-289.
41. Bagorda A & Parent CA (2008) Eukaryotic chemotaxis at a glance. *J Cell Sci* 121(Pt 16):2621-2624.
42. Tessier-Lavigne M (1994) Axon guidance by diffusible repellants and attractants. *Curr Opin Genet Dev* 4(4):596-601.
43. Weijer CJ (2009) Collective cell migration in development. *J Cell Sci* 122(Pt 18):3215-3223.
44. Haeger A, Wolf K, Zegers MM, & Friedl P (2015) Collective cell migration: guidance principles and hierarchies. *Trends Cell Biol* 25(9):556-566.
45. Cortese B, Palama IE, D'Amone S, & Gigli G (2014) Influence of electrotaxis on cell behaviour. *Integr Biol (Camb)* 6(9):817-830.
46. Liu Q & Song B (2014) Electric field regulated signaling pathways. *Int J Biochem Cell Biol* 55:264-268.
47. Zhao M (2009) Electrical fields in wound healing-An overriding signal that directs cell migration. *Semin Cell Dev Biol* 20(6):674-682.
48. Shin Y, *et al.* (2011) In vitro 3D collective sprouting angiogenesis under orchestrated ANG-1 and VEGF gradients. *Lab Chip* 11(13):2175-2181.
49. Eichmann A, Makinen T, & Alitalo K (2005) Neural guidance molecules regulate vascular remodeling and vessel navigation. *Genes Dev* 19(9):1013-1021.
50. Gerhardt H, *et al.* (2003) VEGF guides angiogenic sprouting utilizing endothelial tip cell filopodia. *J Cell Biol* 161(6):1163-1177.
51. Siekmann AF & Lawson ND (2007) Notch signalling limits angiogenic cell behaviour in developing zebrafish arteries. *Nature* 445(7129):781-784.
52. Jakobsson L, *et al.* (2010) Endothelial cells dynamically compete for the tip cell position during angiogenic sprouting. *Nat Cell Biol* 12(10):943-953.
53. Gebala V, Collins R, Geudens I, Phng LK, & Gerhardt H (2016) Blood flow drives lumen formation by inverse membrane blebbing during angiogenesis in vivo. *Nat Cell Biol* 18(4):443-450.
54. Carmeliet P (2003) Angiogenesis in health and disease. *Nat Med* 9(6):653-660.
55. Takakura N, *et al.* (2000) A role for hematopoietic stem cells in promoting angiogenesis. *Cell* 102(2):199-209.
56. Grant MB, *et al.* (2002) Adult hematopoietic stem cells provide functional hemangioblast activity during retinal neovascularization. *Nat Med* 8(6):607-612.
57. Pugh CW & Ratcliffe PJ (2003) Regulation of angiogenesis by hypoxia: role of the HIF system. *Nat Med* 9(6):677-684.
58. Carmeliet P, *et al.* (1996) Abnormal blood vessel development and lethality in embryos lacking a single VEGF allele. *Nature* 380(6573):435-439.
59. Ferrara N, *et al.* (1996) Heterozygous embryonic lethality induced by targeted inactivation of the VEGF gene. *Nature* 380(6573):439-442.
60. Oosthuysen B, *et al.* (2001) Deletion of the hypoxia-response element in the vascular endothelial growth factor promoter causes motor neuron degeneration. *Nat Genet* 28(2):131-138.
61. Leveen P, *et al.* (1994) Mice deficient for PDGF B show renal, cardiovascular, and hematological abnormalities. *Genes Dev* 8(16):1875-1887.

62. Soriano P (1994) Abnormal kidney development and hematological disorders in PDGF beta-receptor mutant mice. *Genes Dev* 8(16):1888-1896.
63. Davis S, *et al.* (1996) Isolation of angiopoietin-1, a ligand for the TIE2 receptor, by secretion-trap expression cloning. *Cell* 87(7):1161-1169.
64. Mochizuki Y, Nakamura T, Kanetake H, & Kanda S (2002) Angiopoietin 2 stimulates migration and tube-like structure formation of murine brain capillary endothelial cells through c-Fes and c-Fyn. *J Cell Sci* 115(Pt 1):175-183.
65. Gale NW & Yancopoulos GD (1999) Growth factors acting via endothelial cell-specific receptor tyrosine kinases: VEGFs, angiopoietins, and ephrins in vascular development. *Genes Dev* 13(9):1055-1066.
66. Dumont DJ, *et al.* (1994) Dominant-negative and targeted null mutations in the endothelial receptor tyrosine kinase, tek, reveal a critical role in vasculogenesis of the embryo. *Genes Dev* 8(16):1897-1909.
67. Beenken A & Mohammadi M (2009) The FGF family: biology, pathophysiology and therapy. *Nat Rev Drug Discov* 8(3):235-253.
68. Bergers G & Hanahan D (2008) Modes of resistance to anti-angiogenic therapy. *Nat Rev Cancer* 8(8):592-603.
69. Pardali E, Goumans MJ, & ten Dijke P (2010) Signaling by members of the TGF-beta family in vascular morphogenesis and disease. *Trends Cell Biol* 20(9):556-567.
70. Carmeliet P & Jain RK (2011) Molecular mechanisms and clinical applications of angiogenesis. *Nature* 473(7347):298-307.
71. Phng LK & Gerhardt H (2009) Angiogenesis: a team effort coordinated by notch. *Dev Cell* 16(2):196-208.
72. Benedito R, *et al.* (2009) The notch ligands Dll4 and Jagged1 have opposing effects on angiogenesis. *Cell* 137(6):1124-1135.
73. Phng LK, *et al.* (2009) Nrarp coordinates endothelial Notch and Wnt signaling to control vessel density in angiogenesis. *Dev Cell* 16(1):70-82.
74. Corada M, *et al.* (2010) The Wnt/beta-catenin pathway modulates vascular remodeling and specification by upregulating Dll4/Notch signaling. *Dev Cell* 18(6):938-949.
75. Dejana E (2010) The role of wnt signaling in physiological and pathological angiogenesis. *Circ Res* 107(8):943-952.
76. Morimoto A, *et al.* (1991) Hepatocyte growth factor modulates migration and proliferation of human microvascular endothelial cells in culture. *Biochem Biophys Res Commun* 179(2):1042-1049.
77. Bussolino F, *et al.* (1992) Hepatocyte growth factor is a potent angiogenic factor which stimulates endothelial cell motility and growth. *J Cell Biol* 119(3):629-641.
78. Aoki M, Morishita R, Taniyama Y, Kaneda Y, & Ogihara T (2000) Therapeutic angiogenesis induced by hepatocyte growth factor: potential gene therapy for ischemic diseases. *J Atheroscler Thromb* 7(2):71-76.
79. Taniyama Y, *et al.* (2001) Therapeutic angiogenesis induced by human hepatocyte growth factor gene in rat diabetic hind limb ischemia model: molecular mechanisms of delayed angiogenesis in diabetes. *Circulation* 104(19):2344-2350.
80. Van Belle E, *et al.* (1998) Potentiated angiogenic effect of scatter factor/hepatocyte growth factor via induction of vascular endothelial growth factor: the case for paracrine amplification of angiogenesis. *Circulation* 97(4):381-390.



81. Xin X, *et al.* (2001) Hepatocyte growth factor enhances vascular endothelial growth factor-induced angiogenesis in vitro and in vivo. *Am J Pathol* 158(3):1111-1120.
82. Ito WD, *et al.* (1997) Monocyte chemotactic protein-1 increases collateral and peripheral conductance after femoral artery occlusion. *Circ Res* 80(6):829-837.
83. Voskuil M, *et al.* (2003) Modulation of collateral artery growth in a porcine hindlimb ligation model using MCP-1. *Am J Physiol Heart Circ Physiol* 284(4):H1422-1428.
84. Moldovan NI, Goldschmidt-Clermont PJ, Parker-Thornburg J, Shapiro SD, & Kolattukudy PE (2000) Contribution of monocytes/macrophages to compensatory neovascularization: the drilling of metalloelastase-positive tunnels in ischemic myocardium. *Circ Res* 87(5):378-384.
85. Salcedo R, *et al.* (2000) Human endothelial cells express CCR2 and respond to MCP-1: direct role of MCP-1 in angiogenesis and tumor progression. *Blood* 96(1):34-40.
86. Takuwa Y, *et al.* (2010) Roles of sphingosine-1-phosphate signaling in angiogenesis. *World J Biol Chem* 1(10):298-306.
87. Pyne NJ & Pyne S (2010) Sphingosine 1-phosphate and cancer. *Nat Rev Cancer* 10(7):489-503.
88. Mizugishi K, *et al.* (2007) Maternal disturbance in activated sphingolipid metabolism causes pregnancy loss in mice. *J Clin Invest* 117(10):2993-3006.
89. Yatomi Y, Ozaki Y, Ohmori T, & Igarashi Y (2001) Sphingosine 1-phosphate: synthesis and release. *Prostaglandins Other Lipid Mediat* 64(1-4):107-122.
90. Venkataraman K, *et al.* (2006) Extracellular export of sphingosine kinase-1a contributes to the vascular S1P gradient. *Biochem J* 397(3):461-471.
91. Hla T, Venkataraman K, & Michaud J (2008) The vascular S1P gradient-cellular sources and biological significance. *Biochim Biophys Acta* 1781(9):477-482.
92. Pappu R, *et al.* (2007) Promotion of lymphocyte egress into blood and lymph by distinct sources of sphingosine-1-phosphate. *Science* 316(5822):295-298.
93. Ryu Y, *et al.* (2002) Sphingosine-1-phosphate, a platelet-derived lysophospholipid mediator, negatively regulates cellular Rac activity and cell migration in vascular smooth muscle cells. *Circ Res* 90(3):325-332.
94. Inoki I, *et al.* (2006) Negative regulation of endothelial morphogenesis and angiogenesis by S1P2 receptor. *Biochem Biophys Res Commun* 346(1):293-300.
95. Peters SL & Alewijnse AE (2007) Sphingosine-1-phosphate signaling in the cardiovascular system. *Curr Opin Pharmacol* 7(2):186-192.
96. Peng X, *et al.* (2004) Protective effects of sphingosine 1-phosphate in murine endotoxin-induced inflammatory lung injury. *Am J Respir Crit Care Med* 169(11):1245-1251.
97. Lee JF, *et al.* (2006) Dual roles of tight junction-associated protein, zonula occludens-1, in sphingosine 1-phosphate-mediated endothelial chemotaxis and barrier integrity. *J Biol Chem* 281(39):29190-29200.
98. Marsolais D & Rosen H (2009) Chemical modulators of sphingosine-1-phosphate receptors as barrier-oriented therapeutic molecules. *Nat Rev Drug Discov* 8(4):297-307.
99. Takuwa Y (2002) Subtype-specific differential regulation of Rho family G proteins and cell migration by the Edg family sphingosine-1-phosphate receptors. *Biochim Biophys Acta* 1582(1-3):112-120.
100. Hla T (2004) Physiological and pathological actions of sphingosine 1-phosphate. *Semin Cell Dev Biol* 15(5):513-520.

101. Lee MJ, *et al.* (1999) Vascular endothelial cell adherens junction assembly and morphogenesis induced by sphingosine-1-phosphate. *Cell* 99(3):301-312.
102. Kimura T, *et al.* (2000) Sphingosine 1-phosphate stimulates proliferation and migration of human endothelial cells possibly through the lipid receptors, Edg-1 and Edg-3. *Biochem J* 348 Pt 1:71-76.
103. Liu Y, *et al.* (2000) Edg-1, the G protein-coupled receptor for sphingosine-1-phosphate, is essential for vascular maturation. *J Clin Invest* 106(8):951-961.
104. Skoura A, *et al.* (2007) Essential role of sphingosine 1-phosphate receptor 2 in pathological angiogenesis of the mouse retina. *J Clin Invest* 117(9):2506-2516.
105. Desgrosellier JS & Cheresh DA (2010) Integrins in cancer: biological implications and therapeutic opportunities. *Nat Rev Cancer* 10(1):9-22.
106. Hodivala-Dilke K (2008)  $\alpha$ v $\beta$ 3 integrin and angiogenesis: a moody integrin in a changing environment. *Curr Opin Cell Biol* 20(5):514-519.
107. Rundhaug JE (2005) Matrix metalloproteinases and angiogenesis. *J Cell Mol Med* 9(2):267-285.
108. Nagase H & Woessner JF, Jr. (1999) Matrix metalloproteinases. *J Biol Chem* 274(31):21491-21494.
109. McCawley LJ & Matrisian LM (2001) Matrix metalloproteinases: they're not just for matrix anymore! *Curr Opin Cell Biol* 13(5):534-540.
110. Stamenkovic I (2003) Extracellular matrix remodelling: the role of matrix metalloproteinases. *J Pathol* 200(4):448-464.
111. Opdenakker G, Van den Steen PE, & Van Damme J (2001) Gelatinase B: a tuner and amplifier of immune functions. *Trends Immunol* 22(10):571-579.
112. Brew K, Dinakarandian D, & Nagase H (2000) Tissue inhibitors of metalloproteinases: evolution, structure and function. *Biochim Biophys Acta* 1477(1-2):267-283.
113. Murphy AN, Unsworth EJ, & Stetler-Stevenson WG (1993) Tissue inhibitor of metalloproteinases-2 inhibits bFGF-induced human microvascular endothelial cell proliferation. *J Cell Physiol* 157(2):351-358.
114. Dejana E, Tournier-Lasserre E, & Weinstein BM (2009) The control of vascular integrity by endothelial cell junctions: molecular basis and pathological implications. *Dev Cell* 16(2):209-221.
115. Strilic B, *et al.* (2009) The molecular basis of vascular lumen formation in the developing mouse aorta. *Dev Cell* 17(4):505-515.
116. Simons M, *et al.* (2015) State-of-the-Art Methods for Evaluation of Angiogenesis and Tissue Vascularization: A Scientific Statement From the American Heart Association. *Circ Res* 116(11):e99-132.
117. Potente M, Gerhardt H, & Carmeliet P (2011) Basic and therapeutic aspects of angiogenesis. *Cell* 146(6):873-887.
118. Ruhrberg C & Bautsch VL (2013) Neurovascular development and links to disease. *Cell Mol Life Sci* 70(10):1675-1684.
119. Claxton S, *et al.* (2008) Efficient, inducible Cre-recombinase activation in vascular endothelium. *Genesis* 46(2):74-80.
120. Fruttiger M (2007) Development of the retinal vasculature. *Angiogenesis* 10(2):77-88.
121. Lawson ND & Weinstein BM (2002) In vivo imaging of embryonic vascular development using transgenic zebrafish. *Dev Biol* 248(2):307-318.

122. Cleaver O & Krieg PA (1998) VEGF mediates angioblast migration during development of the dorsal aorta in *Xenopus*. *Development* 125(19):3905-3914.
123. Levine AJ, Munoz-Sanjuan I, Bell E, North AJ, & Brivanlou AH (2003) Fluorescent labeling of endothelial cells allows in vivo, continuous characterization of the vascular development of *Xenopus laevis*. *Dev Biol* 254(1):50-67.
124. Laib AM, *et al.* (2009) Spheroid-based human endothelial cell microvessel formation in vivo. *Nat Protoc* 4(8):1202-1215.
125. Volkmann I, *et al.* (2013) MicroRNA-mediated epigenetic silencing of sirtuin1 contributes to impaired angiogenic responses. *Circ Res* 113(8):997-1003.
126. Bahramsoltani M, Plendl J, Janczyk P, Custodis P, & Kaesmeyer S (2009) Quantitation of angiogenesis and antiangiogenesis in vivo, ex vivo and in vitro - an overview. *ALTEX* 26(2):95-107.
127. Liang CC, Park AY, & Guan JL (2007) In vitro scratch assay: a convenient and inexpensive method for analysis of cell migration in vitro. *Nat Protoc* 2(2):329-333.
128. Quent VM, Loessner D, Friis T, Reichert JC, & Huttmacher DW (2010) Discrepancies between metabolic activity and DNA content as tool to assess cell proliferation in cancer research. *J Cell Mol Med* 14(4):1003-1013.
129. Heeschen C, *et al.* (2004) Profoundly reduced neovascularization capacity of bone marrow mononuclear cells derived from patients with chronic ischemic heart disease. *Circulation* 109(13):1615-1622.
130. Nakatsu MN & Hughes CC (2008) An optimized three-dimensional in vitro model for the analysis of angiogenesis. *Methods Enzymol* 443:65-82.
131. Koh W, Stratman AN, Sacharidou A, & Davis GE (2008) In vitro three dimensional collagen matrix models of endothelial lumen formation during vasculogenesis and angiogenesis. *Methods Enzymol* 443:83-101.
132. Stratman AN, Malotte KM, Mahan RD, Davis MJ, & Davis GE (2009) Pericyte recruitment during vasculogenic tube assembly stimulates endothelial basement membrane matrix formation. *Blood* 114(24):5091-5101.
133. Saunders WB, *et al.* (2006) Coregulation of vascular tube stabilization by endothelial cell TIMP-2 and pericyte TIMP-3. *J Cell Biol* 175(1):179-191.
134. Nehls V & Drenckhahn D (1995) A microcarrier-based cocultivation system for the investigation of factors and cells involved in angiogenesis in three-dimensional fibrin matrices in vitro. *Histochem Cell Biol* 104(6):459-466.
135. Chung S, *et al.* (2009) Cell migration into scaffolds under co-culture conditions in a microfluidic platform. *Lab Chip* 9(2):269-275.
136. Ridley AJ (2011) Life at the leading edge. *Cell* 145(7):1012-1022.
137. Carman CV (2009) Mechanisms for transcellular diapedesis: probing and pathfinding by 'invadosome-like protrusions'. *J Cell Sci* 122(Pt 17):3025-3035.
138. Heasman SJ & Ridley AJ (2008) Mammalian Rho GTPases: new insights into their functions from in vivo studies. *Nat Rev Mol Cell Biol* 9(9):690-701.
139. Rossman KL, Der CJ, & Sondek J (2005) GEF means go: turning on RHO GTPases with guanine nucleotide-exchange factors. *Nat Rev Mol Cell Biol* 6(2):167-180.
140. Bernardis A (2003) GAPs galore! A survey of putative Ras superfamily GTPase activating proteins in man and *Drosophila*. *Biochim Biophys Acta* 1603(2):47-82.
141. DerMardirossian C & Bokoch GM (2005) GDIs: central regulatory molecules in Rho GTPase activation. *Trends Cell Biol* 15(7):356-363.

142. Jaffe AB & Hall A (2005) Rho GTPases: biochemistry and biology. *Annu Rev Cell Dev Biol* 21:247-269.
143. Amano M, Fukata Y, & Kaibuchi K (2000) Regulation and functions of Rho-associated kinase. *Exp Cell Res* 261(1):44-51.
144. Uchida S, *et al.* (2000) The suppression of small GTPase rho signal transduction pathway inhibits angiogenesis in vitro and in vivo. *Biochem Biophys Res Commun* 269(2):633-640.
145. Hoang MV, Whelan MC, & Senger DR (2004) Rho activity critically and selectively regulates endothelial cell organization during angiogenesis. *Proc Natl Acad Sci U S A* 101(7):1874-1879.
146. Hyvelin JM, *et al.* (2005) Inhibition of Rho-kinase attenuates hypoxia-induced angiogenesis in the pulmonary circulation. *Circ Res* 97(2):185-191.
147. Mavria G, *et al.* (2006) ERK-MAPK signaling opposes Rho-kinase to promote endothelial cell survival and sprouting during angiogenesis. *Cancer Cell* 9(1):33-44.
148. Kroll J, *et al.* (2009) Inhibition of Rho-dependent kinases ROCK I/II activates VEGF-driven retinal neovascularization and sprouting angiogenesis. *Am J Physiol Heart Circ Physiol* 296(3):H893-899.
149. van Nieuw Amerongen GP, Koolwijk P, Versteilen A, & van Hinsbergh VW (2003) Involvement of RhoA/Rho kinase signaling in VEGF-induced endothelial cell migration and angiogenesis in vitro. *Arterioscler Thromb Vasc Biol* 23(2):211-217.
150. Weiss-Haljiti C, *et al.* (2004) Involvement of phosphoinositide 3-kinase gamma, Rac, and PAK signaling in chemokine-induced macrophage migration. *J Biol Chem* 279(41):43273-43284.
151. Rosenfeldt HM, Hobson JP, Milstien S, & Spiegel S (2001) The sphingosine-1-phosphate receptor EDG-1 is essential for platelet-derived growth factor-induced cell motility. *Biochem Soc Trans* 29(Pt 6):836-839.
152. Red-Horse K, Crawford Y, Shojaei F, & Ferrara N (2007) Endothelium-microenvironment interactions in the developing embryo and in the adult. *Dev Cell* 12(2):181-194.
153. Crowther M, Brown NJ, Bishop ET, & Lewis CE (2001) Microenvironmental influence on macrophage regulation of angiogenesis in wounds and malignant tumors. *J Leukoc Biol* 70(4):478-490.
154. Vader P, *et al.* (2011) Examining the role of Rac1 in tumor angiogenesis and growth: a clinically relevant RNAi-mediated approach. *Angiogenesis* 14(4):457-466.
155. D'Amico G, *et al.* (2010) Endothelial-Rac1 is not required for tumor angiogenesis unless alphavbeta3-integrin is absent. *PLoS One* 5(3):e9766.
156. Etienne-Manneville S (2004) Cdc42--the centre of polarity. *J Cell Sci* 117(Pt 8):1291-1300.
157. Cory GO & Cullen PJ (2007) Membrane curvature: the power of bananas, zeppelins and boomerangs. *Curr Biol* 17(12):R455-457.
158. Koleske AJ (2003) Do filopodia enable the growth cone to find its way? *Sci STKE* 2003(183):pe20.
159. Chen TJ, Gehler S, Shaw AE, Bamburg JR, & Letourneau PC (2006) Cdc42 participates in the regulation of ADF/cofilin and retinal growth cone filopodia by brain derived neurotrophic factor. *J Neurobiol* 66(2):103-114.
160. Takai Y & Nakanishi H (2003) Nectin and afadin: novel organizers of intercellular junctions. *J Cell Sci* 116(Pt 1):17-27.

161. Arthur WT, Noren NK, & BurrIDGE K (2002) Regulation of Rho family GTPases by cell-cell and cell-matrix adhesion. *Biol Res* 35(2):239-246.
162. Honda T, *et al.* (2003) Cdc42 and Rac small G proteins activated by trans-interactions of nectins are involved in activation of c-Jun N-terminal kinase, but not in association of nectins and cadherin to form adherens junctions, in fibroblasts. *Genes Cells* 8(5):481-491.
163. Kawakatsu T, *et al.* (2002) Trans-interactions of nectins induce formation of filopodia and Lamellipodia through the respective activation of Cdc42 and Rac small G proteins. *J Biol Chem* 277(52):50749-50755.
164. Srinivasan S, *et al.* (2003) Rac and Cdc42 play distinct roles in regulating PI(3,4,5)P3 and polarity during neutrophil chemotaxis. *J Cell Biol* 160(3):375-385.
165. Phng LK, Stanchi F, & Gerhardt H (2013) Filopodia are dispensable for endothelial tip cell guidance. *Development* 140(19):4031-4040.
166. Snapper SB, *et al.* (2001) N-WASP deficiency reveals distinct pathways for cell surface projections and microbial actin-based motility. *Nat Cell Biol* 3(10):897-904.
167. Peng J, Wallar BJ, Flanders A, Swiatek PJ, & Alberts AS (2003) Disruption of the Diaphanous-related formin Drf1 gene encoding mDia1 reveals a role for Drf3 as an effector for Cdc42. *Curr Biol* 13(7):534-545.
168. De Smet F, Segura I, De Bock K, Hohensinner PJ, & Carmeliet P (2009) Mechanisms of vessel branching: filopodia on endothelial tip cells lead the way. *Arterioscler Thromb Vasc Biol* 29(5):639-649.
169. Peng X, *et al.* (2013) Inactivation of Cdc42 in embryonic brain results in hydrocephalus with ependymal cell defects in mice. *Protein Cell* 4(3):231-242.
170. Jin Y, *et al.* (2013) Deletion of Cdc42 enhances ADAM17-mediated vascular endothelial growth factor receptor 2 shedding and impairs vascular endothelial cell survival and vasculogenesis. *Mol Cell Biol* 33(21):4181-4197.
171. He J, *et al.* (2014) 2564 resected periampullary adenocarcinomas at a single institution: trends over three decades. *HPB (Oxford)* 16(1):83-90.
172. Kleeff J, *et al.* (2016) Pancreatic cancer. *Nat Rev Dis Primers* 2:16022.
173. Hezel AF, Kimmelman AC, Stanger BZ, Bardeesy N, & Depinho RA (2006) Genetics and biology of pancreatic ductal adenocarcinoma. *Genes Dev* 20(10):1218-1249.
174. Kopp JL, *et al.* (2012) Identification of Sox9-dependent acinar-to-ductal reprogramming as the principal mechanism for initiation of pancreatic ductal adenocarcinoma. *Cancer Cell* 22(6):737-750.
175. Klimstra DS & Longnecker DS (1994) K-ras mutations in pancreatic ductal proliferative lesions. *Am J Pathol* 145(6):1547-1550.
176. Bardeesy N & DePinho RA (2002) Pancreatic cancer biology and genetics. *Nat Rev Cancer* 2(12):897-909.
177. Seymour AB, *et al.* (1994) Allelotype of pancreatic adenocarcinoma. *Cancer Res* 54(10):2761-2764.
178. Apte MV, *et al.* (2004) Desmoplastic reaction in pancreatic cancer: role of pancreatic stellate cells. *Pancreas* 29(3):179-187.
179. Apte MV, *et al.* (2015) Pancreatic cancer: The microenvironment needs attention too! *Pancreatology* 15(4 Suppl):S32-38.
180. Rhim AD, *et al.* (2014) Stromal elements act to restrain, rather than support, pancreatic ductal adenocarcinoma. *Cancer Cell* 25(6):735-747.

181. Ponz-Sarvise M, Tuveson DA, & Yu KH (2016) Mouse Models of Pancreatic Ductal Adenocarcinoma. *Hematol Oncol Clin North Am* 29(4):609-617.
182. Jones S, *et al.* (2008) Core signaling pathways in human pancreatic cancers revealed by global genomic analyses. *Science* 321(5897):1801-1806.
183. Hingorani SR, *et al.* (2003) Preinvasive and invasive ductal pancreatic cancer and its early detection in the mouse. *Cancer Cell* 4(6):437-450.
184. Guerra C, *et al.* (2007) Chronic pancreatitis is essential for induction of pancreatic ductal adenocarcinoma by K-Ras oncogenes in adult mice. *Cancer Cell* 11(3):291-302.
185. Olive KP, *et al.* (2009) Inhibition of Hedgehog signaling enhances delivery of chemotherapy in a mouse model of pancreatic cancer. *Science* 324(5933):1457-1461.
186. Jacobetz MA, *et al.* (2013) Hyaluronan impairs vascular function and drug delivery in a mouse model of pancreatic cancer. *Gut* 62(1):112-120.
187. Boj SF, *et al.* (2015) Organoid models of human and mouse ductal pancreatic cancer. *Cell* 160(1-2):324-338.
188. Anzano MA, Roberts AB, Smith JM, Sporn MB, & De Larco JE (1983) Sarcoma growth factor from conditioned medium of virally transformed cells is composed of both type alpha and type beta transforming growth factors. *Proc Natl Acad Sci U S A* 80(20):6264-6268.
189. Massague J, Blain SW, & Lo RS (2000) TGFbeta signaling in growth control, cancer, and heritable disorders. *Cell* 103(2):295-309.
190. Massague J (1998) TGF-beta signal transduction. *Annu Rev Biochem* 67:753-791.
191. Oklu R & Hesketh R (2000) The latent transforming growth factor beta binding protein (LTBP) family. *Biochem J* 352 Pt 3:601-610.
192. Margadant C & Sonnenberg A (2010) Integrin-TGF-beta crosstalk in fibrosis, cancer and wound healing. *EMBO Rep* 11(2):97-105.
193. Wakefield LM & Hill CS (2013) Beyond TGFbeta: roles of other TGFbeta superfamily members in cancer. *Nat Rev Cancer* 13(5):328-341.
194. Derynck R & Zhang YE (2003) Smad-dependent and Smad-independent pathways in TGF-beta family signalling. *Nature* 425(6958):577-584.
195. Goumans MJ, *et al.* (2003) Activin receptor-like kinase (ALK)1 is an antagonistic mediator of lateral TGFbeta/ALK5 signaling. *Mol Cell* 12(4):817-828.
196. Daly AC, Randall RA, & Hill CS (2008) Transforming growth factor beta-induced Smad1/5 phosphorylation in epithelial cells is mediated by novel receptor complexes and is essential for anchorage-independent growth. *Mol Cell Biol* 28(22):6889-6902.
197. Liu IM, *et al.* (2009) TGFbeta-stimulated Smad1/5 phosphorylation requires the ALK5 L45 loop and mediates the pro-migratory TGFbeta switch. *EMBO J* 28(2):88-98.
198. Wrighton KH, Lin X, Yu PB, & Feng XH (2009) Transforming Growth Factor {beta} Can Stimulate Smad1 Phosphorylation Independently of Bone Morphogenetic Protein Receptors. *J Biol Chem* 284(15):9755-9763.
199. Levine AJ, Levine ZJ, & Brivanlou AH (2009) GDF3 is a BMP inhibitor that can activate Nodal signaling only at very high doses. *Dev Biol* 325(1):43-48.
200. Neuzillet C, *et al.* (2015) Targeting the TGFbeta pathway for cancer therapy. *Pharmacol Ther* 147:22-31.
201. Padua D & Massague J (2009) Roles of TGFbeta in metastasis. *Cell Res* 19(1):89-102.
202. Hahn SA, *et al.* (1996) Homozygous deletion map at 18q21.1 in pancreatic cancer. *Cancer Res* 56(3):490-494.

203. Maitra A, Kern SE, & Hruban RH (2006) Molecular pathogenesis of pancreatic cancer. *Best Pract Res Clin Gastroenterol* 20(2):211-226.
204. Baldwin RL, *et al.* (1996) Attenuated ALK5 receptor expression in human pancreatic cancer: correlation with resistance to growth inhibition. *Int J Cancer* 67(2):283-288.
205. Mesnard D, Guzman-Ayala M, & Constam DB (2006) Nodal specifies embryonic visceral endoderm and sustains pluripotent cells in the epiblast before overt axial patterning. *Development* 133(13):2497-2505.
206. Arnold SJ & Robertson EJ (2009) Making a commitment: cell lineage allocation and axis patterning in the early mouse embryo. *Nat Rev Mol Cell Biol* 10(2):91-103.
207. Schier AF (2003) Nodal signaling in vertebrate development. *Annu Rev Cell Dev Biol* 19:589-621.
208. Ramel MC & Hill CS (2012) Spatial regulation of BMP activity. *FEBS Lett* 586(14):1929-1941.
209. Miyazono K, Kamiya Y, & Morikawa M (2010) Bone morphogenetic protein receptors and signal transduction. *J Biochem* 147(1):35-51.
210. Wagner DO, *et al.* (2010) BMPs: from bone to body morphogenetic proteins. *Sci Signal* 3(107):mr1.
211. Magee JA, Piskounova E, & Morrison SJ (2012) Cancer stem cells: impact, heterogeneity, and uncertainty. *Cancer Cell* 21(3):283-296.
212. Waite KA & Eng C (2003) From developmental disorder to heritable cancer: it's all in the BMP/TGF-beta family. *Nat Rev Genet* 4(10):763-773.
213. Hardwick JC, Kodach LL, Offerhaus GJ, & van den Brink GR (2008) Bone morphogenetic protein signalling in colorectal cancer. *Nat Rev Cancer* 8(10):806-812.
214. Lee J, *et al.* (2008) Epigenetic-mediated dysfunction of the bone morphogenetic protein pathway inhibits differentiation of glioblastoma-initiating cells. *Cancer Cell* 13(1):69-80.
215. Sneddon JB, *et al.* (2006) Bone morphogenetic protein antagonist gremlin 1 is widely expressed by cancer-associated stromal cells and can promote tumor cell proliferation. *Proc Natl Acad Sci U S A* 103(40):14842-14847.
216. Strizzi L, Hardy KM, Kirschmann DA, Ahrlund-Richter L, & Hendrix MJ (2012) Nodal expression and detection in cancer: experience and challenges. *Cancer Res* 72(8):1915-1920.
217. Quail DF, Siegers GM, Jewer M, & Postovit LM (2013) Nodal signalling in embryogenesis and tumourigenesis. *Int J Biochem Cell Biol* 45(4):885-898.
218. Topczewska JM, *et al.* (2006) Embryonic and tumorigenic pathways converge via Nodal signaling: role in melanoma aggressiveness. *Nat Med* 12(8):925-932.
219. Lawrence MG, *et al.* (2011) Reactivation of embryonic nodal signaling is associated with tumor progression and promotes the growth of prostate cancer cells. *Prostate* 71(11):1198-1209.
220. Strizzi L, *et al.* (2011) Potential for the embryonic morphogen Nodal as a prognostic and predictive biomarker in breast cancer. *Breast Cancer Res* 14(3):R75.
221. Spiller CM, *et al.* (2012) Endogenous Nodal signaling regulates germ cell potency during mammalian testis development. *Development* 139(22):4123-4132.
222. Lonardo E, *et al.* (2011) Nodal/Activin signaling drives self-renewal and tumorigenicity of pancreatic cancer stem cells and provides a target for combined drug therapy. *Cell Stem Cell* 9(5):433-446.

223. Duan W, *et al.* (2015) Overexpression of Nodal induces a metastatic phenotype in pancreatic cancer cells via the Smad2/3 pathway. *Oncotarget* 6(3):1490-1506.
224. Valastyan S & Weinberg RA (2011) Tumor metastasis: molecular insights and evolving paradigms. *Cell* 147(2):275-292.
225. Auguste P, Lemiere S, Larrieu-Lahargue F, & Bikfalvi A (2005) Molecular mechanisms of tumor vascularization. *Crit Rev Oncol Hematol* 54(1):53-61.
226. Zhao C, *et al.* (2011) Distinct contributions of angiogenesis and vascular co-option during the initiation of primary microtumors and micrometastases. *Carcinogenesis* 32(8):1143-1150.
227. Donnem T, *et al.* (2013) Vessel co-option in primary human tumors and metastases: an obstacle to effective anti-angiogenic treatment? *Cancer Med* 2(4):427-436.
228. Chang YS, *et al.* (2000) Mosaic blood vessels in tumors: frequency of cancer cells in contact with flowing blood. *Proc Natl Acad Sci U S A* 97(26):14608-14613.
229. Maniotis AJ, *et al.* (1999) Vascular channel formation by human melanoma cells in vivo and in vitro: vasculogenic mimicry. *Am J Pathol* 155(3):739-752.
230. Bittner M, *et al.* (2000) Molecular classification of cutaneous malignant melanoma by gene expression profiling. *Nature* 406(6795):536-540.
231. Bissell MJ (1999) Tumor plasticity allows vasculogenic mimicry, a novel form of angiogenic switch. A rose by any other name? *Am J Pathol* 155(3):675-679.
232. Hendrix MJ, Sefter EA, Hess AR, & Sefter RE (2003) Molecular plasticity of human melanoma cells. *Oncogene* 22(20):3070-3075.
233. Cheng N, *et al.* (2003) Inhibition of VEGF-dependent multistage carcinogenesis by soluble EphA receptors. *Neoplasia* 5(5):445-456.
234. Hardy KM, *et al.* (2010) Regulation of the embryonic morphogen Nodal by Notch4 facilitates manifestation of the aggressive melanoma phenotype. *Cancer Res* 70(24):10340-10350.
235. Strizzi L, *et al.* (2009) Nodal as a biomarker for melanoma progression and a new therapeutic target for clinical intervention. *Expert Rev Dermatol* 4(1):67-78.
236. Buchs NC, Chilcott M, Poletti PA, Buhler LH, & Morel P (2010) Vascular invasion in pancreatic cancer: Imaging modalities, preoperative diagnosis and surgical management. *World J Gastroenterol* 16(7):818-831.
237. Hong SM, *et al.* (2012) Vascular invasion in infiltrating ductal adenocarcinoma of the pancreas can mimic pancreatic intraepithelial neoplasia: a histopathologic study of 209 cases. *Am J Surg Pathol* 36(2):235-241.
238. Bandyopadhyay S, *et al.* (2009) Isolated solitary ducts (naked ducts) in adipose tissue: a specific but underappreciated finding of pancreatic adenocarcinoma and one of the potential reasons of understaging and high recurrence rate. *Am J Surg Pathol* 33(3):425-429.
239. Folkman J (1995) Angiogenesis in cancer, vascular, rheumatoid and other disease. *Nat Med* 1(1):27-31.
240. Witmer AN, Vrensen GF, Van Noorden CJ, & Schlingemann RO (2003) Vascular endothelial growth factors and angiogenesis in eye disease. *Prog Retin Eye Res* 22(1):1-29.
241. Harmey JH & Bouchier-Hayes D (2002) Vascular endothelial growth factor (VEGF), a survival factor for tumour cells: implications for anti-angiogenic therapy. *Bioessays* 24(3):280-283.



242. Staton CA, Reed MW, & Brown NJ (2009) A critical analysis of current in vitro and in vivo angiogenesis assays. *Int J Exp Pathol* 90(3):195-221.
243. Jain RK, Schlenger K, Hockel M, & Yuan F (1997) Quantitative angiogenesis assays: progress and problems. *Nat Med* 3(11):1203-1208.
244. Donovan D, Brown NJ, Bishop ET, & Lewis CE (2001) Comparison of three in vitro human 'angiogenesis' assays with capillaries formed in vivo. *Angiogenesis* 4(2):113-121.
245. Nakatsu MN, *et al.* (2003) Angiogenic sprouting and capillary lumen formation modeled by human umbilical vein endothelial cells (HUVEC) in fibrin gels: the role of fibroblasts and Angiopoietin-1. *Microvasc Res* 66(2):102-112.
246. Meier F, *et al.* (2000) Human melanoma progression in skin reconstructs : biological significance of bFGF. *Am J Pathol* 156(1):193-200.
247. Debnath J & Brugge JS (2005) Modelling glandular epithelial cancers in three-dimensional cultures. *Nat Rev Cancer* 5(9):675-688.
248. Schmeichel KL & Bissell MJ (2003) Modeling tissue-specific signaling and organ function in three dimensions. *J Cell Sci* 116(Pt 12):2377-2388.
249. Montesano R, Vassalli JD, Baird A, Guillemin R, & Orci L (1986) Basic fibroblast growth factor induces angiogenesis in vitro. *Proc Natl Acad Sci U S A* 83(19):7297-7301.
250. Silvagno F, *et al.* (1995) In vivo activation of met tyrosine kinase by heterodimeric hepatocyte growth factor molecule promotes angiogenesis. *Arterioscler Thromb Vasc Biol* 15(11):1857-1865.
251. Fong GH, Rossant J, Gertsenstein M, & Breitman ML (1995) Role of the Flt-1 receptor tyrosine kinase in regulating the assembly of vascular endothelium. *Nature* 376(6535):66-70.
252. Kono M, *et al.* (2004) The sphingosine-1-phosphate receptors S1P1, S1P2, and S1P3 function coordinately during embryonic angiogenesis. *J Biol Chem* 279(28):29367-29373.
253. Montesano R & Orci L (1985) Tumor-promoting phorbol esters induce angiogenesis in vitro. *Cell* 42(2):469-477.
254. Lampugnani MG, *et al.* (2010) CCM1 regulates vascular-lumen organization by inducing endothelial polarity. *J Cell Sci* 123(Pt 7):1073-1080.
255. Mendel DB, *et al.* (2000) Development of SU5416, a selective small molecule inhibitor of VEGF receptor tyrosine kinase activity, as an anti-angiogenesis agent. *Anticancer Drug Des* 15(1):29-41.
256. Mendel DB, *et al.* (2000) The angiogenesis inhibitor SU5416 has long-lasting effects on vascular endothelial growth factor receptor phosphorylation and function. *Clin Cancer Res* 6(12):4848-4858.
257. Inai T, *et al.* (2004) Inhibition of vascular endothelial growth factor (VEGF) signaling in cancer causes loss of endothelial fenestrations, regression of tumor vessels, and appearance of basement membrane ghosts. *Am J Pathol* 165(1):35-52.
258. Bayless KJ & Davis GE (2003) Sphingosine-1-phosphate markedly induces matrix metalloproteinase and integrin-dependent human endothelial cell invasion and lumen formation in three-dimensional collagen and fibrin matrices. *Biochem Biophys Res Commun* 312(4):903-913.
259. Lee OH, *et al.* (1999) Sphingosine 1-phosphate induces angiogenesis: its angiogenic action and signaling mechanism in human umbilical vein endothelial cells. *Biochem Biophys Res Commun* 264(3):743-750.

260. LaMontagne K, *et al.* (2006) Antagonism of sphingosine-1-phosphate receptors by FTY720 inhibits angiogenesis and tumor vascularization. *Cancer Res* 66(1):221-231.
261. Brown PD (1997) Matrix metalloproteinase inhibitors in the treatment of cancer. *Med Oncol* 14(1):1-10.
262. Steward WP & Thomas AL (2000) Marimastat: the clinical development of a matrix metalloproteinase inhibitor. *Expert Opin Investig Drugs* 9(12):2913-2922.
263. Chrobak KM, Potter DR, & Tien J (2006) Formation of perfused, functional microvascular tubes in vitro. *Microvasc Res* 71(3):185-196.
264. Miller JS, *et al.* (2012) Rapid casting of patterned vascular networks for perfusable engineered three-dimensional tissues. *Nat Mater* 11(9):768-774.
265. Zheng Y, *et al.* (2012) In vitro microvessels for the study of angiogenesis and thrombosis. *Proc Natl Acad Sci U S A* 109(24):9342-9347.
266. Song JW & Munn LL (2011) Fluid forces control endothelial sprouting. *Proc Natl Acad Sci U S A* 108(37):15342-15347.
267. Yeon JH, Ryu HR, Chung M, Hu QP, & Jeon NL (2012) In vitro formation and characterization of a perfusable three-dimensional tubular capillary network in microfluidic devices. *Lab Chip* 12(16):2815-2822.
268. Newman AC, Nakatsu MN, Chou W, Gershon PD, & Hughes CC (2011) The requirement for fibroblasts in angiogenesis: fibroblast-derived matrix proteins are essential for endothelial cell lumen formation. *Mol Biol Cell* 22(20):3791-3800.
269. Stratman AN, Davis MJ, & Davis GE (2011) VEGF and FGF prime vascular tube morphogenesis and sprouting directed by hematopoietic stem cell cytokines. *Blood* 117(14):3709-3719.
270. Holderfield MT & Hughes CC (2008) Crosstalk between vascular endothelial growth factor, notch, and transforming growth factor-beta in vascular morphogenesis. *Circ Res* 102(6):637-652.
271. Iruela-Arispe ML & Davis GE (2009) Cellular and molecular mechanisms of vascular lumen formation. *Dev Cell* 16(2):222-231.
272. Eilken HM & Adams RH (2010) Dynamics of endothelial cell behavior in sprouting angiogenesis. *Curr Opin Cell Biol* 22(5):617-625.
273. Carmeliet P, De Smet F, Loges S, & Mazzone M (2009) Branching morphogenesis and antiangiogenesis candidates: tip cells lead the way. *Nat Rev Clin Oncol* 6(6):315-326.
274. Hellstrom M, *et al.* (2007) Dll4 signalling through Notch1 regulates formation of tip cells during angiogenesis. *Nature* 445(7129):776-780.
275. Suchting S, *et al.* (2007) The Notch ligand Delta-like 4 negatively regulates endothelial tip cell formation and vessel branching. *Proc Natl Acad Sci U S A* 104(9):3225-3230.
276. le Noble F, *et al.* (2005) Control of arterial branching morphogenesis in embryogenesis: go with the flow. *Cardiovasc Res* 65(3):619-628.
277. Hasan J, *et al.* (2004) Quantitative angiogenesis assays in vivo--a review. *Angiogenesis* 7(1):1-16.
278. Huh D, *et al.* (2010) Reconstituting organ-level lung functions on a chip. *Science* 328(5986):1662-1668.
279. Barrila J, *et al.* (2010) Organotypic 3D cell culture models: using the rotating wall vessel to study host-pathogen interactions. *Nat Rev Microbiol* 8(11):791-801.
280. Govck EE, Newey SE, & Van Aelst L (2005) The role of the Rho GTPases in neuronal development. *Genes Dev* 19(1):1-49.

281. Nguyen DH, *et al.* (2013) Biomimetic model to reconstitute angiogenic sprouting morphogenesis in vitro. *Proc Natl Acad Sci U S A* 110(17):6712-6717.
282. Yamao M, *et al.* (2015) Distinct predictive performance of Rac1 and Cdc42 in cell migration. *Sci Rep* 5:17527.
283. Surviladze Z, *et al.* (2010) A Potent and Selective Inhibitor of Cdc42 GTPase.
284. Chen F, *et al.* (2000) Cdc42 is required for PIP(2)-induced actin polymerization and early development but not for cell viability. *Curr Biol* 10(13):758-765.
285. Garvalov BK, *et al.* (2007) Cdc42 regulates cofilin during the establishment of neuronal polarity. *J Neurosci* 27(48):13117-13129.
286. Yang L, Wang L, & Zheng Y (2006) Gene targeting of Cdc42 and Cdc42GAP affirms the critical involvement of Cdc42 in filopodia induction, directed migration, and proliferation in primary mouse embryonic fibroblasts. *Mol Biol Cell* 17(11):4675-4685.
287. Johnson DI (1999) Cdc42: An essential Rho-type GTPase controlling eukaryotic cell polarity. *Microbiol Mol Biol Rev* 63(1):54-105.
288. Koh W, Mahan RD, & Davis GE (2008) Cdc42- and Rac1-mediated endothelial lumen formation requires Pak2, Pak4 and Par3, and PKC-dependent signaling. *J Cell Sci* 121(Pt 7):989-1001.
289. Bayless KJ & Davis GE (2002) The Cdc42 and Rac1 GTPases are required for capillary lumen formation in three-dimensional extracellular matrices. *J Cell Sci* 115(Pt 6):1123-1136.
290. Gupton SL & Gertler FB (2007) Filopodia: the fingers that do the walking. *Sci STKE* 2007(400):re5.
291. Monypenny J, *et al.* (2009) Cdc42 and Rac family GTPases regulate mode and speed but not direction of primary fibroblast migration during platelet-derived growth factor-dependent chemotaxis. *Mol Cell Biol* 29(10):2730-2747.
292. Wan H, *et al.* (2013) CDC42 is required for structural patterning of the lung during development. *Dev Biol* 374(1):46-57.
293. Lee CY & Bautch VL (2011) Ups and downs of guided vessel sprouting: the role of polarity. *Physiology (Bethesda)* 26(5):326-333.
294. Wakayama Y, Fukuhara S, Ando K, Matsuda M, & Mochizuki N (2015) Cdc42 mediates Bmp-induced sprouting angiogenesis through Fmnl3-driven assembly of endothelial filopodia in zebrafish. *Dev Cell* 32(1):109-122.
295. Fantin A, *et al.* (2015) NRP1 Regulates CDC42 Activation to Promote Filopodia Formation in Endothelial Tip Cells. *Cell Rep* 11(10):1577-1590.
296. Rhim AD, *et al.* (2014) Detection of circulating pancreas epithelial cells in patients with pancreatic cystic lesions. *Gastroenterology* 146(3):647-651.
297. Steeg PS (2016) Targeting metastasis. *Nat Rev Cancer* 16(4):201-218.
298. Gupta GP & Massague J (2006) Cancer metastasis: building a framework. *Cell* 127(4):679-695.
299. Steeg PS (2006) Tumor metastasis: mechanistic insights and clinical challenges. *Nat Med* 12(8):895-904.
300. Tuveson DA & Neoptolemos JP (2012) Understanding metastasis in pancreatic cancer: a call for new clinical approaches. *Cell* 148(1-2):21-23.
301. Valiente M, *et al.* (2014) Serpins promote cancer cell survival and vascular co-option in brain metastasis. *Cell* 156(5):1002-1016.

302. Jeon JS, *et al.* (2015) Human 3D vascularized organotypic microfluidic assays to study breast cancer cell extravasation. *Proc Natl Acad Sci U S A* 112(1):214-219.
303. Zervantonakis IK, *et al.* (2012) Three-dimensional microfluidic model for tumor cell intravasation and endothelial barrier function. *Proc Natl Acad Sci U S A* 109(34):13515-13520.
304. Craven KE, Gore J, & Korc M (2015) Overview of pre-clinical and clinical studies targeting angiogenesis in pancreatic ductal adenocarcinoma. *Cancer Lett.*
305. Rhim AD, *et al.* (2012) EMT and dissemination precede pancreatic tumor formation. *Cell* 148(1-2):349-361.
306. Haeno H, *et al.* (2012) Computational modeling of pancreatic cancer reveals kinetics of metastasis suggesting optimum treatment strategies. *Cell* 148(1-2):362-375.
307. Rehders A, *et al.* (2012) Vascular invasion in pancreatic cancer: tumor biology or tumor topography? *Surgery* 152(3 Suppl 1):S143-151.
308. Elmore S (2007) Apoptosis: a review of programmed cell death. *Toxicol Pathol* 35(4):495-516.
309. Jang CW, *et al.* (2002) TGF-beta induces apoptosis through Smad-mediated expression of DAP-kinase. *Nat Cell Biol* 4(1):51-58.
310. Gaur U & Aggarwal BB (2003) Regulation of proliferation, survival and apoptosis by members of the TNF superfamily. *Biochem Pharmacol* 66(8):1403-1408.
311. Lacana E & D'Adamio L (1999) Regulation of Fas ligand expression and cell death by apoptosis-linked gene 4. *Nat Med* 5(5):542-547.
312. Gonzalvez F & Ashkenazi A (2010) New insights into apoptosis signaling by Apo2L/TRAIL. *Oncogene* 29(34):4752-4765.
313. Inman GJ, *et al.* (2002) SB-431542 is a potent and specific inhibitor of transforming growth factor-beta superfamily type I activin receptor-like kinase (ALK) receptors ALK4, ALK5, and ALK7. *Mol Pharmacol* 62(1):65-74.
314. Korc M (2003) Pathways for aberrant angiogenesis in pancreatic cancer. *Mol Cancer* 2:8.
315. Postovit LM, Margaryan NV, Seftor EA, & Hendrix MJ (2008) Role of nodal signaling and the microenvironment underlying melanoma plasticity. *Pigment Cell Melanoma Res* 21(3):348-357.
316. Gogna R, Shee K, & Moreno E (2015) Cell Competition During Growth and Regeneration. *Annu Rev Genet* 49:697-718.
317. Morata G & Ripoll P (1975) Minutes: mutants of drosophila autonomously affecting cell division rate. *Dev Biol* 42(2):211-221.
318. Kebers F, *et al.* (1998) Induction of endothelial cell apoptosis by solid tumor cells. *Exp Cell Res* 240(2):197-205.
319. Boussoimmier-Calleja A, Li R, Chen MB, Wong SC, & Kamm RD (2016) Microfluidics: A new tool for modeling cancer-immune interactions. *Trends Cancer* 2(1):6-19.
320. Kim S, Lee H, Chung M, & Jeon NL (2013) Engineering of functional, perfusable 3D microvascular networks on a chip. *Lab Chip* 13(8):1489-1500.
321. Lim SH, Kim C, Aref AR, Kamm RD, & Raghunath M (2013) Complementary effects of ciclopirox olamine, a prolyl hydroxylase inhibitor and sphingosine 1-phosphate on fibroblasts and endothelial cells in driving capillary sprouting. *Integr Biol (Camb)* 5(12):1474-1484.

322. Jeong GS, *et al.* (2011) Sprouting angiogenesis under a chemical gradient regulated by interactions with an endothelial monolayer in a microfluidic platform. *Anal Chem* 83(22):8454-8459.
323. Greek R & Menache A (2013) Systematic reviews of animal models: methodology versus epistemology. *Int J Med Sci* 10(3):206-221.
324. Mroue R & Bissell MJ (2013) Three-dimensional cultures of mouse mammary epithelial cells. *Methods Mol Biol* 945:221-250.
325. Sato T & Clevers H (2013) Growing self-organizing mini-guts from a single intestinal stem cell: mechanism and applications. *Science* 340(6137):1190-1194.
326. Lancaster MA, *et al.* (2013) Cerebral organoids model human brain development and microcephaly. *Nature* 501(7467):373-379.
327. Muranen T, *et al.* (2012) Inhibition of PI3K/mTOR leads to adaptive resistance in matrix-attached cancer cells. *Cancer Cell* 21(2):227-239.
328. Jang KJ & Suh KY (2010) A multi-layer microfluidic device for efficient culture and analysis of renal tubular cells. *Lab Chip* 10(1):36-42.
329. Huh D, *et al.* (2010) ) Reconstituting organ-level lung functions on a chip. *Science* 328(5986):1662-1668.
330. Booth R & Kim H (2012) Characterization of a microfluidic in vitro model of the blood-brain barrier (muBBB). *Lab Chip* 12(10):1784-1792.
331. Bhatia SN & Ingber DE (2014) Microfluidic organs-on-chips. *Nat Biotechnol* 32(8):760-772.
332. Inoue T, Heo WD, Grimley JS, Wandless TJ, & Meyer T (2005) An inducible translocation strategy to rapidly activate and inhibit small GTPase signaling pathways. *Nat Methods* 2(6):415-418.
333. Shen CJ, *et al.* (2011) Decreased cell adhesion promotes angiogenesis in a Pyk2-dependent manner. *Exp Cell Res* 317(13):1860-1871.
334. Fantin A, *et al.* (2010) Tissue macrophages act as cellular chaperones for vascular anastomosis downstream of VEGF-mediated endothelial tip cell induction. *Blood* 116(5):829-840.